INTERNATIONAL ATOMIC ENERGY AGENCY
UNITED NATIONS EDUCATIONAL, SCIENTIFIC AND CULTURAL ORGANIZATION

INTERNATIONAL CENTRE FOR THEORETICAL PHYSICS
34100 TRIESTE (ITALY) - P.O.B. 586 - MIRAMARE - STRADA COSTIERA 11 - TELEPHONE: 2240-1
CABLE: CENTRATOM - TELEX 460392 - I

H4.SMR/285 - 19

WINTER COLLEGE ON
LASER PHYSICS: SEMICONDUCTOR LASERS
AND INTEGRATED OPTICS

(22 February - 11 March 1988)

# ADVANCED STRUCTURES OF SEMICONDUCTOR OPTOELECTRONIC DEVICES FOR TELECOMMUNICATIONS

A. CARTER
Plessey Research Ltd (Caswell)
Northants
U.K.

# Advanced Structures of
# Semiconductor Optoelectronic Devices for
# Telecommunications

Andrew C. Carter 29/2/1988

A

## Lecture Outlines

1. Introduction
2. Optical Links
3. System Budgets
4. Operating Wavelengths
5. Light Emitting Diodes
6. Laser Diodes
7. Lasers for Coherent Communication
8. Integrated Devices
9. Detectors and Receivers

## Laser Diodes

* Outline of basic operation
* Structures
* Fabry- Perot lasers
* Limitations of FP lasers
* Mode Partition Noise
* Single Mode device options
* DFB laser basics
* DFB laser structures
* Systems implications
* Quantum Well and High Speed Lasers

---

## Light Emitting Diodes

* Introduction
* Why Leds?
* Structures
* Reliability
* LED based systems
* LEDs for Single Mode Systems
* Packaging etc
* Conclusions

## Integrated Devices

- etched facet lasers
- Dual and multisection devices
- Optoelectronic integrated circuits

PLESSEY RESEARCH CASWELL

---

## Lasers for Coherent Communications

- System basics
- Linewidth requirements
- Alternative Configurations
- DFB lasers
- DFB/external cavity
- external grating feedback
- Linewidth reduction/ tunability
- Multisection devices

PLESSEY RESEARCH CASWELL

## BASIC PARAMETERS

SOURCES

Fibre type
Launch power; mean, peak
Wavelength; wavelength tolerance
Detail of spectrum; modes, spectral width
Modulation parameters; bandwidth, tr,tf
Temperature effects; TEC provision
Operating point stabilisation
Operating current, voltage
Reliability
Noise
Reflection sensitivity
Linearity

PLESSEY RESEARCH CASWELL

---

## Detectors and Receivers

* Detection principles
* Materials
* Detector structures
* Detector technology
* Receivers
* Integrated devices
* Future requirements and trends

PLESSEY RESEARCH CASWELL

## LINK OPTICAL BUDGETS

Gross Budget = Source mean launch power - Receiver Sensitivity

Allowances for:
- Fibre loss
- Connector loss
- Dispersion impairments
- Equipment impairments
- Temperature variations
- Repair and maintainance
- Component degradation
- Operating margin
- Upgrade (WDM etc. )

---

## BASIC PARAMETERS

<u>DETECTORS</u>

- Operating wavelength
- Detector type; APD, PIN, RX
- Responsivity (A/W)
- Leakage current
- Resistance, capacitance
- Bandwidth, pole frequencies; (Hi Z, TZ)
- Amplifier noise
- APD gain, Gain-Bandwidth product
- Receiver sensitivity, at given BER
- Temperature derating
- Reliability

ACC/16

II

# LIGHT EMITTING DIODES FOR OPTICAL FIBRE SYSTEMS

Andrew C. Carter

Plessey Research (Caswell) Limited
Allen Clark Research Centre
Caswell, Towcester, Northants NN12 8EQ,
England

K

## 1. INTRODUCTION

Optical fibre technology is now firmly established as a superb medium for the transmission of both analogue and digital data. World wide exploitation of the technology is proceeding on a broad spectrum of applications, from low cost links of only a few metres operating at data rates of a few thousand bit/s right up to long haul telecommunication links in excess of 100 km at greater than 1 Gbit/s. There is now an exhilarating urgency in the development of the necessary optoelectronic components for these systems; the basic device technology is now maturing with many components in full production, yet the research is being continually driven by the need for enhanced system performance and lower device cost in a competitive and rapidly growing market.

The broad spectrum of applications for optical fibre technology demands an equally wide range of source devices; the requirements for a source to transmit at 1 Gb/s over 100 km being radically different to the simple minimal cost LED (light emitting diode) used for short links.

It is now clear that long haul telecommunication systems will be monomode, on grounds of both cost and performance. Such systems demand high performance laser sources. Multimode systems, which can be used in applications from the junction network down to the simplest control links, can utilise LED sources, with both cost and performance benefits.

In this article the range of applicability of the LED in the fibre optics field is discussed and the structure, design and optimisation of suitable LEDs described.

## 2. THE ROLE OF LEDs IN SYSTEMS

Light emitting diodes (LEDs) are playing an increasingly important role as fibre optic sources. LEDs are not only the obvious device for short haul links, but also, with the development of low loss fibres in the 1.3 µm band, they have become viable sources for medium range, medium data rate telecommunication links, where the laser has long been regarded as the essential source element.

The maximum link lengths at high data rates which can be achieved using 0.8 - 0.9 µm LEDs is limited by 'chromatic' or 'material' dispersion in the fibre acting on the inherently large spectral linewidth of the LED. For this reason, 'first generation' 140 Mb/s links, which operate in this band, use laser sources, with spectral linewidths generally less than ~ 5 nm. However, narrow spectral linewidth can lead to severe modal noise with multimode fibre, which imposes a severe loss penalty. Hence an idea frequently advanced is that lasers should only be used with monomode fibres and LEDs only should be used with multimode fibres. For LEDs centred near 1.3 µm, the maximum data rate is not limited by chromatic dispersion, as this passes through zero for silica fibres near this wavelength. Fibre modal dispersion imposes a more severe limit, and this is independent, to first order, of the source linewidth. Figure 1 shows estimates of the maximum link lengths and data rates attainable using near state-of-the-art fibres and current sources and detectors. Results are shown for two wavelengths, 0.9 and 1.3 µm and assume source energy widths of 3 kT, corresponding to linewidths of 32 and 100 nm respectively.

In the dispersion limited regime, to the right of the figure, the relative contributions from fibre modal dispersion and material dispersion can be seen. The material dispersion limit at 1.3 µm, in this case allowing for

some narrowing of the LED linewidth by the filtering action of the fibre (1) is up to 100 GHz km, well in excess of the likely modal dispersion of the fibre, of which three examples, 0.75, 1.5 and 3 GHz km are shown on the diagram.

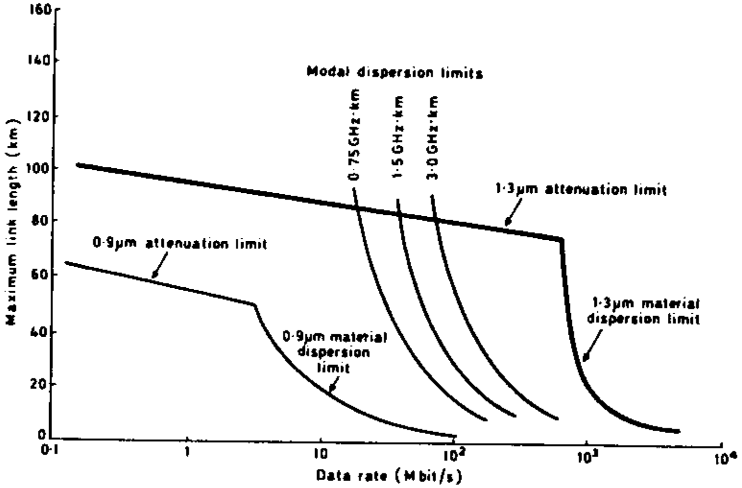

Figure 1. Estimates of maximum link lengths and data rates attainable with LED based systems.

In the power limited region of the diagram (left side) no allowance is made for splice or connector losses or for system margin. Consequently practical link lengths will lie well within the bounded region. LED based 1.3 µm 140 Mbit/s systems have already been installed widely within the U.K., with link lengths in excess of 10 km.

It is thus clear that LED sources can be used for the majority of single channel point to point multimode links, as the extra power and narrower linewidth given by laser sources is often unnecessary.

Additional advantages arise from using LEDs wherever possible. There is no modal noise, which can be a severe problem with lasers on multimode fibre, and freedom from self pulsation and reflection generated noise together with simple drive circuitry, in that optical stabilisation of the operating point is unnecessary.

Table 1 details some of the LED based systems which are under development or are in production by Plessey. The range extends from short haul military up to medium haul (10 km) telecommunications and includes the major growth areas of CATV and local area networks, where the low cost and high performance of modern LEDs is likely to have a catalytic impact.

TABLE 1 - SUMMARY OF LED BASED MULTIMODE SYSTEMS

| SYSTEM | SOURCE | DETECTOR | OPERATIONAL |
|---|---|---|---|
| Telecommunications | | | |
| 2, 8 Mbit/s | 0.9 μm SLED<br>1.3 μm SLED | Silicon APD<br>PIN-FET | 1979<br>1982 |
| 34 Mbit/s | 1.3 μm SLED/ELED | PIN-FET | 1982 |
| 140 Mbit/s | 1.3 μm ELED | PIN-FET | 1983 |
| Local Area Network | | | |
| 50 Mbit/s, short haul | 0.9 μm SLED | Silicon PIN | 1983 |
| CATV | 1.3 μm ELED | PINFET | 1984-5 |
| Military | | | |
| Analogue, Digital DC - 30 Mbit/s | 0.9 μm SLED | Silicon PIN | 1982-83 (Military Qualified) |
| Wavelength Multiplexing | 0.75-1.55 μm | Silicon,<br>III-V PIN | 1984-5 |

## 3. LED PHYSICS

### 3.1. Emission Wavelengths

Both cost and performance dictate the wavelength of operation for an LED based optical transmission system. There are potential applications for LEDs from the near visible (ultra low cost polymer fibres) through the near infra red (0.7 - 0.9 μm) for moderate performance systems to the long wavelength (1.3 - 1.65 μm) band for the longest haul, highest performance applications.

Two III-V semiconductor materials systems can be conveniently used to virtually cover the entire wavelength range of interest, these being the GaAs/GaInAs and InP/GaInAsP combinations for 0.7 - 0.9 and 0.95 - 1.65 μm respectively. These materials are grown with the active layer lattice matched to the confining material, for low internal stress and high reliability.

### 3.2. Light Generation

Light is generated in an LED under forward bias due to the recombination of the carriers which are injected at the p-n junction. LEDs for optical communication are generally fabricated from direct gap semiconductor materials and alloys as radiative recombination is rapid and dominates other non-radiative processes. Conveniently the GaAlAs alloy remains direct gap for emission between ~ 0.7 μm and 0.9 μm (2) and the GaInAsP alloy is direct over the full lattice matched compositional range on InP substrates (0.95 - 1.65 μm). Both of these material systems are also used to fabricate laser diodes for optical communication.

### 3.3. Heterojunctions

The ability to form heterojunctions in both material systems is used to advantage in LED structures. Figure 2 illustrates the band structures of GaAs homojunction and GaAlAs/GaAs double heterojunction diodes under zero bias. In the former, under forward bias electrons are injected into the p-type material, resulting in radiative recombination. The electrons are poorly confined as they can diffuse several microns into the p-type material before recombining. The LED material is also absorbtive at the emission wavelength; care must be taken to minimise substrate thickness to ensure efficient light extraction.

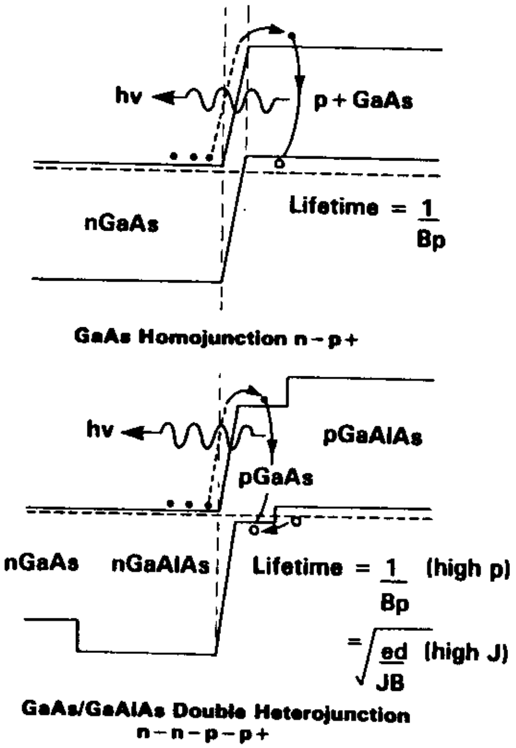

Figure 2 Band structures of GaAs homojunction and GaAlAs/GaAs double heterojunctions.

In the double heterojunction device, carriers are injected into the narrow bandgap active layer from the two wider bandgap confining layers. Carriers can no longer diffuse away and efficient, recombination occurs within the active layer. The confining layers are now transparent to the emitted light, and can be utilised as windows for very efficient light extraction. A similar layer configuration is applcable for the long wavelengths. Here the cladding layers are of InP and the active layer GaInAsP.

### 3.4. Recombination Rates

Electron-hole spontaneous recombination in direct bandgap materials takes place at a rate R depending upon the electron and hole concentrations:

$$R = Bnp$$

where B is the recombination coefficient which depends on the nature of the transition. B is effectively similar for both band to band and band to shallow acceptor transitions, as although the capture probability at an acceptor is higher, this is largely offset by only a proportion of the acceptors being ionised at normal temperatures (3).

For a fast radiative process an increased R is needed. Now R is defined as

$$R = \frac{\Delta n}{\tau_{rad}}$$

where $\Delta_n$ is the excess electron concentration, thus

$$\tau_{rad} = \frac{\Delta n}{Bnp}$$

For p-type material, $p \sim N_A$ and $\Delta n = n$ so the lifetime is inversely proportional to the doping level. Alternatively, if the diode is fabricated in undoped material the lifetime is inversely proportional to $\Delta p$, and thus becomes short at high current densities, giving a fast modulation rate. Both approaches can be used to control the lifetime in high speed LEDs; this is discussed further, with respect to LED structures, in Section 5.1.

# 4. LED OPTICS

## 4.1. External Efficiency

Although minority-carrier injection-induced electroluminescence in LEDs can be of very high quantum efficiency, the measured external efficiency of rectangular shaped LEDs is only a few per cent. This is because only a small fraction of the light is radiated from the active region within the crystal toward the crystal surfaces at less than the critical angle, so the majority of the light generated is trapped by total interal reflection. The power coupled into a medium of low index $n_o$ from the planar face of an LED crystal of index $n_x$ is approximately

$$P_{in} \; T \; \frac{n_o^2}{4n_x^2}$$

where $P_{in}$ is the power generated internally and T is the transmission factor at the crystal/air interface. This is 1.3% of $P_{in}$ for GaAs into air where $n_x = 3.5$ and $n_o = 1$.

The power P coupled from an LED of radiance R into a fibre with acceptance angle Ω is

$$P = RA\Omega = RA\pi(NA)^2$$

for small values of numerical aperture NA. A is the smaller of the areas of the emitter and the fibre core cross section. For highest coupled powers the product RA must be maximised.

## 4.2. Burrus-type Emitters

One simple way of achieving a high radiance is to restrict the emission to a small region within a larger chip. This approach was first adopted by Burrus and Dawson (4) and high-radiance LEDs of this geometry are commonly termed

'Burrus' emitters. With such designs, low thermal impedances can be achieved at the active region allowing very high current-density operation. With the high internal efficiencies $\eta_{int}$ usually achieved this results in high-radiance emission at the front surface. If it is assumed that the emission distribution from the active region is isotropic, the external emission distribution, after transformation by refraction from a high- to a low-index medium at the front face, is approximately lambertian (i.e. $I_\theta = I_o \cos\theta$).

The axial radiance P is approximated by

$$R \approx \frac{T\eta_{int}JV}{4n_x^2\pi}$$

where T is the transmission factor which may take into account the absorption loss through the crystal and losses at the surface due to reflection at the dielectric/air interface, J is the current density and V is the junction voltage.

If the internal absorption is low and the reflection coefficient at the back crystal face very high, the radiance may be up to twice that predicted above.

With the fibre butt-coupled to the emitting area of the LED as shown, there is obviously no advantage in making the emitting area larger than the fibre core area as light would only be coupled into the fibre cladding and ultimately be lost or otherwise wasted. With a step-index fibre, the emitting area may therefore be matched to that of the fibre core so that the active region will then have lowest thermal impedance and therefore a high maximum operating current.

With graded-index fibres, the effective acceptance numerical aperture is a maximum on the fibre axis and decreases radially so that increased butt coupling efficiency results with smaller sources but thermal impedance increases with decreasing source area so some compromise dimension must be determined.

## 4.3. Lens Coupling

The situation where the fibre is butted directly to the emitting aperture of the device is very far from optimum since a large fraction of the lambertian emission distribution is not coupled into the relatively narrow acceptance angle of the fibre. Much more efficient coupling can be achieved if lenses are used to collimate the emission from the LED.

The aim is to magnify the active area so that firstly the size of the image of the active area matches the fibre core, and secondly the radiance of the image over the acceptance solid angle of the fibre is not significantly reduced. Highest lens-coupling efficiencies are obtained when the active area is considerably less than the fibre-core area. This places severe constraints on the thermal and electrical design of the structure in order that high radiance is achieved in very small-area devices at reasonable drive levels.

Several lens-coupling configurations have been adopted and are summarised in Figure 3. In all cases radiation within a larger acceptance solid angle is transformed by the lens to have a smaller solid angle which can be accepted by the fibre. The main limit to the increase in coupling efficiency which can be achieved with lenses is set by the fraction of emitted radiation which

can be collected by the lens. With the simple lens and bulb-ended fibre configurations, the lenses collect a fraction of the radiation emitted into air from the front face of the LED. With the sphere-lens configurations, the adhesive used to hold the lens in place acts as an immersion medium with a higher index than that of air and so the lens acts on a larger proportion of the internally emitted radiation. The best coupling efficiencies will be achieved where the LED-lens interface is completely eliminated, as in the integral-lens LED, because the lens can act upon a large proportion of the internally generated power. The coupling efficiency of both separate and integral sphere lens configurations has been calculated by Abram, Allen and Goodfellow (5,6). King et al and Alferov et al (7,8) have described GaAlAs DH LEDs with an integral-lens geometry. This was formed by the growth of GaAlAs in near-hemisherical holes in a GaAs substrate which is etched away later in the process.

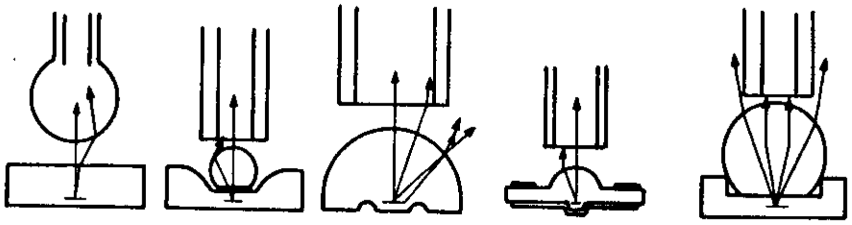

**Bulb ended fibre** **Truncated sphere** **Spherically polished** **Integral lensed** **'Sweet Spot' (Honeywell)**

Figure 3. LED-Fibre Lens Coupling Schemes.

Improvements in the coupling efficiency compared with the butt-coupling case (with 0.16 NA fibres) of around 3-5 times are typically obtained with bulb-ended fibres, and up to 18-20 times with sphere-lens coupling. However, in principle, gains of several hundredfold are feasible with the integral-lens geometry if active regions of just a few micrometres diameter are realised.

From thermodynamic considerations it is not possible to increase radiance by means of lens systems, but magnification without loss of axial radiance at the image can be readily achieved if the acceptance aperture of the lens is sufficiently large. The advantages which can result from sphere-lens coupling depend on the operating conditions one allows for the LED

Figure 4 shows the results of our theoretical analysis of the LED-lens system, based on the optimum truncated sphere lens system of Reference 6. To read the figure, fibre core diameter and NA are selected. Device parameters (drive current, source diameter) can then be read off the right hand scales and launch power off the left hand axis. The results assume an LED of the lens coupled type shown in Figure 6, and assume 100% internal efficiency, step index fibres and reflective back contacts. In the following section, optimised LED structures are described, and results compared with the predictions of this model.

The sweet spot (Honeywell) configuration included in Figure 3 employs a relatively large lens, giving an output beam which is larger than the fibre core. This has the advantage that reduced accuracy is necessary in the fibre placement, at the cost of lower coupled power than attainable with the optimised truncated sphere lens configuration.

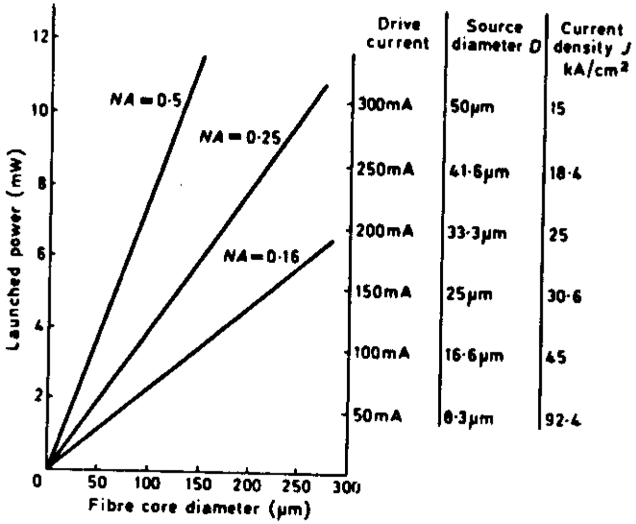

Figure 4. Theoretical coupled power levels for optimised surface emitter with truncated sphere lens. Read by first selecting fibre parameters, giving diode dimensions, current and coupled power.

## 5. LED STRUCTURES

### 5.1. Lens Coupled Surface Emitter (SLED)

The lens coupled surface emitting LED developed by Plessey is illustrated in section in Figure 5. Two active layer configurations are shown, for the GaAs/GaAlAs and InP/GaInAsP systems. A third alternative is the simple diffused device, where the junction is made by zinc diffusion into an n-type GaAs substrate. The basic unlensed device is derived from the configuration first adopted by Burrus (4). The current is confined to flow through a small central area (10 - 50 μm in diameter) by either dielectric isolation by a film of $SiO_2$ or by proton implantation of the passive area of the device, which renders the material semi-insulating. Efficient radiative recombination occurs between electrons and holes in the relatively narrow bandgap active layers of the double heterojunction devices and between injected electrons and majority holes in the p-side of the junction in the case of the Zn-diffused device. Light, which is radiated isotropically, exits from the top face of the device (into which is etched a well to reduce absorption), is collected by the lens and coupled into the fibre. Heat is effectively removed from the device by the integral plated gold heatsink, which is 5 - 10 µm thick. Overall chip dimensions are typically 200 x 300 µm, the etched well being offset to enable a thermocompression gold wire bond to be made to the n-side of the device. A bonded and lensed device is shown in Figure 6. Here the lens diameter is ~ 110 µm and the device is of the GaAlAs/GaAs type.

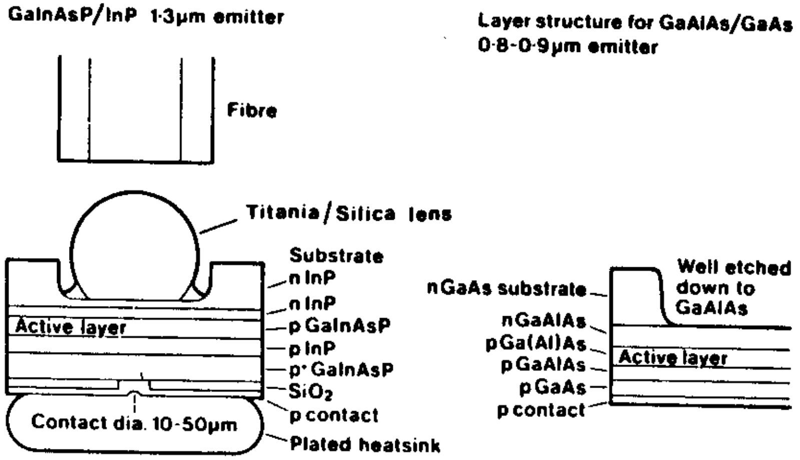

Figure 5. The Lens Coupled Surface Emitting LED - Schematic

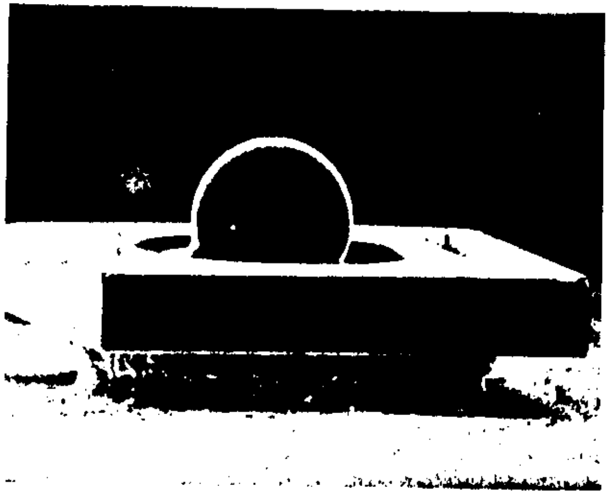

Figure 6. The Lens Coupled Surface Emitting LED. Scanning Electron Micrograph.

We have achieved power levels up to a third of those predicted from Figure 4 for GaAlAs/GaAs and GaInAsP/InP LEDs into the larger core fibres. Saturation of the LED output occurs for the very small emitting areas required for small core fibres (particularly 50 µm, 0.2 NA telecomms), due to both thermal and non-thermal effects (8). Of particular importance are Auger recombination and in-plane superluminescence.

In addition, it becomes difficult to control current spreading in the device, which gives rise to wasted light generation outside the desired area. Consequently some design compromises have to be made. At present best performance with 50 µm core fibre is obtained for LEDs with emitting areas of 20 µm diameter.

### 5.2. The Edge Emitting LED (ELED)

The edge emitting LED configuration has significant advantages over the surface emitting geometry when coupling into the 50 µm core fibre, particularly for the long wavelength devices (9). This is due to reduced non-thermal saturation and exploitation of super-radiance.

Figure 7 shows the edge emitting LED (ELED) configuration developed by Plessey. Particularly important features of the device which contribute to the excellent reliability and high performance include (i) the n-contact window to allow screening of the device for defects by observation of the spontaneous emission perpendicular to the stripe; (ii) the plated gold heatsink which allows the use of high temperature bonding solders; (iii) the refractory p-side metallisation to eliminate contact metal diffusions; and (iv), as shown in the scanning electron micrograph of the device in Figure 8, the facet mounted truncated sphere microlens, which enhances the power coupled into the fibre by typically a factor of five over butt coupling.

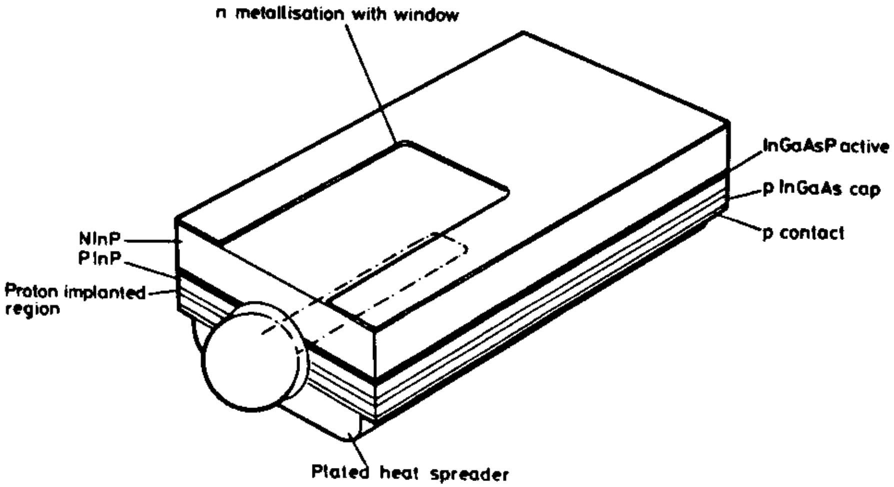

Figure 7. 1.3 µm Wavelength Edge Emitting LED - Schematic

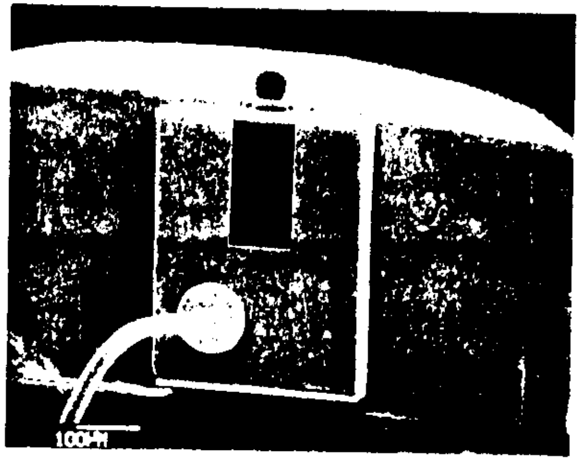

Figure 8. Edge Emitting LED - Scanning Electron Micrograph.

Contact stripe isolation is generally by proton implantation through the $p^+$ GaInAs contact layer. Stripe widths and lengths are 10 and 150 µm respectively, with a 250 µm unpumped region, which inhibits round trip gain, preventing lasing action.

## 6. LED PERFORMANCE

### 6.1. Bandwidth and Efficiency

The injected carrier lifetime for spontaneous emission has been derived from Namizaki (10) from the recombination rates outlined in Section 3.4 to be

$$\tau = \frac{edN}{2J}\left[\sqrt{1 + \frac{4J}{edN^2 B}} - 1\right]$$

Where e is the electronic charge; d is the active layer thickness; N is the acceptor doping concentration; B is the radiative recombination coefficient; and J is the injection current density. For low-injection conditions this yields a current density independent lifetime of

$$\tau \propto (N)^{-1}$$

and for high-injection conditions

$$\tau \propto J^{-\frac{1}{2}}$$

Since the high-injection situation applies when the density of the injected carrier in the active layer exceeds the majority carrier density, the latter relationship for $\tau$ clearly applies for low-doped active-layer material. The current density dependence of modulation bandwidth follows because it is related theoretically, to lifetime by

$$P(\omega)=P(o)\left[1+(\omega\tau)^2\right]^{-\frac{1}{2}}$$

Figure 9 shows the small signal frequency responses of several quaternary 1.3 µm SLEDs with different active layer doping levels. Here the frequency response is plotted against $\sqrt{I}$, where I is the drive current, such that the different speed determining mechanisms are apparent. The reduction in bandwidth of the heavily doped device at low current is due to device parasitics in the oxide isolated device shown and is improved by the used of proton implant isolation, which reduces the effects of passive junction capacitance.

We have fabricated 1.3 µm SLEDs for data transmission at 140 Mb/s. Such devices are typically a factor of two less efficient than slower devices and launch up to about 40 µW into 50 µm core fibre. Other workers (11,12) have reported very wide (1 GHz) bandwidth devices with similar geometry. Despite relatively low power, these devices have many potential applications in short haul, high data rate systems.

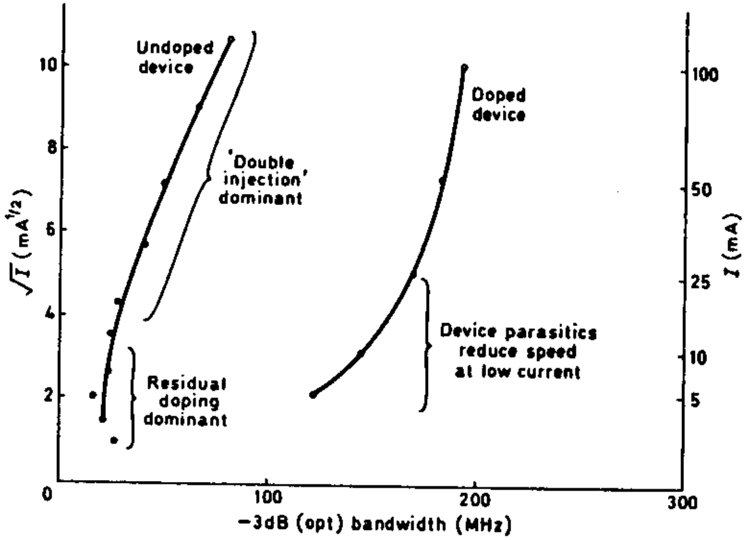

Figure 9. Frequency Responses of Doped and Undoped SLEDs.

Switching speeds below 2ns can also be attained in the 1300 nm ELED. Here there can be a degree of speed enhancement due to super-radiance, which effectively shortens the radiative lifetime. Figure 10 shows a single pulse response of an ELED designed for 140 Mb/s, together with the corresponding eye diagram for NRZ coding. There is clearly little penalty due to eye closure.

## 6.2. Launch Powers

Table 2 summarises the launch powers which have been obtained into various fibres from GaAs, GaAlAs and GaInAsP surface emitting LEDs, together with GaInAsP ELEDs. In all cases the cladding modes were stripped and the fibre apertured into a detector at the stated NA of the fibre.

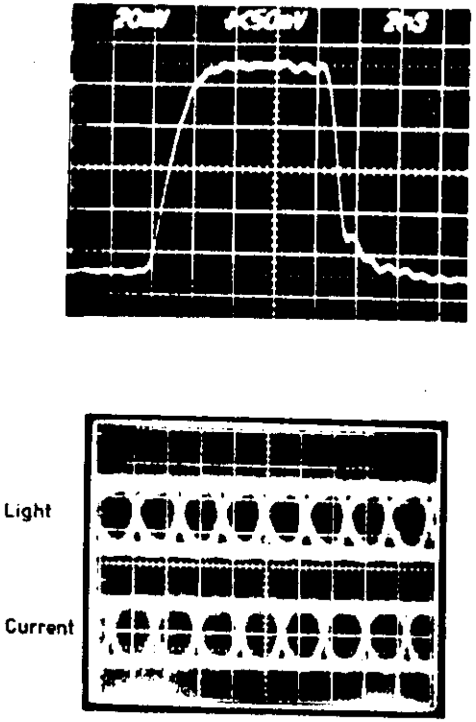

Figure 10. Pulse Response and Eye Diagram for 140 Mb/s ELED.

For telecommunications applications the 50 µm core 0.2 NA graded, index fibre is most important. Here power levels in excess of 250 µW (DC) have been obtained with GaAlAs/GaAs SLEDs and 70 µW (DC) with 1.3 µm SLEDs. The lower power from the 1.3 µm devices is due to saturation effects but is none the less sufficient for many long haul applications, such as 34 Mb/s, 12 km junction links.

TABLE 2 - LED COUPLED POWER LEVELS

| Device Type | Bandwidth at max. current | $T_r$ | Coupled power 50µm 0.2NA Graded Index | Current | Coupled power 100µm 0.3NA Step Index | Current |
|---|---|---|---|---|---|---|
| GaInAsP/InP Double Heterostructure Surface Emitter | 50MHz | 7ns | 70µW(DC) | 100mA | 400µW(DC) | 100mA |
| GaInAsP/InP Double Heterostructure Surface Emitter | 300MHz | 1.5ns | 38µW(DC) | 100mA | - | - |
| GaAlAs/GaAs Double Heterostructure Surface Emitter | 150MHz | 3ns - 5ns | 250µW(DC) | 150mA | 2·05mW(DC) | 150mA |
| GaAlAs/GaAs Double Heterostructure Surface Emitter | 300MHz | 1.5 - 2ns | - | - | 1·2mW(DC) | 150mA |
| GaAs Zinc Diffused Surface Emitter | 30MHz | 10ns | 150µW(DC) | 150mA | 800µW(DC) | 150mA |
| GaInAsP/InP Double Heterostructure Edge Emitter | 150MHz | 2ns | 150 - 300µW(DC) | 150mA | - | - |

For longer links or higher data rates the 1.3 µm ELED is a better option. Figure 11 shows the light current characteristic for a premium device, which couples over 300 µW at 150 mA. Values in excess of 150 µW are typical for this device.

The GaAlAs/GaAs SLED has many applications in the military and avionic fields, where short haul, high loss systems dominate. These devices typically launch 2.5 mW into 200 µm core and >1 mW into 100 µm core quasi-step index fibres.

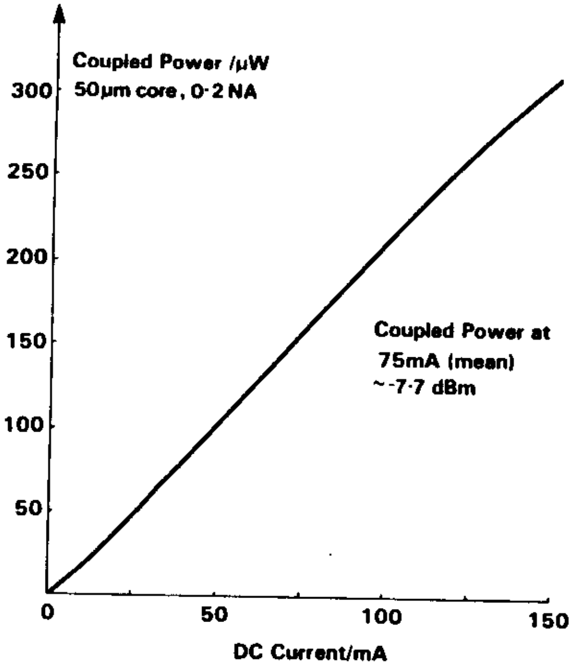

Figure 11. Light-Current Characteristic of ELED.

### 6.3. Spectral Linewidths

Although the disadvantage of broad spectral linewidth inherent in the LED largely disappears at 1.3 µm due to the low material dispersion of the fibre, control and reduction of linewidth is still highly desirable to improve reproducibility and to reduce the need for receiver equalisation. The linewidth of 1.3 µm SLEDs increases with increasing doping level due to the

formation of band tail states. Figure 12 shows the linewidths of two devices, with Zn doping levels of $5.10^{17}$ $cm^{-3}$ and $10^{19}$ $cm^{-3}$ in the active layer, such devices exhibit rise times of 15 ns and 1.5 ns respectively. The linewidths (full width at half maximum) increase from 75 to 95 nm with increasing doping level. A shift to lower energy is also apparent so that the active layer composition must be adjusted to maintain the same centre wavelength. The 1.3 µm ELED has a reduced linewidth due to self absorption and superluminescence - giving 50-60 nm linewidth.

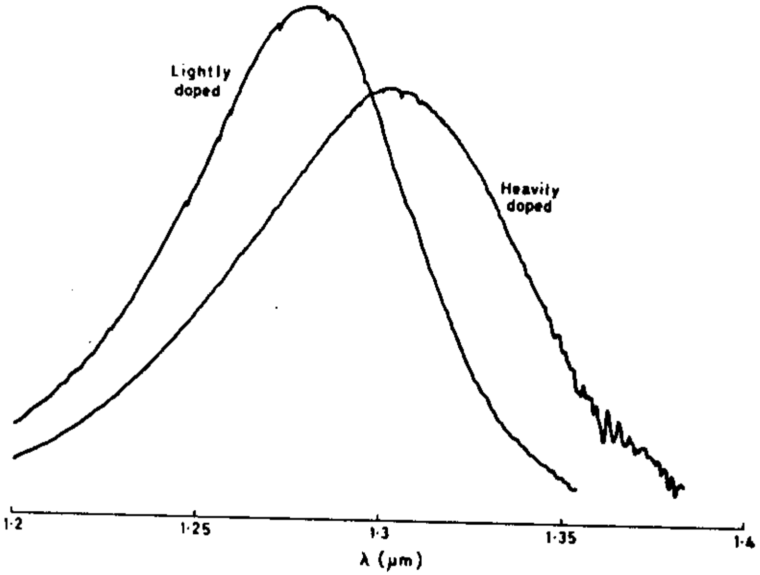

Figure 12. Emission spectra of lightly and heavily doped 1.3 µm wavelength SLEDs.

### 6.4. Thermal Behaviour

The optical power from a LED changes only relatively slowly with temperature so that optical feedback to stabilise the working point is unnecessary. For a 1.3 μm GaInAsP/InP SLED in the range 20-100°C the output falls by ~ 0.7%°C$^{-1}$, reaching half power at ~ 130°C. GaAlAs/GaAs devices tend to be even less temperature sensitive, falling by ~ 0.5%°C$^{-1}$.

The basic ELED is considerably more temperature sensitive than the SLED, as the power increases rapidly with decreasing temperature due to the onset of super-radiance. For telecomms applications, where device operation up to a temperature of 60°C is necessary, we have found it advantageous to reduce super-radiance by adjusting the LED doping and geometry. Figure 13 shows a comparison between an ELED with considerable super-radiance, a doped ELED and an SLED. The doped ELED clearly is as good as the undoped device at 60°C, and imposes less demands on receiver dynamic range at the lower temperature.

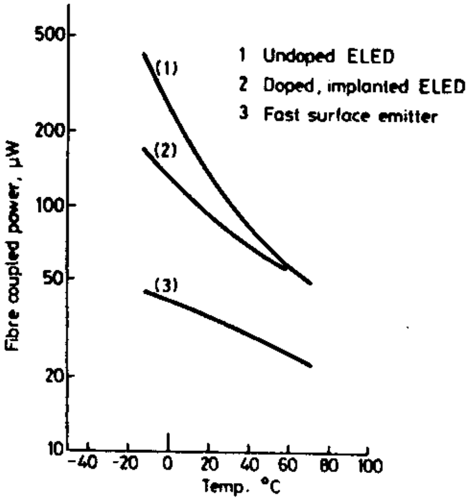

Figure 13. Power v/s Temperature for 1.3 μm Wavelength ELEDs and SLEDs.

## 7. RELIABILITY

The surface emitting high radiance LED is a particularly long lived, reliable device. GaAs zinc diffused devices have been operating at Plessey since 1974 and results of high temperature accelerated ageing, indicate lives at room temperature around ~ 5.10$^5$ hours, the particular failure mechanism being gold diffusion from the contact. Diffused devices with improved contacts have lives well in excess of 10$^6$ hours.

The GaAlAs/GaAs double heterostructure SLED has been extensively investigated by ourselves and others (13,14) with excellent results. Even with the most pessimistic assumptions, operation over 10$^6$ hours can be confidently predicted.

The GaInAsP/InP devices are proving to be even more reliable than the shorter wavelength diodes. Device temperatures have to exceed 170°C before degradation rates become measurable (15,16) and even at this temperature batch lives are around 10$^4$ hours. Predicted room temperature lives are 10$^7$-10$^8$ hours. Our accelerated ageing studies on 1.3 μm ELED have given activation energies of ~ 0.5 eV, with batch lives of > 5000 hours at 155°C, giving room temperature lives well in excess of 10$^6$ hours.

## 8. SUMMARY AND CONCLUSIONS

High power, fast, reliable LEDs have been developed for all wavelengths of current interest in optical fibre systems. The range includes minimal cost devices for very short haul links, 0.85 μm wavelength devices for LAN and military systems, 1.3 μm wavelength devices for LAN, CATV and high speed links and 1.3 μm devices for telecommunications systems.

LEDs are simple to use, requiring no feedback control, and are immune to modal noise, self pulsation and reflection induced noise. Increasingly LEDs will be used in preference to lasers for multimode fibre systems, whereas lasers will exclusively be used for monomode links.

Future developments of LEDs will give cost reductions with improvements in power, bandwidth and linearity. Integration of high performance LEDs into optoelectronic integrated circuits for high speed, low cost data transmission can also be expected as the trend towards a worldwide integrated communications network continues.

## REFERENCES

(1) Stewart WJ. Proc. 5th European Conf. on Optical Communications. Amsterdam, Sept 1979, Paper 12.3

(2) Casey HC and Panish MB. J. Appl. Phys. 40, 4910, 1969

(3) Rees G and Milne W. Gallium Arsenide and Related Compounds. pp.362-369, Edinburgh 1976.

(4) Burrus CA and Dawson RW. Appl. Phys. Lett. 17 (3), pp.97-99, 1970.

(5) Abram RA, Allen RW and Goodfellow RC. J. Appl. Phys. 46 (8), 3468-3474, 1975.

(6) Abram RA and Goodfellow RC. Electronic Letters, 3rd Jan 1980, 16, 1, pp.14-16.

(7) King FD and Springthorpe AJ. J. Electronic Matls, 4, 2, p.243-252, 1975.

(8) Alferov Zh.I, Andreev VM, Egoros BV and Syrbu AV. Sov. Phys. Semicond. 11 (10) 1123-1127, 1977.

(9) Goodfellow RC, Carter AC, Rees GJ and Davis R. IEEE Trans. ED., Vol.ED-28, 4 Apl. 1981, pp.365-371.

(10) Carter AC, Ure J, Harding M and Goodfellow RC, IOOC, June 1983, Tokyo.

(11) Namizaki H, Kan H, Ishii M and Ito A. Appl. Phys. Lett. 24, p.486-487, May 1974.

(12) Grothe H, et al. El. Lett. 15, pp.702-3, 1979

(13) Suzuki et al. IOOC 1983, Tokyo. Paper 27C2-2

(14) Abe M, et al. IEEE Trans. ED, ED-24, No.7, pp.990-994, July 1977

(15) Dawson LR, Keramidas VG and Zipfel CL. Bell Syst. Tech. J.59, 2, p.161-8, 1980

(16) Wada O, et al. IEEE J. QE, QE18, No.3, pp.368-374, 1982.

## BIBLIOGRAPHY

Andrew C. Carter was born in 1951 in Helensburgh, Scotland. In 1973 he graduated in physics from Oxford University, England, where he continued after graduation to study the infra red properties of impurities in semiconductors, leading to the degree of D.Phil in 1977. After this time he joined the scientific staff at the Allen Clark Research Centre of the Plessey Company to work on infra red diodes for optical fibre systems. He is now leader of the Optoelectronic Device Physics Research Group, with interests including LEDs, lasers, wavelength multiplexing, detectors, integrated optoelectronics and semiconductor integrated optics.

### 3.2.4 Light Emitting Diodes for Single Mode Optical Fibre Systems

Light emitting diodes used with single mode fibre (SMF) are attractive sources for local loop and other short haul applications due to cost and reliability advantages over laser diodes [1]. Their output power is less temperature dependent and they do not normally need external control circuits. LEDs are currently being investigated for short haul low, medium and high data rate links to meet the evolutionary demands of the emerging broadband integrated services digital network (B-I DN). This section examines the structure and performance of such LEDs and discusses their system limitations.

#### 3.2.4.1 Device Structures and Performance

Two basic device structures are available for monomode LEDs, these being the surface emitting and edge emitting geometry. In general higher optical powers can be achieved with the latter whereas the former offers simpler processing and packaging, with hence potentially lower cost, and a lower temperature coefficient.

In edge emitting LEDs, lasing action needs to be reliably inhibited. This can be done by using a structure incorporating a proton-implanted absorbing region behind the emitting stripe [2]. The alternative structure widely used is similar to the conventional injection laser but with high performance anti- reflection coatings to inhibit laser action, e.g. [3].

Coupled power levels from single mode ELEDs are typically in the range 2-10μW peak at room temperature. Greater power is available from devices which are strongly super radiant. However this extra power is accompanied by a worsening in the temperature de-rating of power, from typically 1.2% per degree C to around 2.6% per degree C. Figure 3.7 shows light current characteristics for a super radiant device coupled into single mode fibre at 20,25 and 40°C.

Modulation rates are somewhat dependent on device structure and drive conditions. Commercial devices are now readily available for data rates upt to 200 Mbit/s but many experiments have been performed with edge emitting LEDs at 565 Mbit/s and even 1.2 Gbit/s [4].

Surface emitting LEDs have also been proposed and demonstrated for use in single mode fibre systems [5,6]. The advantage of the surface geometry is in simple bonding, non critical fibre placement and planar processing (no facet). The main disadvantage is the relatively low power, with 1.5μW being reported for a device suitable for 565 Mbit/s operation [6] and the wider spectral width, although the lower temperature coefficient partially compensates for these disadvantages in practical systems.

Table 3.2 summarizes the performance of currently available high speed ELEDs.

Table 3.2: Typical ELED Performance

| | |
|---|---|
| Output power into SM-fibre (25°C, 150m A drive) | 2-10μW |
| rise/fall times | 3ns max |
| half power line width (25°C) | 80-100nm |
| Output power temperature coefficient | 1.2%/°C typ. |
| Centre Wavelength Variation with Temperature | 0.5-0.8nm/°C |
| Spectral broadening | 0.4nm/°C typ. |

### 3.2.4.2 Systems Applications

Figure 3.8 shows published experiments using LEDs with single mode fibre. Link lengths of up to 9.8km have been reported at 2Gbit/s [33] and in excess of 100km at 16 Mbit/s [34]. Link lengths are limited by either the available power budget or by chromatic dispersion due to the spectral width of the LED. A 3dB power penalty may be seen for a 3.5 Gbit.km/s link length data rate product for SLEDs increasing to ~5 Gbit.km/s for ELEDs due to their intrinsically narrower line width.

For practical system applications, however, it is necessary to allow for manufacturing tolerance and temperature variation of the LED centre wavelength and spectral width and for fibre dispersion and attenuation variation over the entire LED wavelength spectrum (see Fig. 3.9). The fibre attenuation characteristic will not only affect the system loss, but also the system bandwidth due mainly to the filtering effect of the water peaks. This can drastically reduce the achievable section length compared with those reported above. Bitrate distance products in commercial single mode systems are likely to be similar to those achieved in long wavelength multimode systems, i.e. less than 1.5 Gbit.km/s and will depend on control of LED-wavelength and spectral characteristics. The overall bit rate limit will be set by achievable modulation speed and by receiver sensitivity.

In conclusion, both surface and edge emitting LEDs are suitable for use with single mode fibre. The prime advantages of these devices over lasers are reduced cost together with excellent reliability. These advantages enable these devices to offer cost effective solutions to many low and medium bit rate local loop applications for link lengths up to a few km.

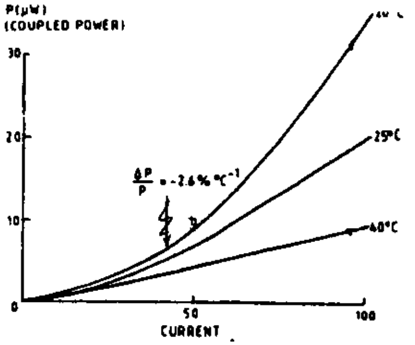

FIG 2.7 COUPLED POWER/CURRENT CHARACTERISTIC SUPER-RADIANT E-LED

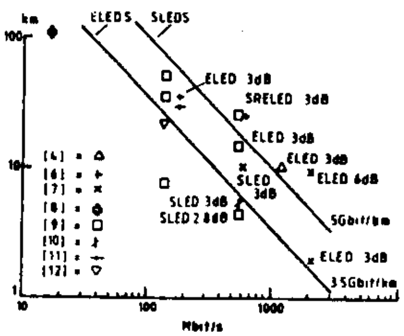

FIG 2.8 PUBLISHED EXPERIMENTS USING LEDS ON SINGLE MODE FIBRE
(DEVICE TYPE AND DISPERSION PENALTY ARE INDICATED)

---

## STRUCTURE OF REPRESENTATIVE EDGE-EMITTING LEDS

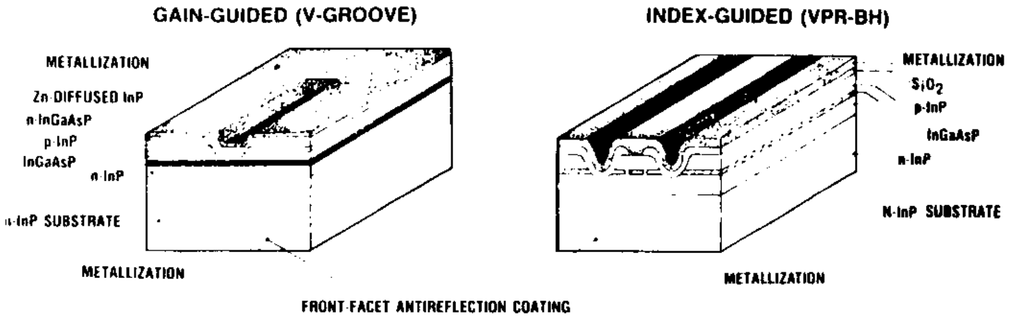

OLSHANSKI - OFC MINI TUTORIAL
G.T.E.

# INDEX-GUIDED EDGE-EMITTING LED

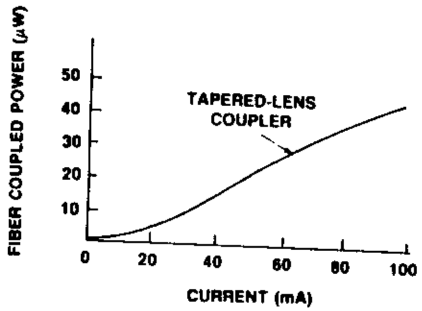

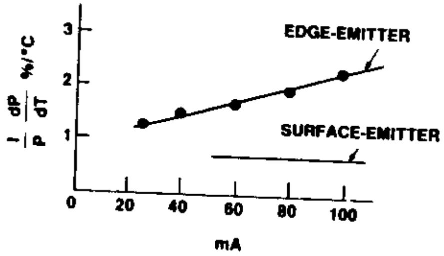

R. OLSHANSKI OFC MINITUTORIAL
G.T.E.

References

[1] Kaiser, P. Proceedings of IOOC/ECOC, Venice 1985

[2] Carter, A.C. et al. Proc. IOOC, Tokyo 1983, p210-211

[3] Fye, D.M. et al. El. Lett. 16th January, 1986 22, 2, pp87-88 and Fye, D.M. JLT, Vol. LT-4, 10th October, 1986, pp 1546-51. The latter reference gives also a useful review of system experiments with LEDs.

[4] Fujimoto N. et al OFC/IOOC 1987 paper M15 Reno, 1987.

[5] Uji T. and Hayashi, J. El. Lett. 21 10, pp418-9, 1985.

[6] Uji, T et al IOOC/ECOC 1985, Venice, Postdeadline papers pp57-60.

[7] Hayashi, J. et al OFC/IOOC 1987 PDP17-1, RENO.

[8] Plastow et al. El. Lett. 21, pp369-370.

[9] Gimlett, J.L. et al. IOOC/ECOC 1985, Venice, Postdeadline papers pp 53-56.

[10] Saul, R.H. et al. El. Lett. 21, 17, pp773-5, 1985.

[11] Ullricht, L.W. et al. El Lett. 21, 19 pp860-1, 1985.

[12] Schumati, P.W., et al. El Lett. 21, 12 pp522-4, 1985.

# LASER OSCILLATOR

- Medium with gain
- Optical feedback

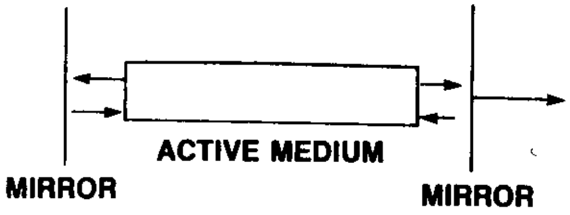

FABRY-PEROT CAVITY

Real medium has losses (absorption, scattering, end losses)

Laser oscillation occurs with gain = losses

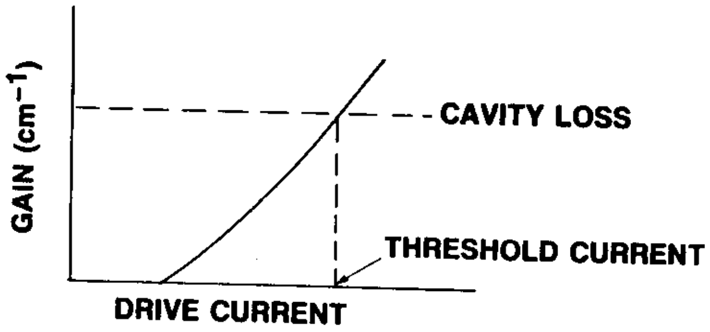

# TWO CONDITIONS FOR LASING

- Gain = loss
- Phase condition

$$\frac{m\lambda}{2} = nL$$

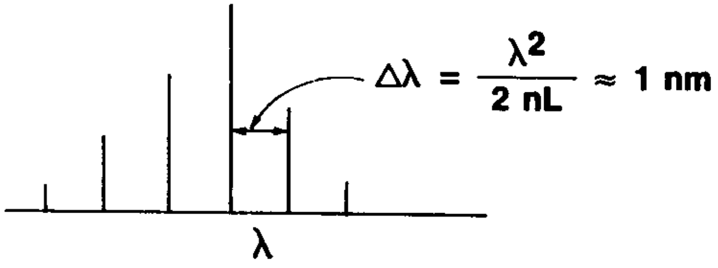

FABRY-PEROT SPECTRUM

# PLANAR ACTIVE LAYERS

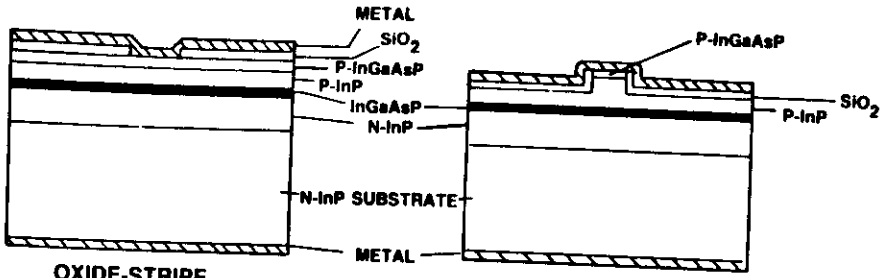

**OXIDE-STRIPE**
GAIN-GUIDED

**RIDGE**
WEAKLY
INDEX-GUIDED

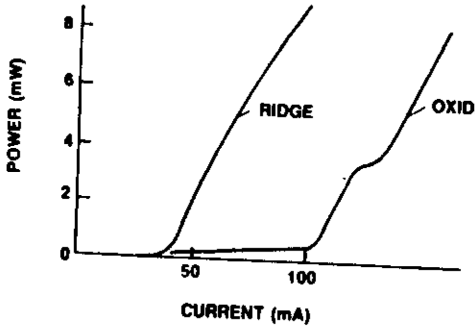

OLSHANSKI OFC

# TYPES OF BURIED-HETEROSTRUCTURE LASERS

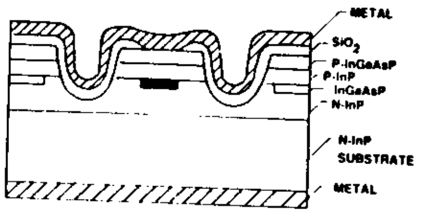

MESA

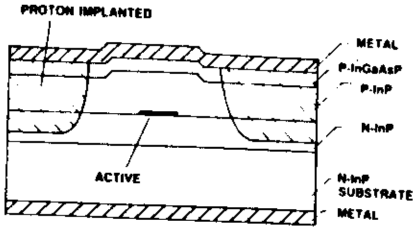

BURIED MESA

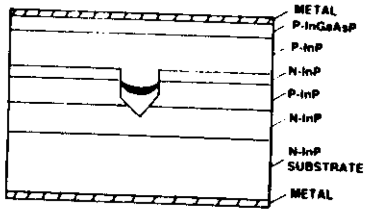

BURIED-CRESCENT

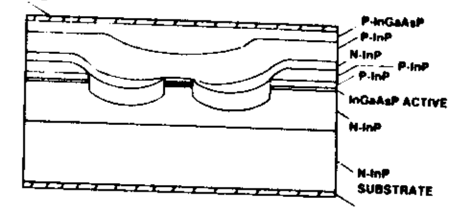

DOUBLE-CHANNEL

# CONSEQUENCES OF STRONG WAVEGUIDING
## ($\delta n = 0.2$)

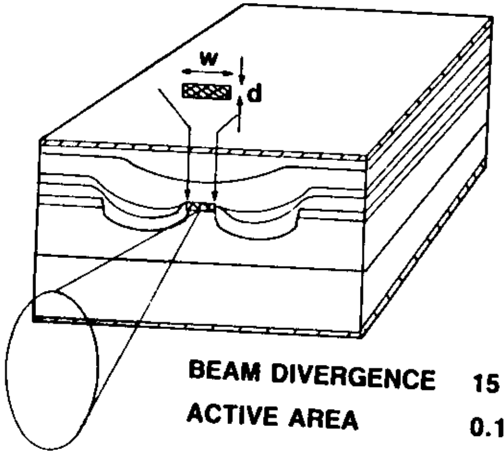

| | |
|---|---|
| **BEAM DIVERGENCE** | 15° × 30° |
| **ACTIVE AREA** | 0.15 $\mu m$ × 1.5 $\mu m$ |

- **Small dimensions for single spatial mode**
  - — Low threshold current
  - — Difficult to process (reduced yield)
- **Large beam divergence**
  - — Lens required for 25–50% coupling efficiency
  - — Very sensitive to fiber alignment

OLSHANSKI OFC

---

## Buried Ridge

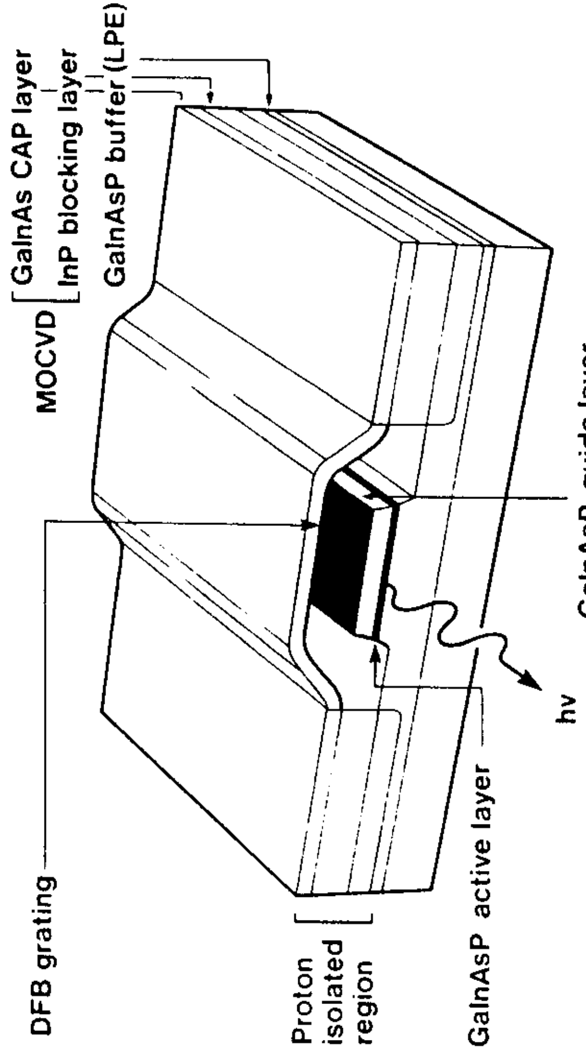

PLESSEY RESEARCH CASWELL

## 1.3μm Laser High Power Performance

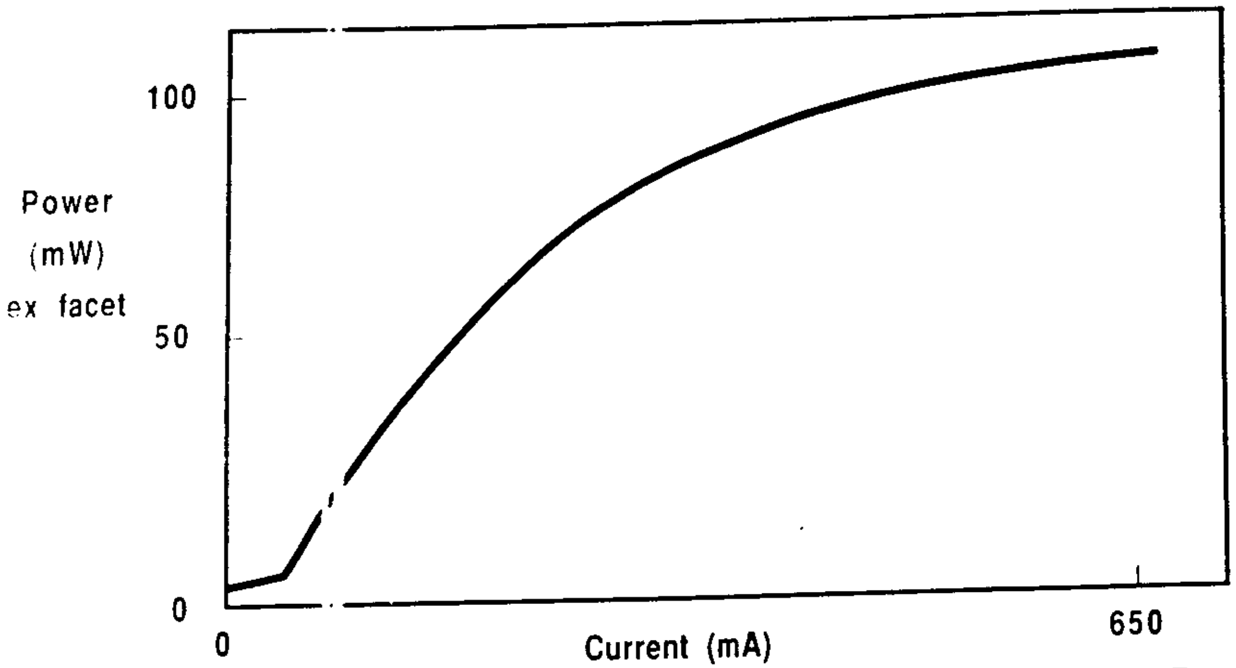

PLESSEY RESEARCH CASWELL

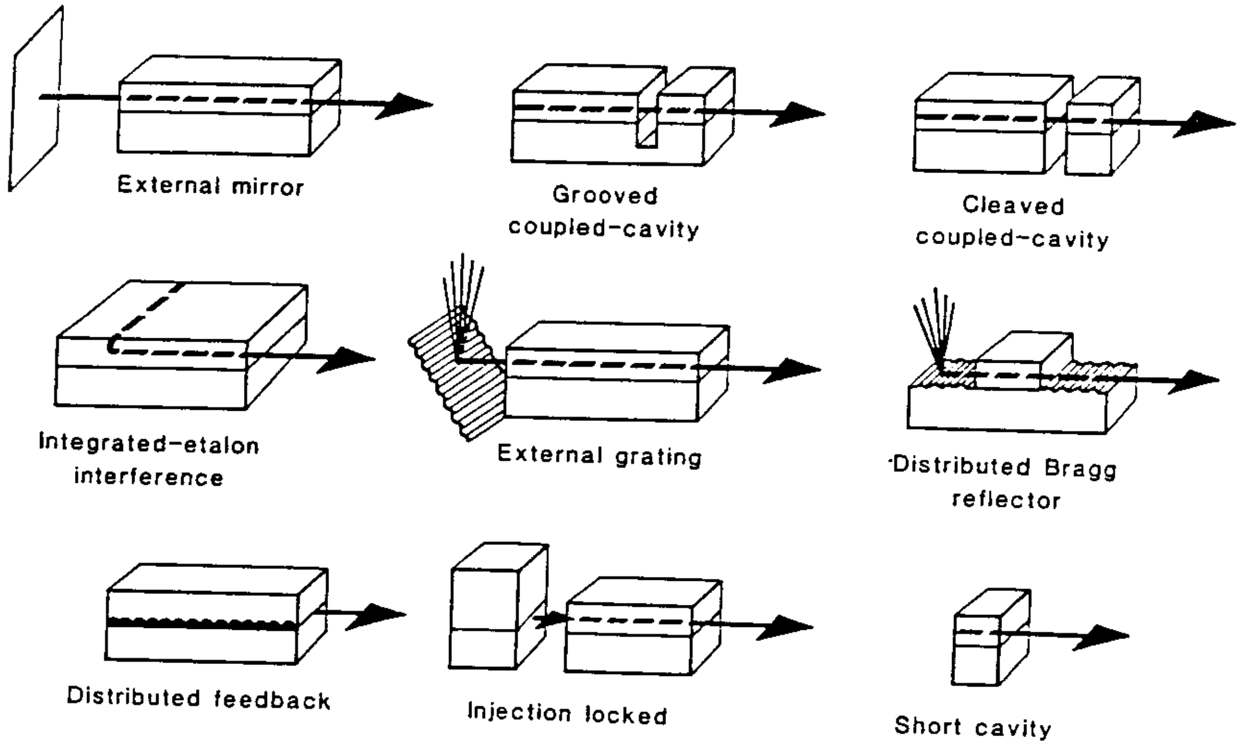

## SINGLE LONGITUDINAL MODE LDs
(by G.H.B.Thompson)

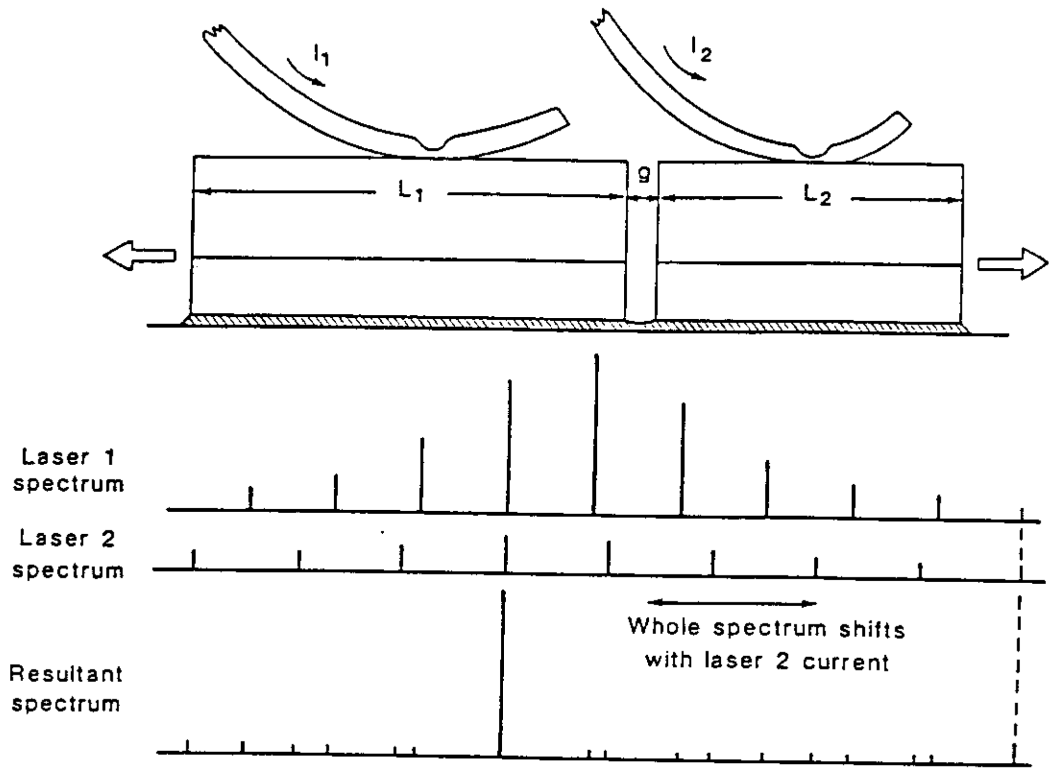

***SINGLE LONGITUDINAL MODE OPERATION OF CLEAVED COUPLED CAVITY ($C^3$) LD***

---

## Distributed Feedback Lasers- - Wavelength Selection by Grating

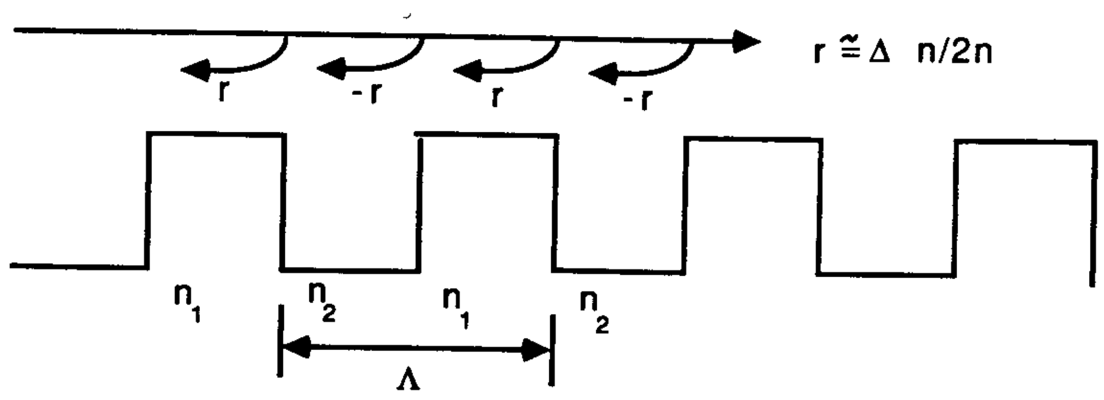

$r \cong \Delta\ n/2n$

Constructive Interference for:

$(2\pi/\lambda)n\Lambda + \pi = 2\pi \rightarrow \Lambda = \lambda/2n \rightarrow \lambda_B = \Lambda/2n$

Bragg wavelength

Coupling Coefficient = Coupling per unit length

$\kappa \cong 2r/\Lambda \cong 2\Delta n/\lambda$

## DFB Feedback Phase Problem

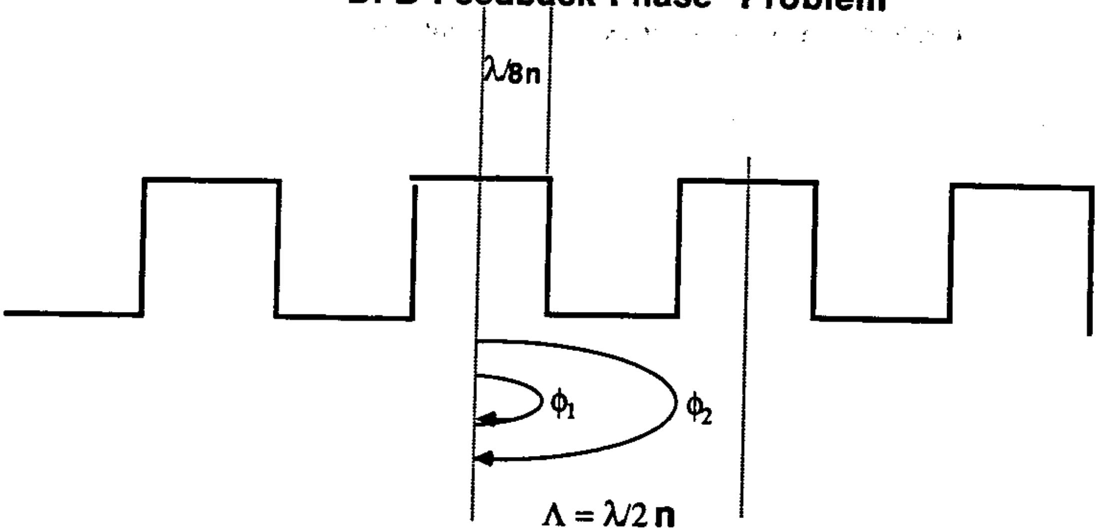

$\phi_1 = \lambda/4\,n = \pi/2$  $\phi_2 = \phi_1 + \pi + \pi = \phi_1 + 2\pi$

Round Trip Phase = $2\phi_1 = \pi$ at $\lambda_B$ ; wanted $2\pi$

---

Wavelength and required gain found by solving complex transcendental equation

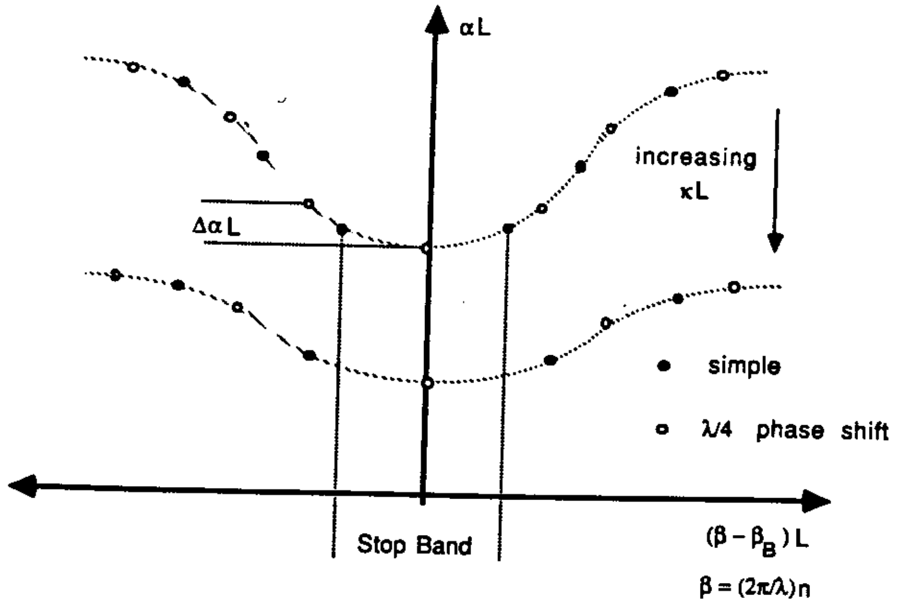

## Phase shifted DFB Configuration

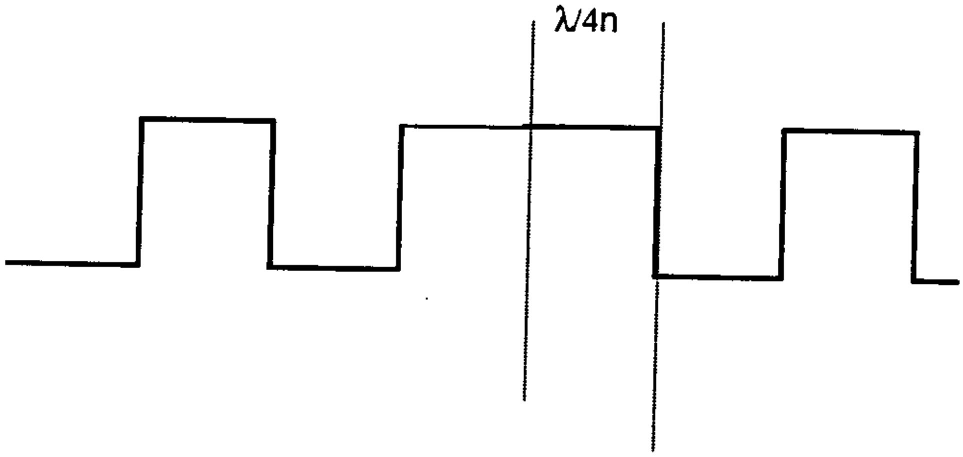

$\lambda/4n$ Phase shift $\longrightarrow$ $2\phi_1 = 2\pi$ at $\lambda_B$

---

DFB + FACET REFLECTION LEADS TO
INTERFERENCE BETWEEN DISTRIBUTED AND DISCRETE FEEDBACK;
MODE SELECTION DEPENDS ON 'GRATING PHASE'

YIELD = % OF HIGH $\alpha$ L CASES

# MODE SELECTIVITY IN DFB LASERS WITH CLEAVED FACETS

*Indexing terms: Lasers and laser applications, Semiconductor lasers*

The mode selectivity of distributed feedback lasers with cleaved facets is examined for various positions of the grating relative to the facets. The expected yield of single-mode lasers is calculated for several values of the coupling coefficient.

*Introduction:* In order to take full advantage of the low loss in optical fibres in the 1·55 μm region a light source with a narrow spectral linewidth is required. A possible candidate is a semiconductor laser incorporating a grating in order to provide distributed feedback (DFB). Although the DFB favours modes near the Bragg wavelength, a laser with nonreflecting mirrors may be multimoded since one mode on each side of the stopband will have the same threshold gain. The resulting spectrum is then determined by the spectral gain which will shift with temperature or under modulation. In a DFB laser with reflecting mirrors (i.e. cleaved facets) the situation is more complicated since the threshold for the various modes depends on the position of the facet relative to the grating ('facet phase'). Various schemes have been proposed in order to bypass this problem:

(i) use a phase shift in the grating[1,2]

(ii) use a structure where the gratings have been partly removed[3]

(iii) employ a tuning section[4]

(iv) adjust the thickness of the facet coating for each laser.[5]

These schemes all complicate the fabrication, and in the following we therefore examine the mode selectivity of devices with cleaved facets in order to assess how serious the problem is.

*Analysis and results:* The strength of the distributed feedback depends on the product of the coupling coefficient $\kappa$ and the length of the grating $L$. A good second-order grating has $\kappa \sim 100\ \mathrm{cm}^{-1}$, and for $L \sim 300\ \mu m$ this gives $\kappa L \sim 3$. Higher values can be obtained for larger values of $L$. In theory a higher value of $\kappa$ can be obtained by using a first-order grating, but this requires a more complicated processing technology. An analysis of various published results has shown that the reported first-order gratings do not have higher values of $\kappa$ than those obtained by good second-order gratings.

We consider DFB lasers with one or two cleaved facets. In order to simplify the analysis we assume the maximum gain to occur close to the Bragg wavelength, and hence the spectral properties are mainly determined by the threshold gain of the first few modes on each side of the stopband. For given magnitudes and phases of the facet reflection coefficients we find, using the formulas from Reference 6, the difference in threshold gain for the two modes with the lowest thresholds. This calculation is performed for a number of facet phases and we define the 'yield' as the percentage of cases where the difference in threshold gain exceeds a given value. (A possible difference in the radiation loss[7] for the various modes is neglected.)

An analysis along the same lines was reported in Reference 8. In Reference 8 the mode selectivity for DFB lasers with one cleaved facet was given in terms of the threshold currents. For the case of two cleaved facets, results for the variation of the threshold current for the dominating mode due to various facet phases were given. A systematic investigation of the mode selectivity in terms of the difference in threshold gain has not been reported for this case, however.

For the case with one nonreflecting mirror, 32 different values for the phase of the reflecting mirror were examined. In the case of two reflecting mirrors 16 values of each phase were considered. Owing to the symmetry properties of the problem,[6] only 73 different combinations need to be considered. Using multiples of $\pi/8$ as the values for the phases we may slightly overestimate the number of extreme cases (i.e. those with either very high or very low threshold difference). If instead the phases were taken to be random variables we would, of course, get smooth curves if a sufficient number of cases were examined.

The results are shown in Figs. 1 and 2, which show the 'yield' as a function of $\Delta\alpha L$, which is the required difference in threshold gain multiplied by the length; the results are shown for three values of the product $\kappa L$. Note that $\Delta\alpha$ refers to the field and not to the intensity.

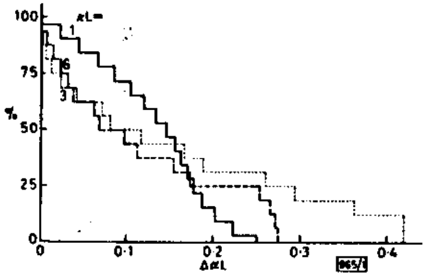

Fig. 1 *Yield of single-mode lasers, defined as the percentage of cases with a threshold difference ΔαL above the value given on the abscissa*

Calculated for lasers with one reflecting and one nonreflecting mirror, using three different values for the product of the coupling coefficient and the length

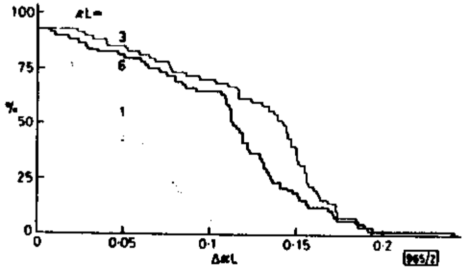

Fig. 2 *As Fig. 1, but for lasers with two reflecting mirrors*

For a laser with a length of 250 μm the value $\Delta\alpha L = 0 \cdot 1$ corresponds to a difference in the intensity threshold gain of $8\ \mathrm{cm}^{-1}$. Based on a simple two-mode rate-equation model[9] this should give a 100:1 ratio of the intensity of the dominating mode to the intensity of the next mode. In this calculation a high-speed modulation and a bias below threshold is assumed. The yield results for $\Delta\alpha L = 0 \cdot 1$ are summarised in Table 1.

A further analysis of the case of one cleaved facet shows that for a region of $\kappa L$ values around 1·5 very low selectivity is obtained. For $\kappa L \lesssim 1$ a good selectivity is obtained, but at the expense of a higher threshold current.

**Table 1**

| Value of $\kappa L$ | 1 | 3 | 6 |
|---|---|---|---|
| Yield with 1 cleaved facet | 72% | 50% | 44% |
| Yield with 2 cleaved facets | 7% | 70% | 65% |

The mode selectivity arises from the interference of the discrete facet reflections and the distributed reflections from the grating. Maximum interference, and hence maximum selectivity, occurs when the two contributions are of comparable strength. Since a Fabry-Perot laser with power reflectivities near 0·3 and a DFB laser with two nonreflecting mirrors have the same threshold gain for $\kappa L \sim 3 \cdot 2$, we expect good selectivity for $\kappa L$ products near this value.

Experimental results for the spectral properties of DFB lasers were reported in Reference 10. A yield for single-mode lasers of 66% was reported; some of the 'failed' lasers, however, had other problems. The value of $\kappa L$ was not given.

We see that a DFB laser with two cleaved mirrors gives a good yield of single-mode lasers for moderate values of $\kappa L$ (these can be obtained using a second-order grating). For low values of $\kappa L$ the yield is significantly improved if the reflectivity for one of the mirrors is reduced.

Finally, we note that the output power distribution between the two facets depends on the facet phases and differs from mode to mode.[8]

The author is grateful to one of the referees for helpful comments.

J. BUUS

*Plessey Research (Caswell) Limited*
*Allen Clark Research Centre*
*Caswell, Towcester, Northants NN12 8EQ, England*

*17th December 1984*

## References

1 UTAKA, K., AKIBA, S., SAKAI, K., and MATSUSHIMA, Y.: 'Analysis of quarter-wave-shifted DFB laser', *Electron. Lett.*, 1984, **20**, pp. 326-327

2 SEKARTEDJO, K., EDA, N., FURUYA, K., SUEMATSU, Y., KOYAMA, F., and TANBUN-EK, T.: '1·5 μm phase-shifted DFB lasers for single-mode operation', *ibid.*, 1984, **20**, pp. 80-81

3 KOYAMA, F., SUEMATSU, Y., KOJIMA, K., and FURUYA, K.: '1·5 μm phase-adjusted active distributed reflector laser for complete dynamic single-mode operation', *ibid.*, 1984, **20**, pp. 391-393

4 KITAMURA, M., YAMAGUCHI, M., EMURA, K., MITO, I., and KOBAYASHI, K.: 'Lasing mode and spectral linewidth control by phase tunable DFB-DC-PBH LD'. Ninth IEEE international semiconductor laser conference, Rio de Janeiro, August 1984, Paper A5

5 ITAYA, Y., WAKITA, K., MOTOSUGI, G., and IKEGAMI, T.: 'Phase control by coating in 1·5 μm DFB lasers', *ibid.*, paper E1

6 STREIFER, W., BURNHAM, R. D., and SCIFRES, D. R.: 'Effect of external reflectors on longitudinal modes of distributed feedback lasers', *IEEE J. Quantum Electron.*, 1975, **QE-11**, pp. 154-161

7 STREIFER, W., SCIFRES, D. R., and BURNHAM, R. D.: 'Coupled wave analysis of DFB and DBR lasers', *ibid.*, 1977, **QE-13**, pp. 134-141

8 UTAKA, K., AKIBA, S., SASAKI, K., and MATSUSHIMA, Y.: 'Effect of mirror facets on lasing characteristics of distributed feedback InGaAsP/InP laser diodes at 1·5 μm range', *ibid.*, 1984, **QE-20**, pp. 236-245

9 KOYAMA, F., SUEMATSU, Y., KOMORI, K., and TAKAHASHI, S.: 'Dynamic single mode condition for semiconductor lasers'. Tenth European conference on optical communications, Stuttgart, September 1984, Paper 5B3

10 KITAMURA, M., YAMAGUCHI, M., MURATA, S., MITO, I., and KOBAYASHI, K.: 'High-performance single-longitudinal-mode operation of InGaAsP/InP DFB-DC-PBH LDs', *IEEE J. Lightwave Technol.*, 1984, **LT-2**, pp. 363-369

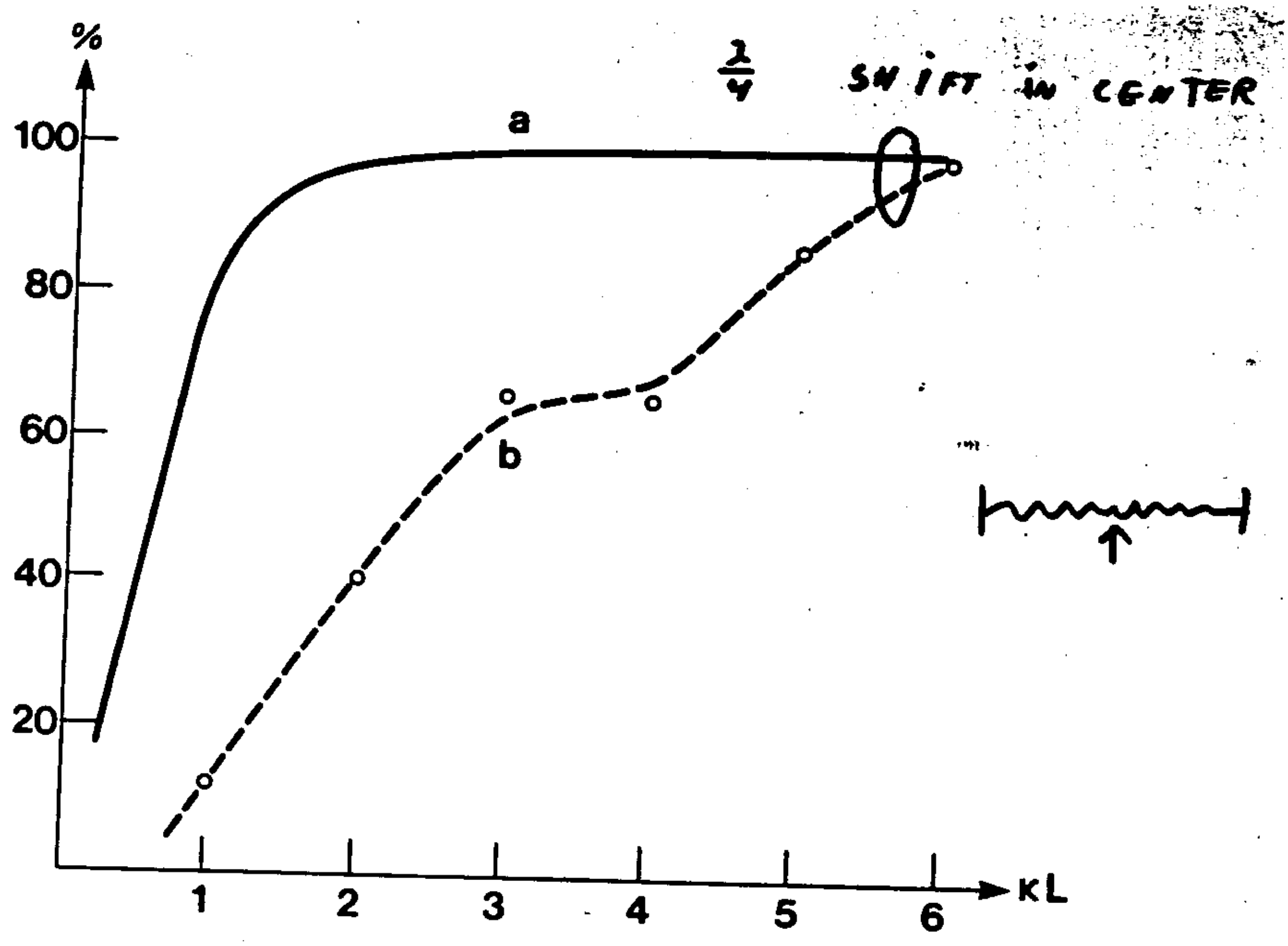

$\frac{\lambda}{4}$ SHIFT IN CENTER

49

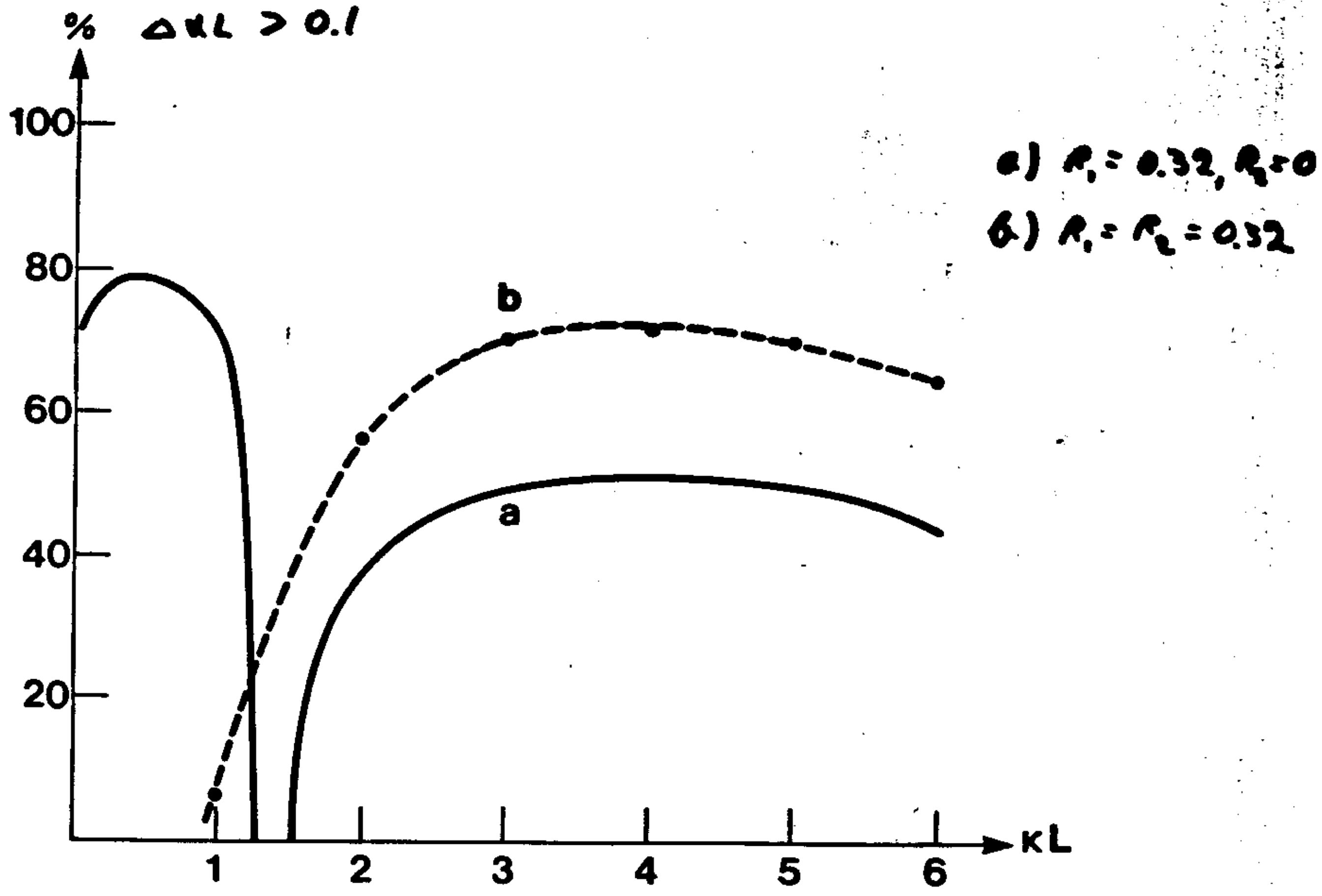

$\Delta \kappa L > 0.1$

a) $R_1 = 0.32, R_2 = 0$

b) $R_1 = R_2 = 0.32$

50

# Buried Ridge DFB Laser

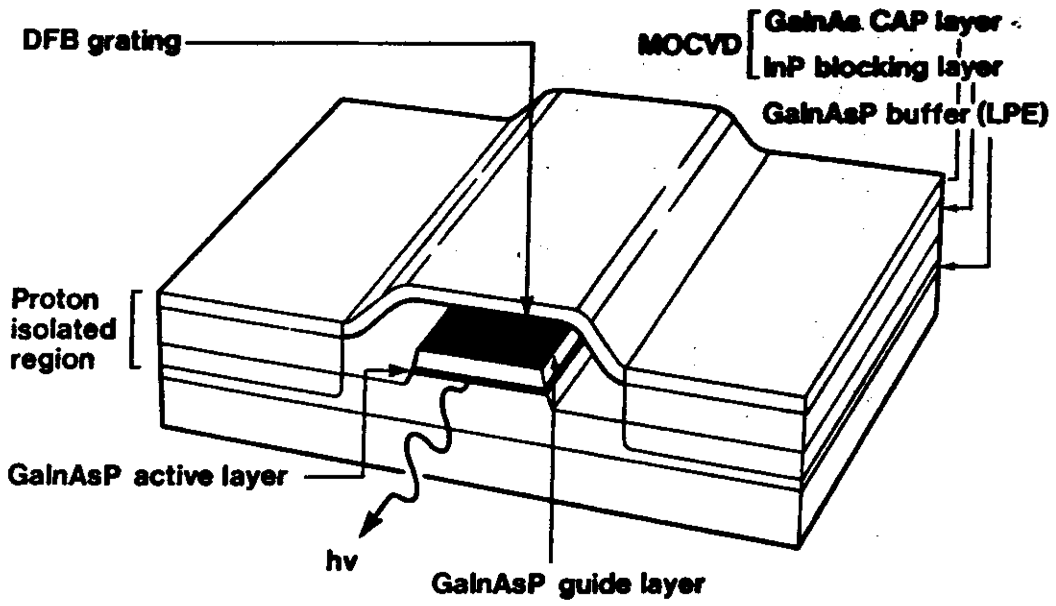

PLESSEY RESEARCH CASWELL

51

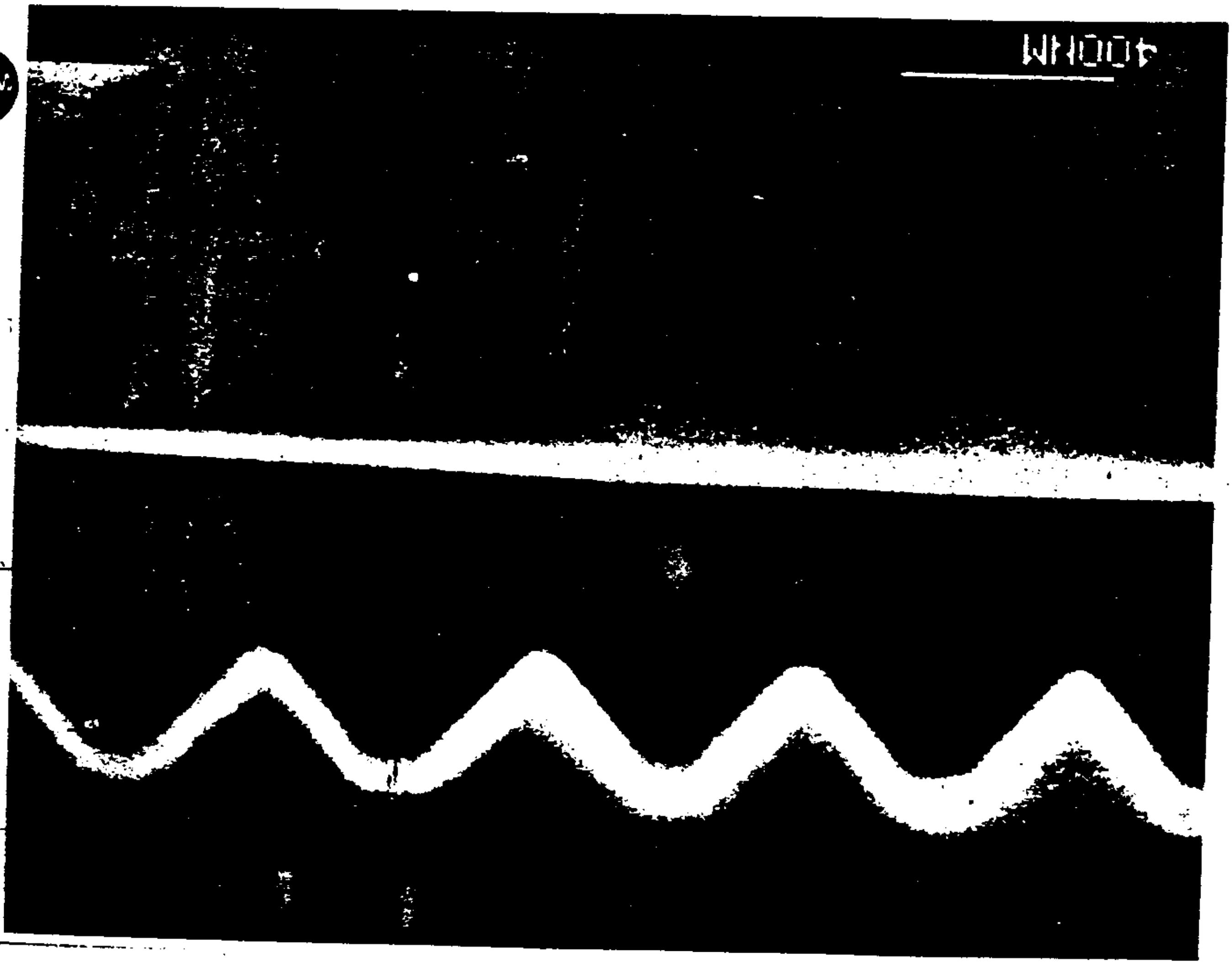

1.55µm

1.3µm

52

DEVICE BATCH/NUMBER
G7AB/ 9/ CHIP

DATE 26/8/86

TEMPERATURE 19C

DETECTOR G474

DISTRIBUTED FEEDBACK LASER
THRESHOLD Ith = 18.9 mA

PULSED AT 5mW=038

Reject

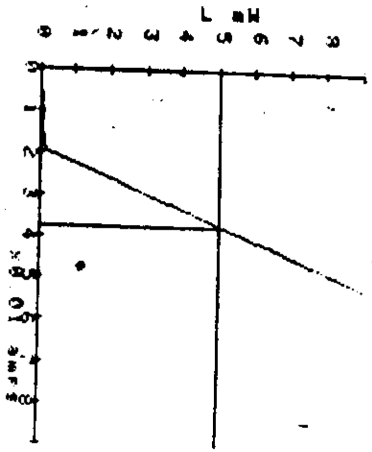

PULSED SLOPE

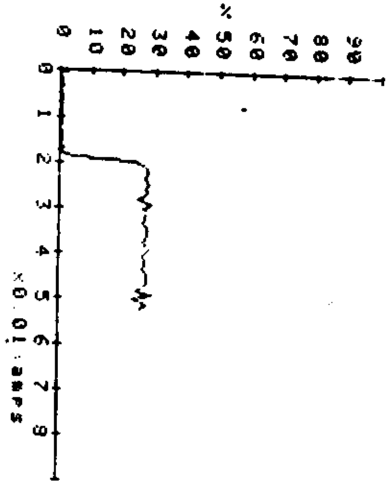

Sub

DEVICE BATCH/NUMBER
G7AB 9 CHIP

DATE 26/8/86

TEMPERATURE 19C

DETECTOR G474

DISTRIBUTED FEEDBACK LASER
THRESHOLD Ith = 18.9 mA

PULSED AT 5mW=068

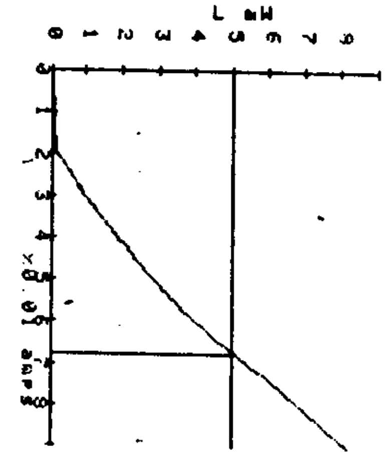

PULSED SLOPE

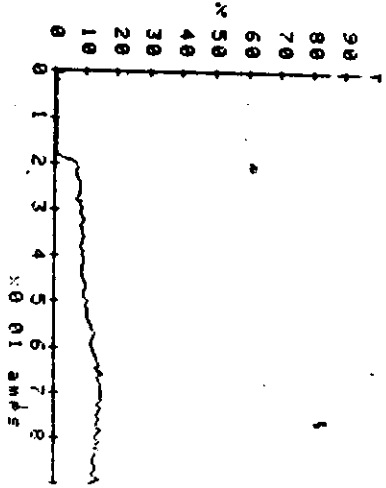

# WAVELENGTH "CHIRPS" UNDER MODULATION

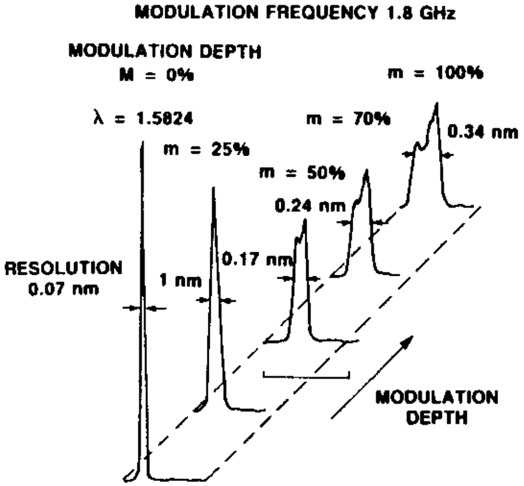

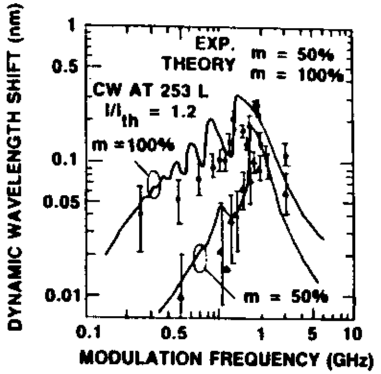

Introduces dispersion penalty at multigigabit data rates
and maximum distances (50–200 km)

Koyama et al. (1983

# LASING SPECTRAM CHANGE under DIRECT MODURATION

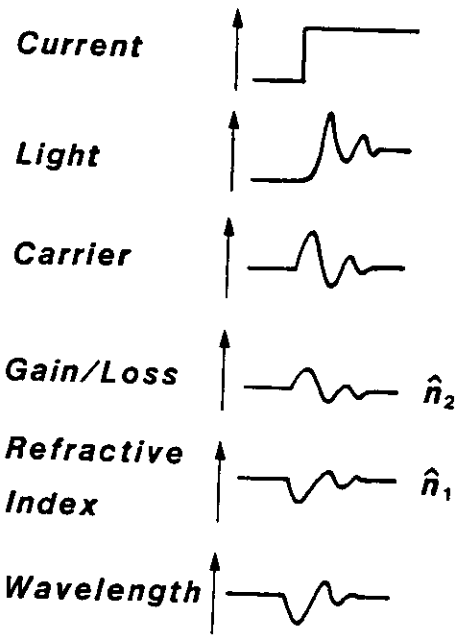

- In INTENSITY MODULATION:

Spectrum Broadening "CHIRPING"

→ Pulse Distortion due to Dispersion

"CHIRPING LIMIT"

- In FM MODULATION:

Modulation Sensitivity $\Delta\lambda m/\Delta Im$

$$\alpha = \frac{\text{change of real part of } \hat{n} \text{ with respect to change of carrier density}}{\text{change of imaginal part of } \hat{n} \text{ with respect to change of carrier density}}$$

(Linewidth Enhancement Factor : -4~-7)

55 IKEGAMI - OFC MINITUTORIAL
NTT

## CHIRPING LIMIT

$\sqrt{\text{Fiber Length due to Chirping Limit}}$ × Bit Rate =

K ( |α| ,Dispersion, Power Penalty)

4.5, 20ps / nm / km, -1dB 20.7 Gb / s $\sqrt{km}$

(T.L.Koch et al, F. Koyama et al)

Exp. : 4Gb/s × 103km (A.H.Gnauk et al)

COUNTERMEASURE :

1) EQUALIZATION (Not Random …) Could be but …
2) MULTI-TERMINAL DFB LD
3) MQW LD (N.K.Dutta et al)
4) SMOOTH DIRECT MODULATION
5) BIAS CURRENT ABOVE THE THRESHOLD
6) EXTERNAL MODULATION (Give up Direct Mod.)

IKEGAMI - OFC MINITUTORIAL
NTT

56

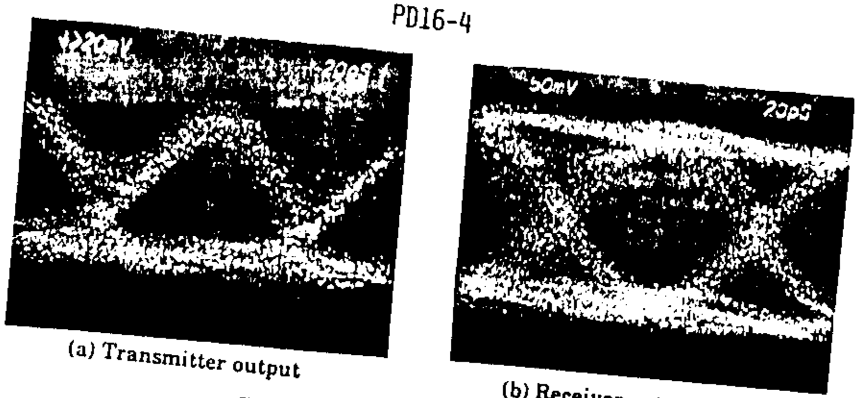

(a) Transmitter output

(b) Receiver output (80km)

Fig.2 10Gb/s Signal waveforms

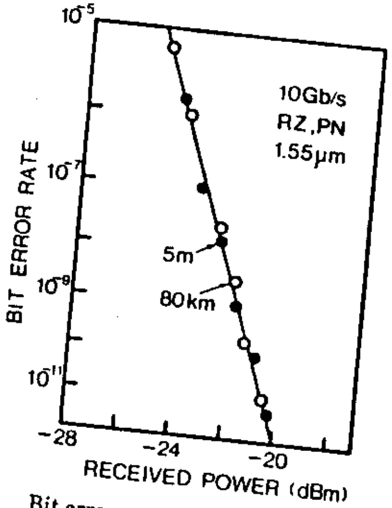

Fig.3 Bit error rate vs. average received power characteristics

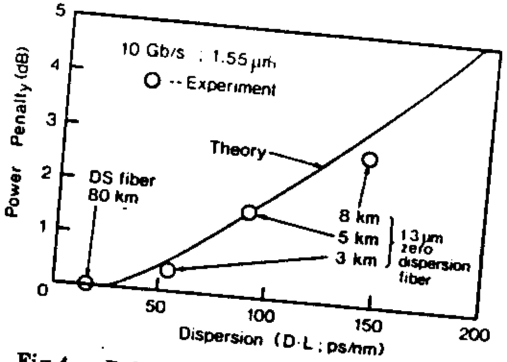

Fig.4 Relation between power penalty and total dispersion

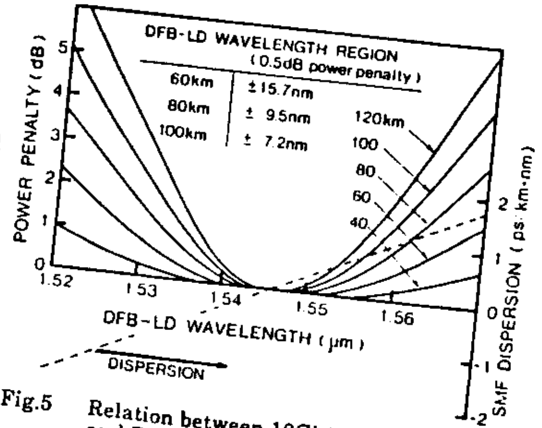

Fig.5 Relation between 10Gb/s power penalty and DFB-LD wavelength

FUJITA et al
OFC'88 NEC.

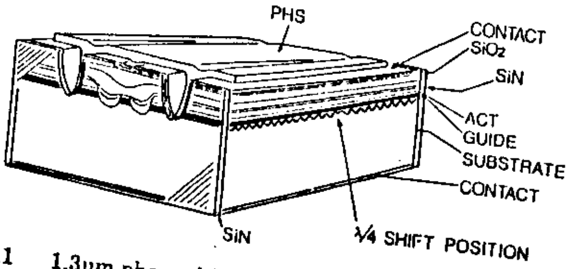

Fig.1 1.3μm phase shifted DFB-DC-PBH LD structure.

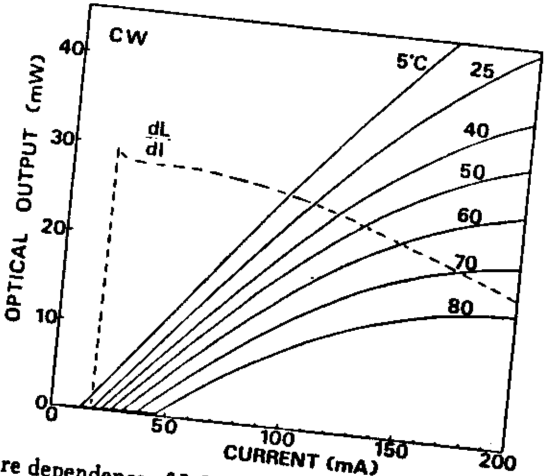

Fig.2 Temperature dependence of L-I curves up to high power level in phase shifted DFB-DC-PBH LD.

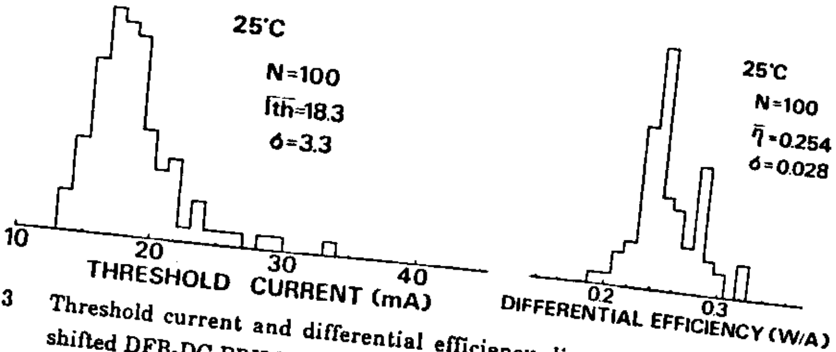

Fig.3 Threshold current and differential efficiency distribution of 1.3μm phase shifted DFB-DC-PBH LD.

Mito et al OFC'88 NEC

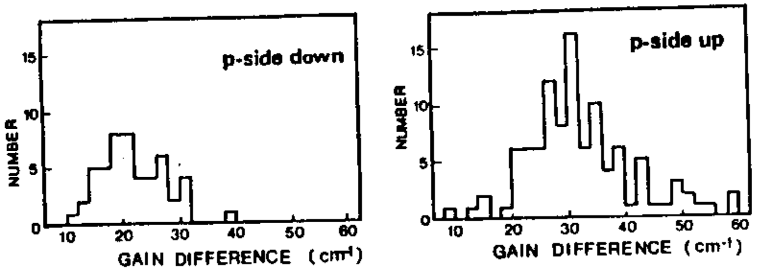

**Fig.4** Gain difference distribution between main mode and sub mode measured with the spectra at 0.9xIth bias current level.

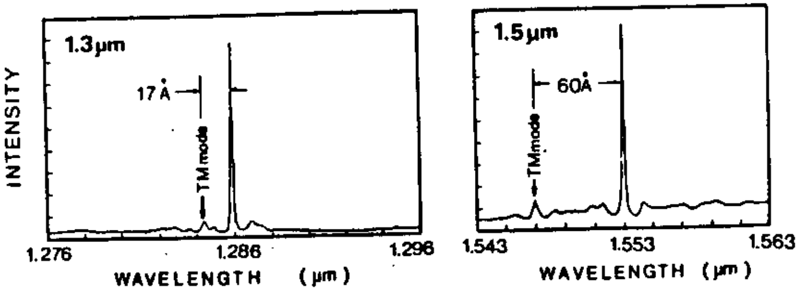

**Fig.5** Spectra at 0.9xIth bias current for 1.3μm and 1.5μm wavelength phase shifted DFB-DC-PBH LD.

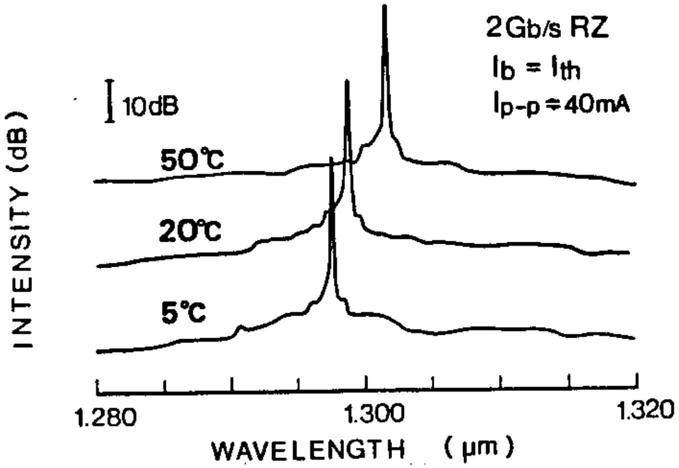

**Fig.6** Temperature dependence of the spectrum measured under 2Gb/s RZ pulse modulation condition. Ib=Ith. Ip-p=40mA.

59

Mito et al
OFC '98 (NEC)

# QUANTUM WELL LD

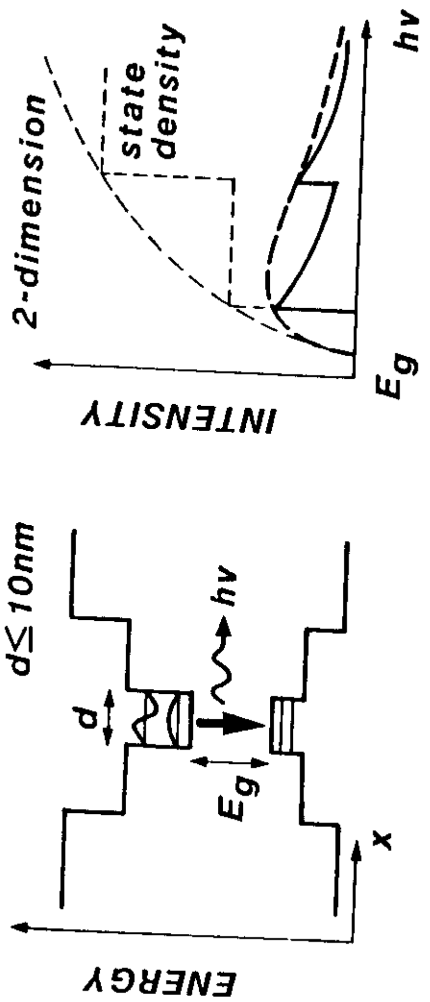

1. Large Gain (Low $J_{th}$)
2. Large Differential Efficiency $\Delta\eta_{ex}$
3. Reduced Temperature Sensitivity
4. Visible LD

→ zero dimension : "Solid-State Laser"

IKEGAMI - OFC MINITUTORIAL
NTT

60

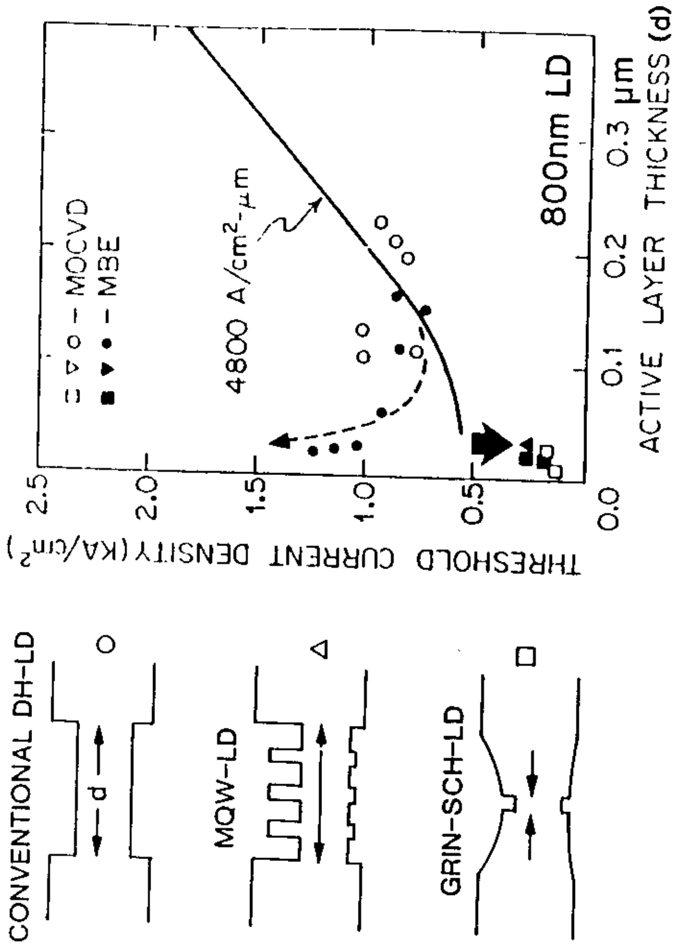

THINNER ACTIVE LAYER → QUANTUM EFFECT

IKEGAMI -OFC MINITUTORIAL
NTT
61

# Requirements of a Coherent Optical Heterodyne System

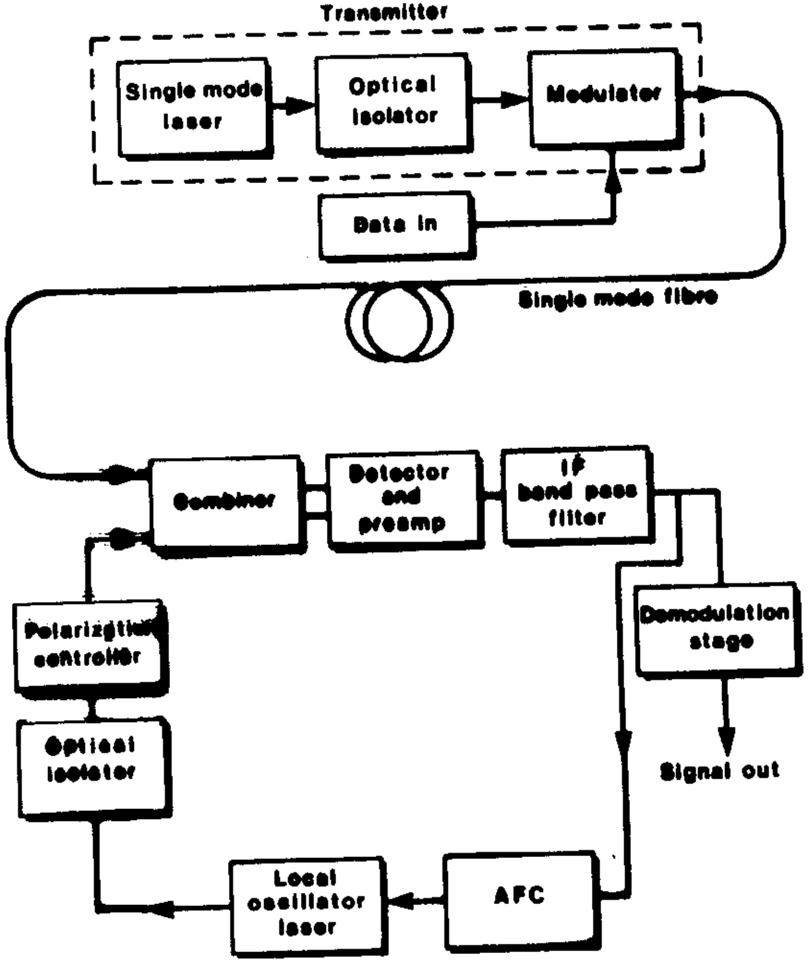

# Importance of Narrow Linewidths

| | | | | If B = 140Mbit/s |
|---|---|---|---|---|
| ASK | HET | Δv/B | ~9% | ~12.6MHz |
| PSK | HET | Δv/B | ~9% | ~12.6MHz |
| PSK | HET | Δv/B | ~0.1% | ~140kHz |
| PSK | HOM | Δv/B | ~0.01% | ~14kHz |

Δv= 3dB laser linewidths and B = transmission data rate
Figures depend on demodulation schemes but give reasonable guidelines

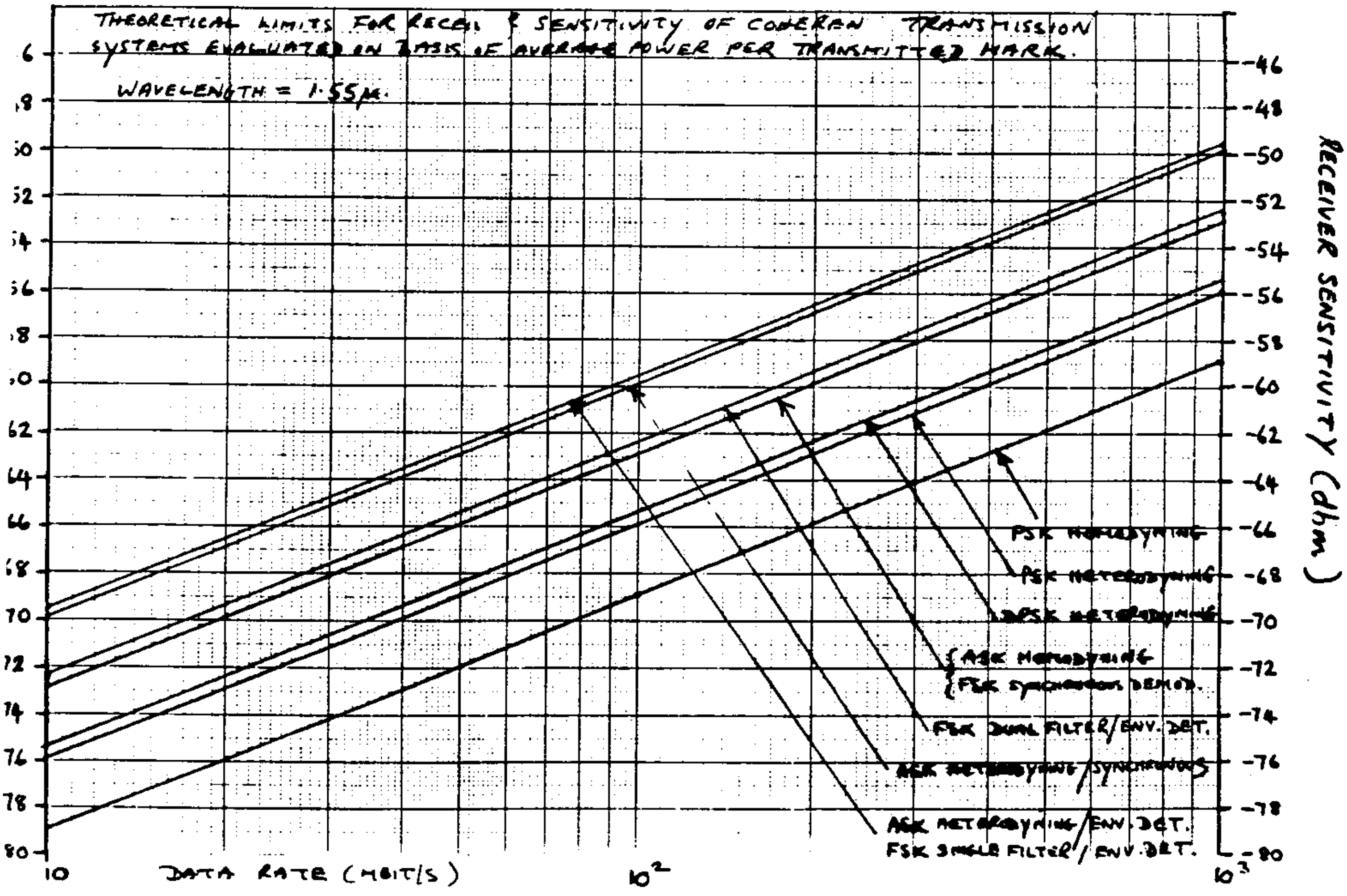

## Milestones in the Development of Coherent Optical Communications

| | | | |
|---|---|---|---|
| ● | 1980 | First Demonstration of Optical FSK Heterodyne Detection | NTT |
| ● | 1982 | First System Experiment; FSK at 100Mb/s | NTT |
| ● | 1983 | First Demonstration of an Optical Phase Locked Loop for Homodyning | Glasgow University |
| ● | 1984 | First System Experiment Demonstrating PSK Homodyne Detection with OPLL; 140Mb/s | BT |
| ● | 1984 | First System Experiment Using DFB Lasers as Transmitter and Local Oscillator | NEC |
| ● | 1986 | FSK Transmission Experiment over 301 Km Fibre | NEC |
| ● | 1986 | Ten Channel Coherent Subscriberline Experiment | HHI |
| ● | 1987 | 2Gb/s Transmission Experiment over 170 Km Fibre | AT & T |

## ADVANTAGES

- Higher receiver sensitivity
  - 10 to 20 db better than IM/DD
- Frequency selectivity of heterodyne receive
  - use of Optical Frequency Division Multiplex (OFDM). Channel spacing ~ GHz
    'Optical Radio" concept.

## APPLICATIONS

- Trunk – longer unrepeatered links
  - upgrade of existing installed links to higher data rates

- Local BroadBand – greater use of passive signal distribution
  - multichannel broadcast capability

# Cavity Schemes Studied

- Simple DFB
- DFB + graded index lens cavity
- DFB + fibre cavity
- Fabry Perot laser + fibre grating

---

# Delayed Self Heterodyne Technique

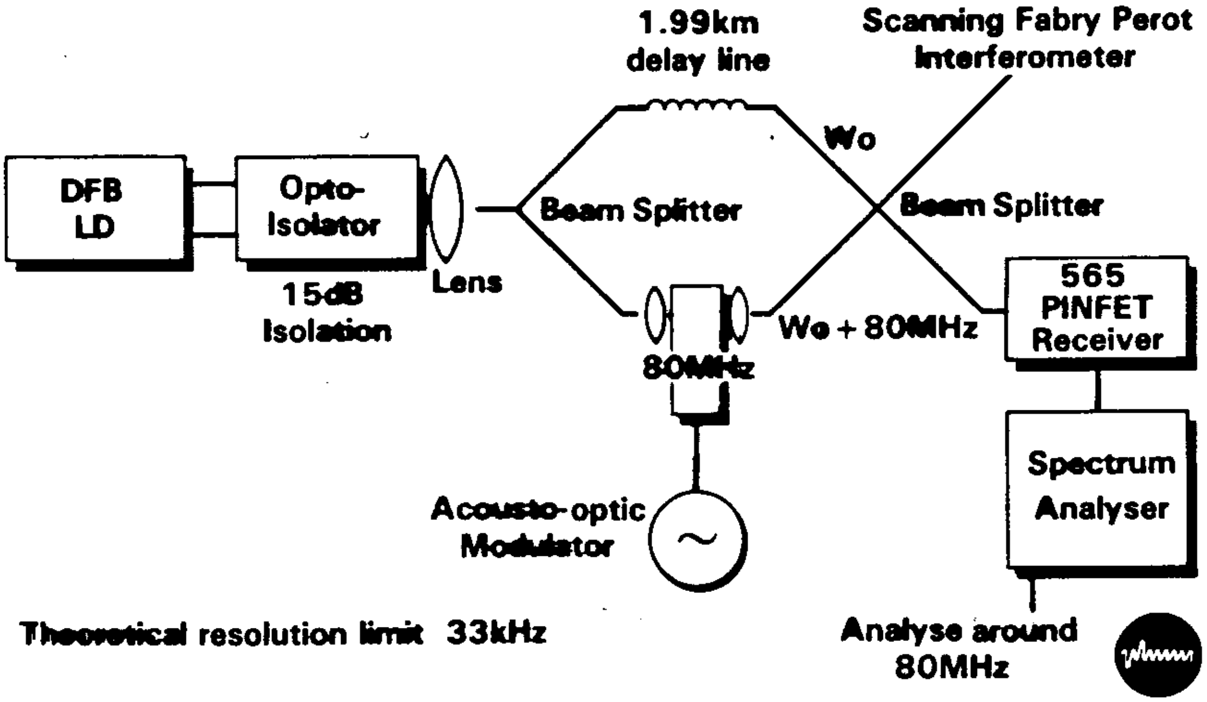

Theoretical resolution limit 33kHz

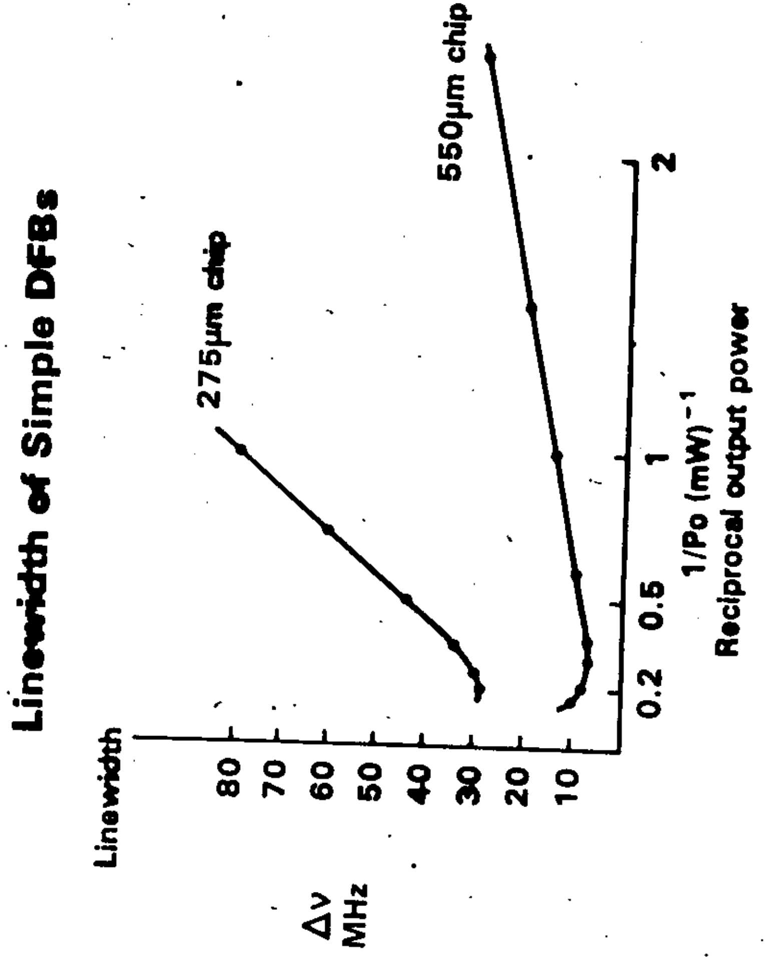

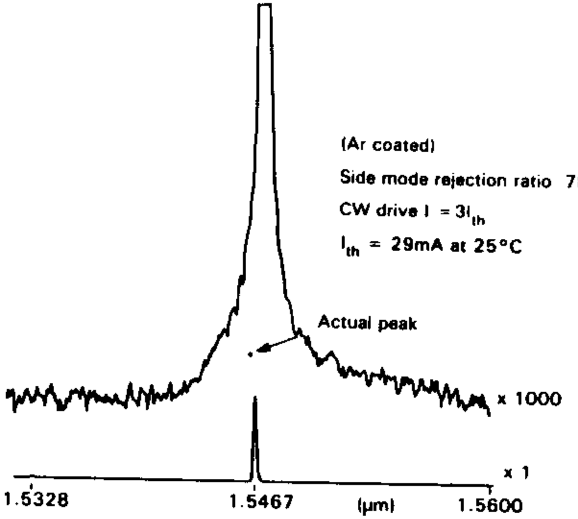

Fig. 6. SPECTRAL PLOT FOR A PLESSEY DFB LASER

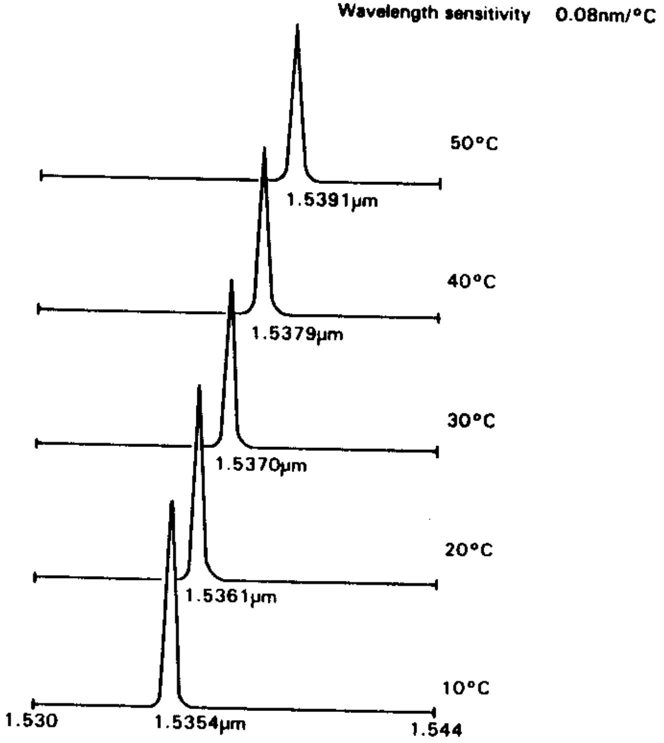

Fig. 7. WAVELENGTH SHIFT OF DFB LASER MODE WITH TEMPERATURE, MEASURED UNDER CONDITIONS OF CONSTANT OUTPUT POWER

# Delayed Self Heterodyne Linewidth Measurement of 550μm Cavity DFB at 3.4mW Output Power

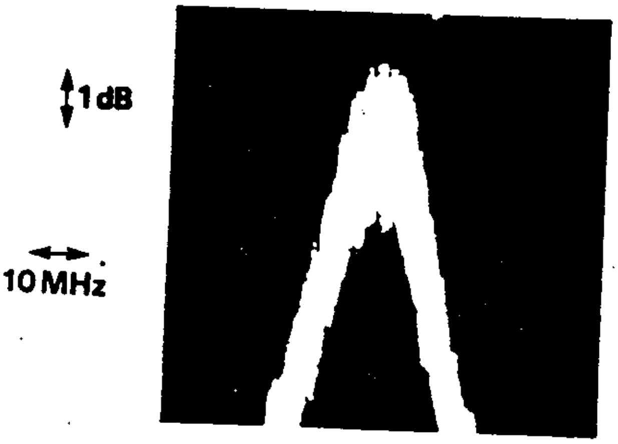

# FM Response of Solitary DFB and Graded Index Rod Lens External Cavity DFB Lasers

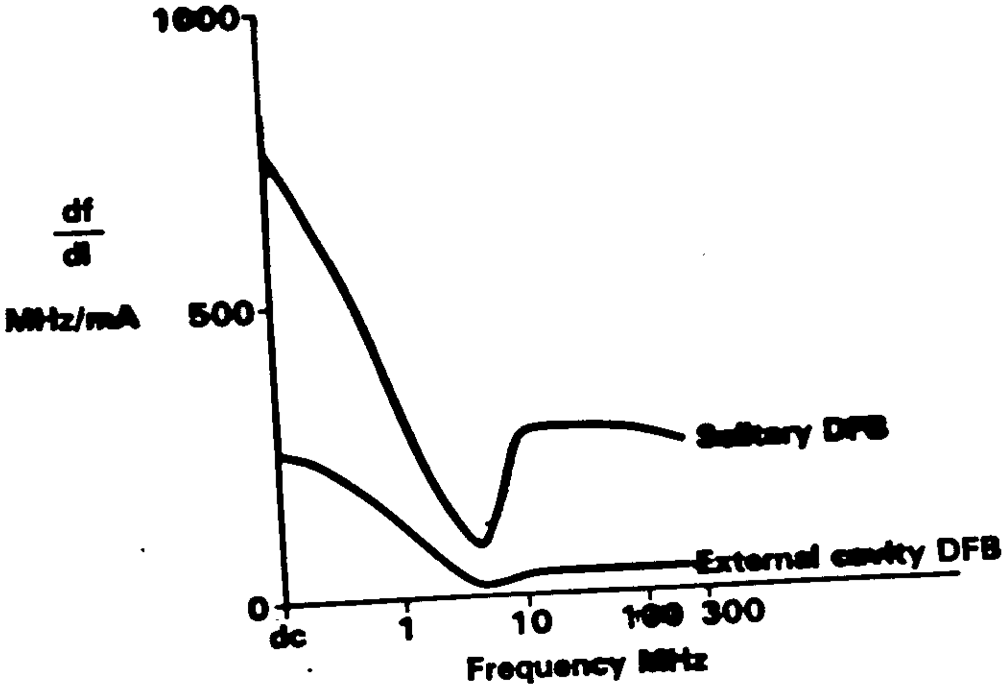

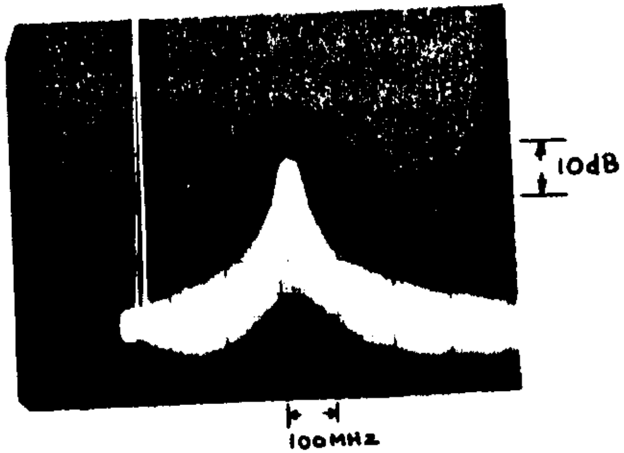

M1632

#15 104.1mA
3·98V

#95 49·7mA
3·82V

$\Delta\nu_{IF} \sim 30\,MHz$

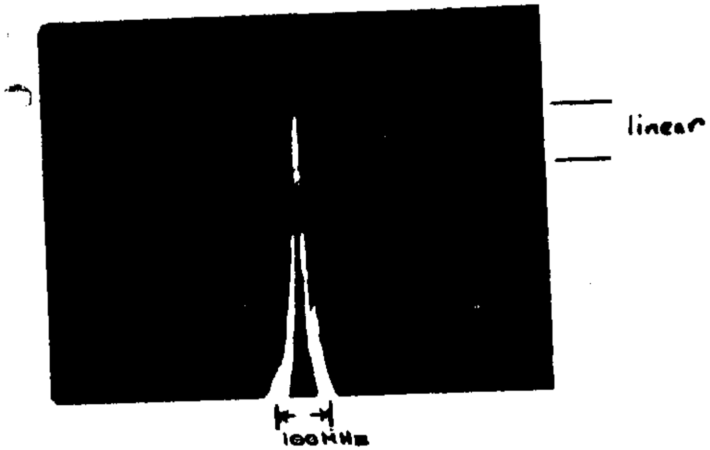

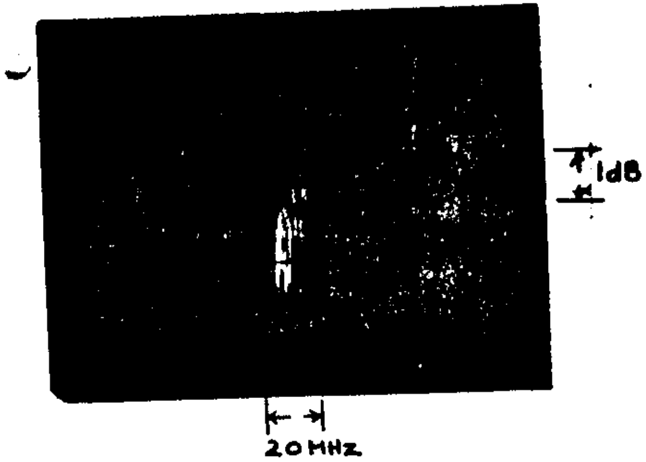

## EXTERNAL CAVITY LASERS

- 1·55μm DFB with:
  - external fibre cavity
  - GRIN lens external cavity

aiming for linewidth of ~ 1 MHz

- 1·55μm Fabry-Perot laser with external fibre grating

Single mode behaviour with linewidth down to 3KHz achieved.

## EXTERNAL CAVITY SEMICONDUCTOR LASER

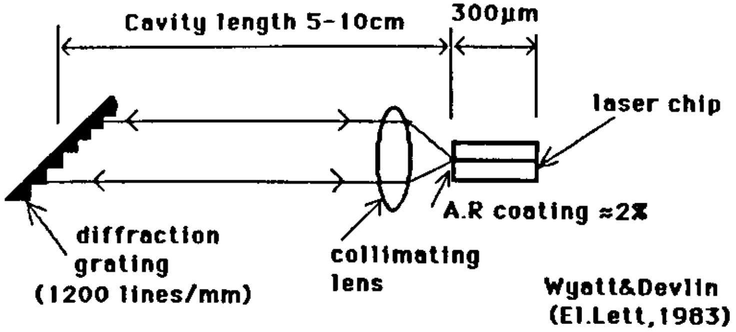

## MEASURED SPECTRUM OF LEC LASER

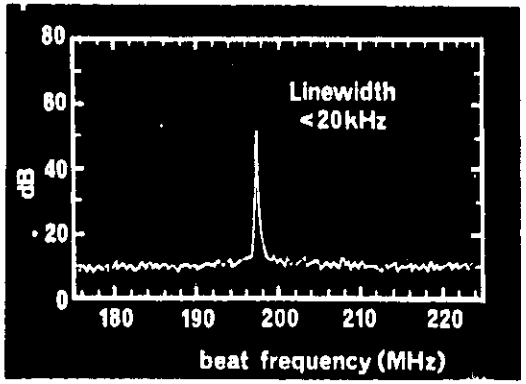

## CHARACTERISTICS OF LEC LASER

- Linewidth : Short term (millisecond) ≈ kHz
  : Medium term (seconds) ≈ MHz
  : Long term (hours) ≈ 100MHz
- Tuning range by rotating grating ≈ 10,000GHz optical bench components
  ≈ 100GHz packaged laser

(For packaged LEC laser see Matthews et-al, Electron. lett, pp113-115,1985.)

## IF SIGNAL OF 2 DFBs

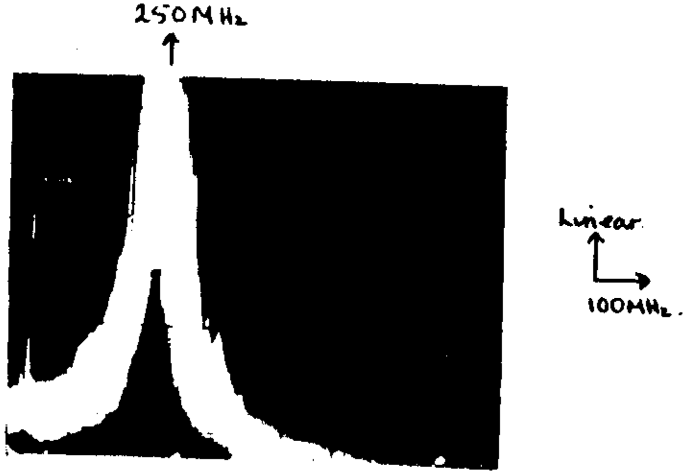

DFB M1632 13 * 15

Under identical drive conditions ~ 1½ nm apart.

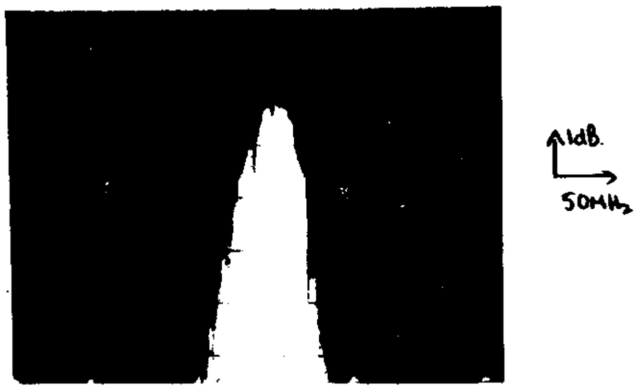

3dB linewidth of IF signal about 100MHz.

Frequency stability ~ 100MHz for short periods (~15minutes).

~ 400MHz for an afternoon.

Signal very sensitive to mechanical/reflection disturbance.

## Schematic Arrangement of DFB with Taper Lensed Fibre External Cavity

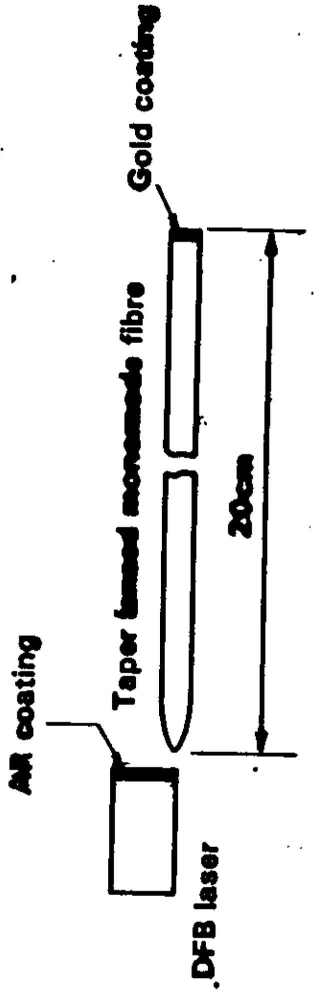

# Experimental Arrangement for Assembly of DFB Lasers with External Fibre Cavities

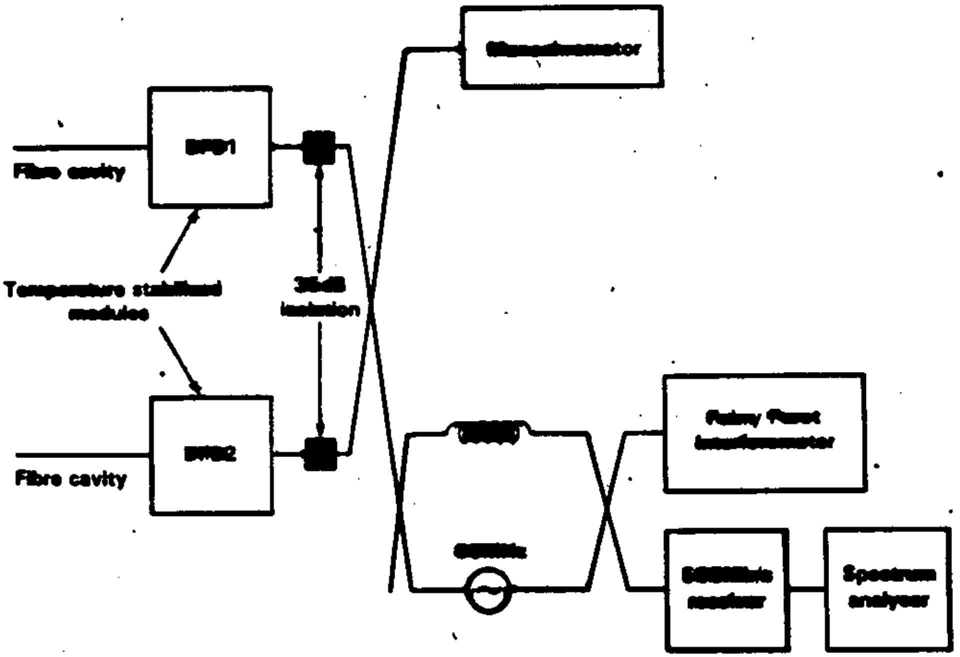

---

# DFBs with Taper Lensed Fibre External Cavities

a) Linewidth of one device measured by delayed self heterodyne method ($\Delta\nu$ 200KHz)
b) Beat spectrum of two devices −3dB width 2.5MHz due to acoustic disturbance

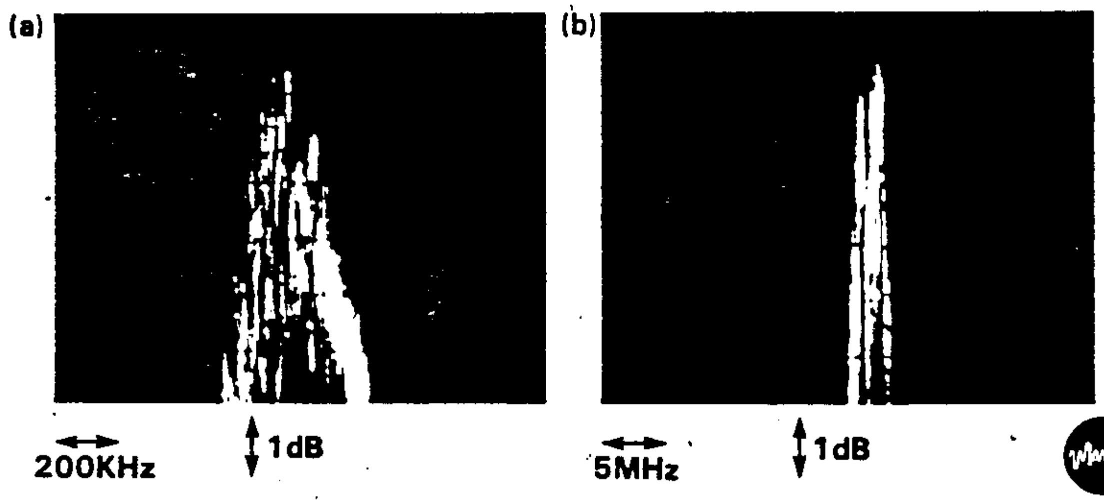

# Schematic Arrangement of External Cavity DFB Laser

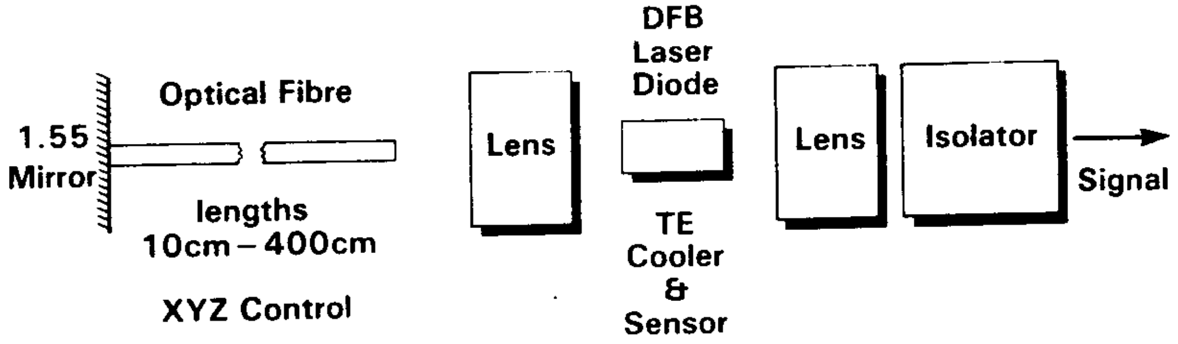

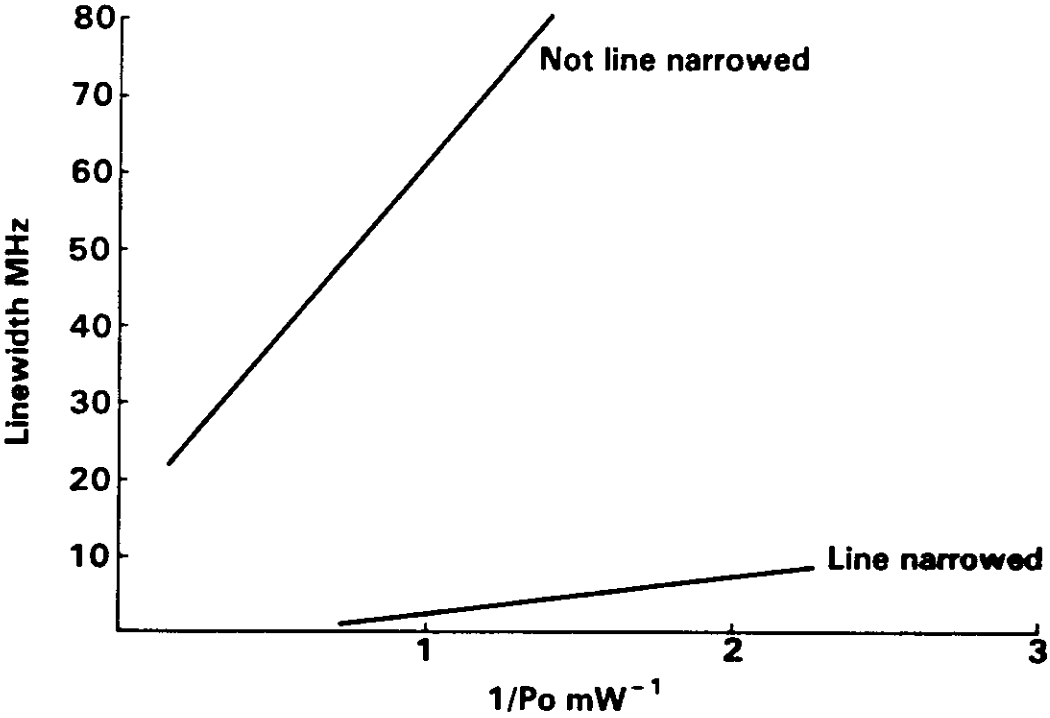

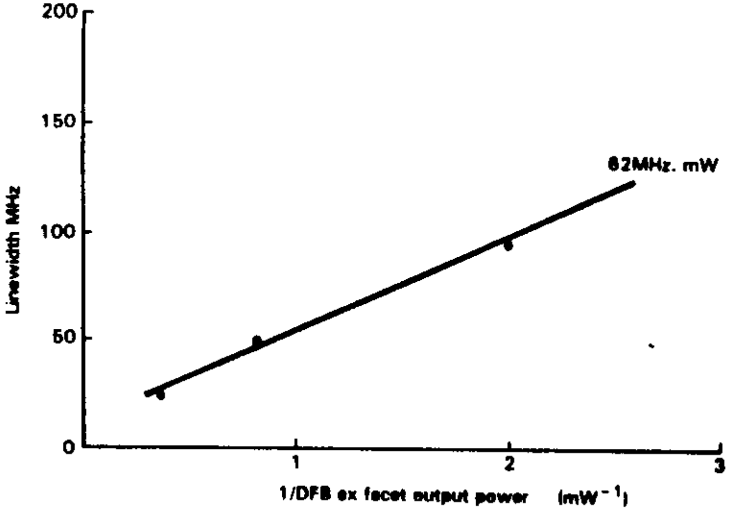

Fig. 8. LINEWIDTH VERSUS RECIPROCAL OUTPUT POWER FOR A STANDARD LENGTH (275μm) DFB LASER. THE LINEWIDTH POWER PRODUCT OF 60MHz. mW IS FAIRLY TYPICAL OF RESULTS OBTAINED FOR THIS TYPE OF LASER.

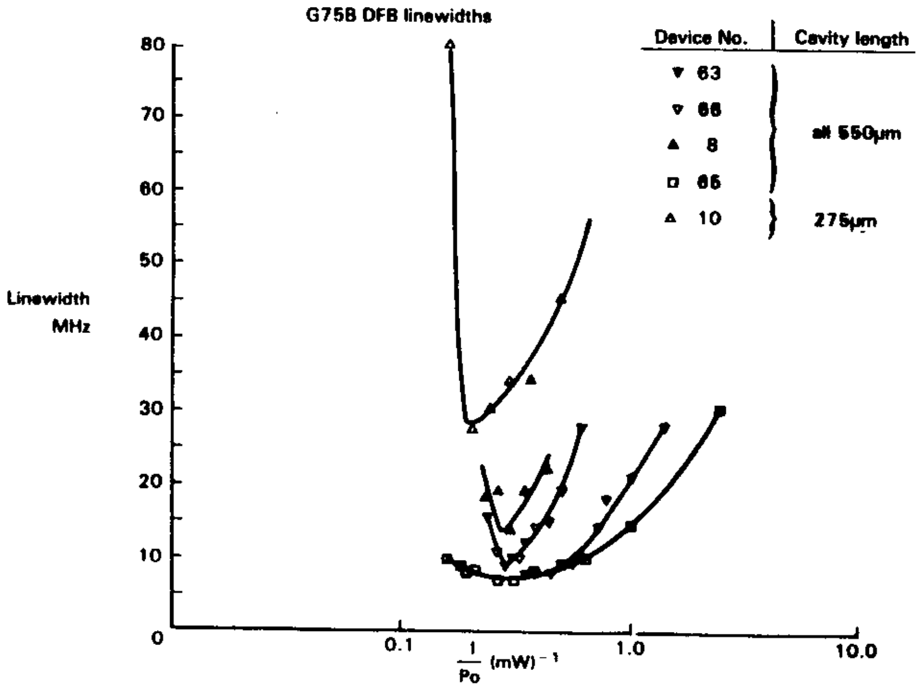

Fig. 9. MEASURED LINEWIDTH VERSUS RECIPROCAL OUTPUT POWER FOR BOTH LONG AND STANDARD CHIP LENGTH DFB LASER DIODES

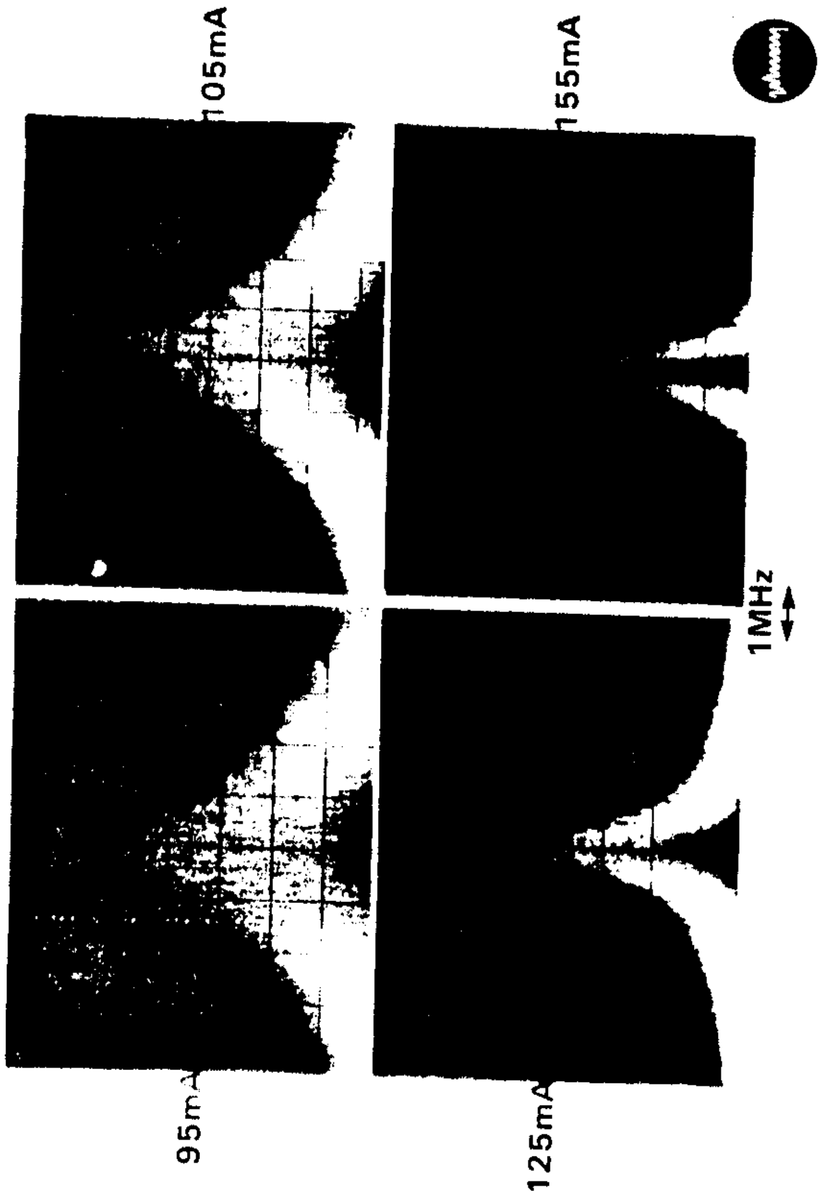

DFB laser, 20cm external/fibre cavity.

# Spectrum of Line Narrowed DFB Laser

Linewidth 500kHz

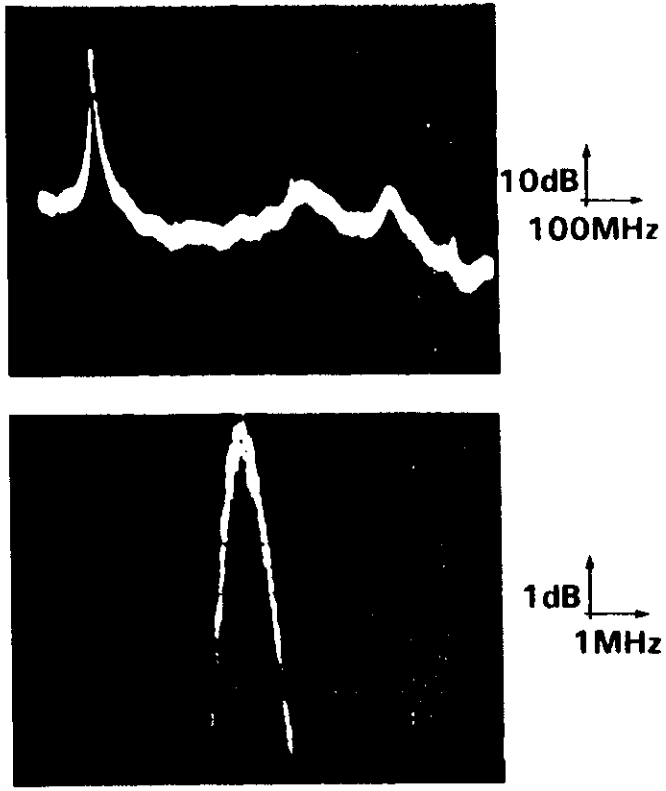

# Schematic Arrangement of DFB with Graded Index Rod Lens External Cavity

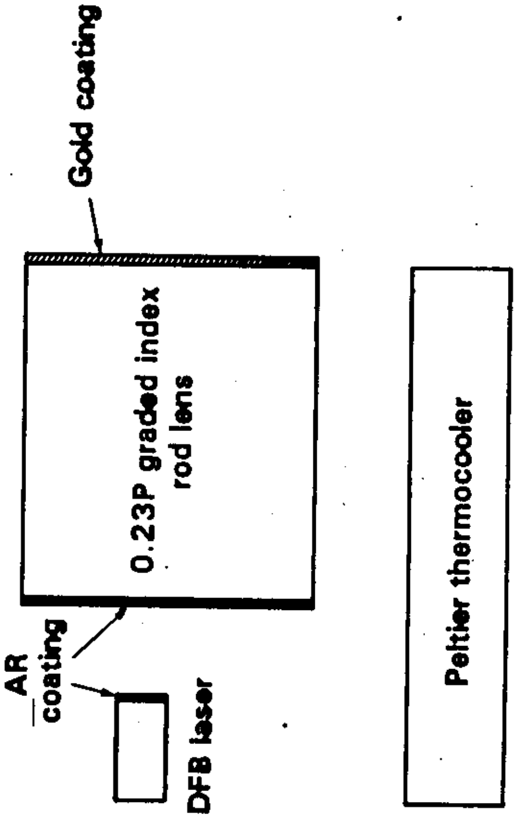

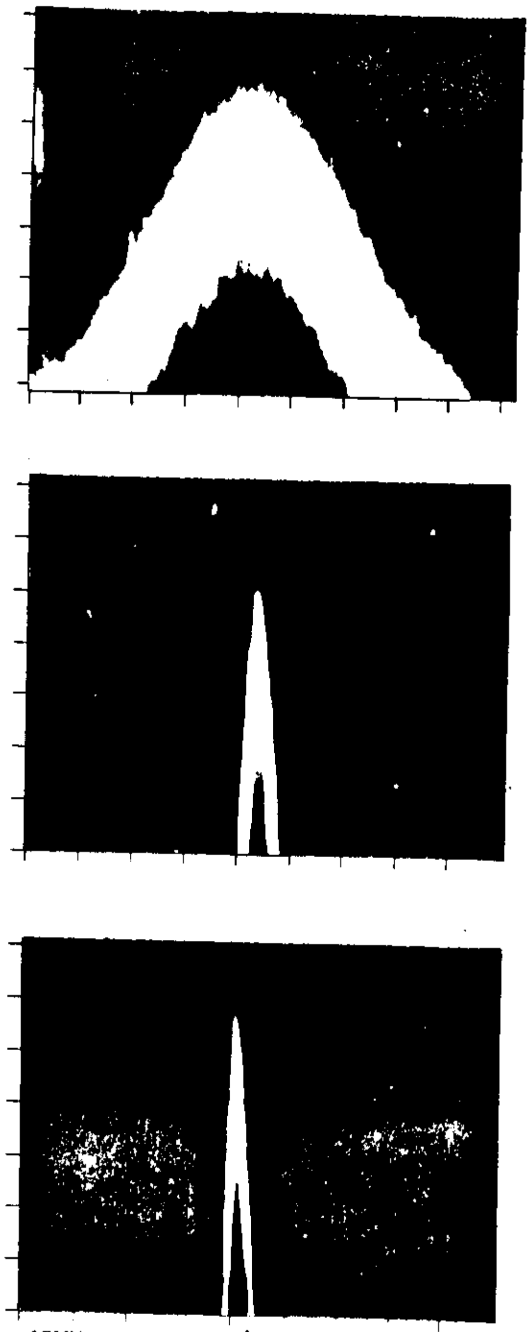

(a) Solitary laser

(b) Cavity in optimum position

(c) After assembly and fixing of cavity

10MHz per div horizontal
1dB per div vertical

14. MEASURED LINEWIDTH OF A DFB LASER BEFORE AND AFTER ASSEMBLY WITH A GRIN LENS EXTERNAL CAVITY

---

## Delayed Self Heterodyne Linewidth Measurement of a DFB Laser

(a) Without an external cavity and (b) With a GRIN lens external cavity fixed in position.

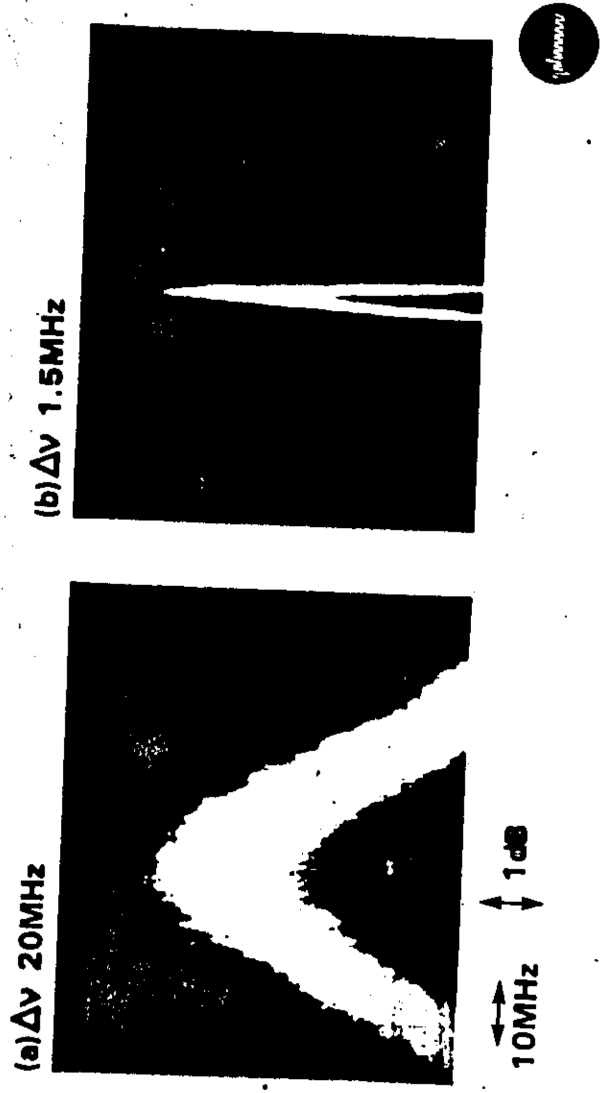

## Delayed Self Heterodyne Linewidth Measurement of GRIN Cavity DFB Laser

(a) Unmodulated, (b) Directly modulated 4mA @ 50MHz

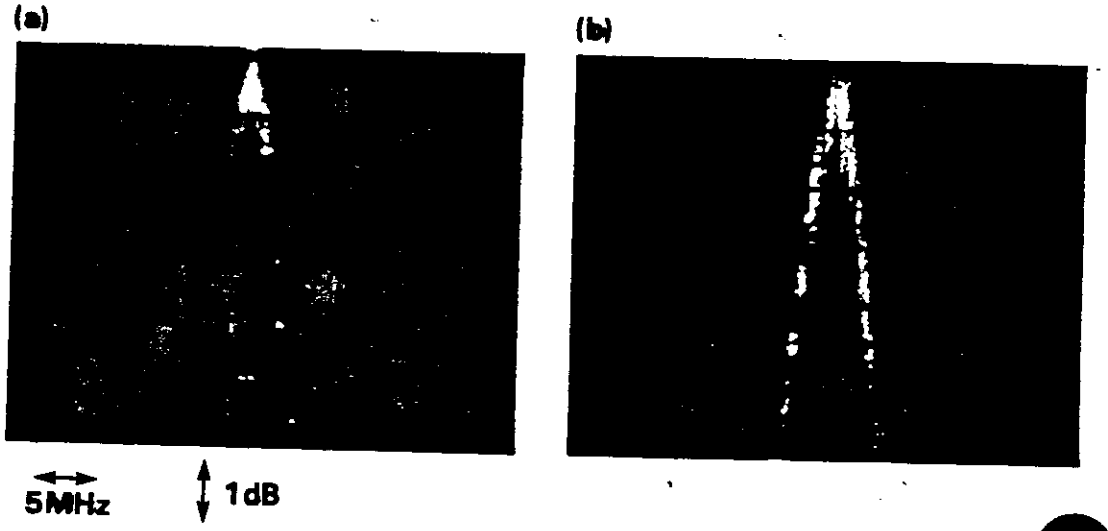

## Effect of Laser Drive Current on Linewidth of DFB Coupled to Graded Index Rod Lens External Cavity

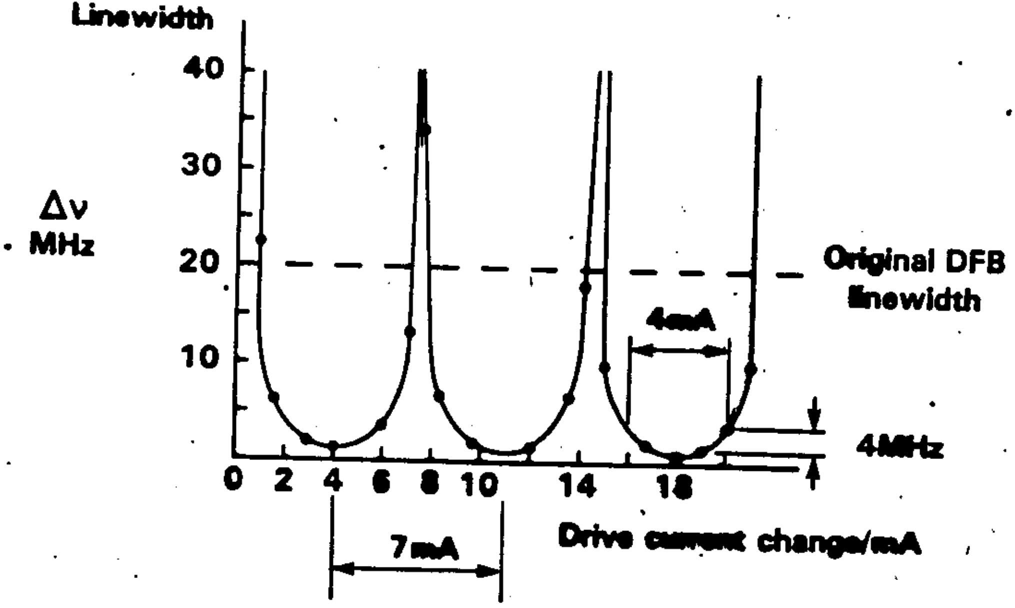

# Schematic Arrangment of Fabry Perot Laser with Fibre Grating External Cavity

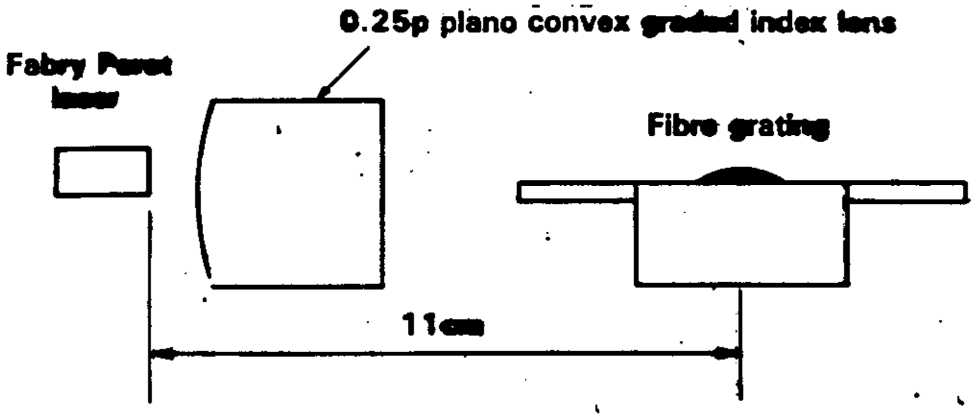

91

# Cross Section of Fibre Grating Device

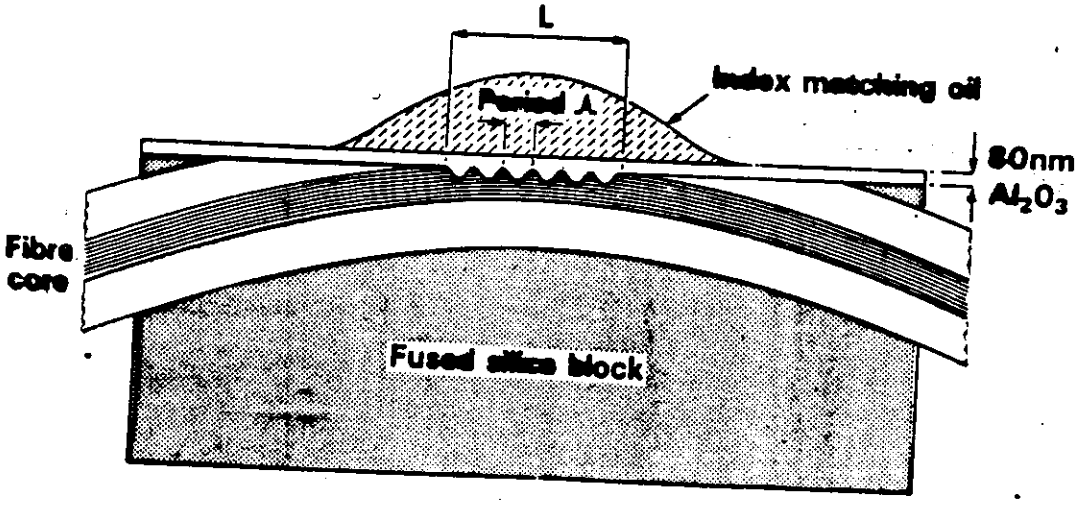

92

## Spectra of 1.55 Laser

(a) Without. (b) With fibre grating external cavity. One mode is selected at 1562nm with a side mode rejection ratio of 320.

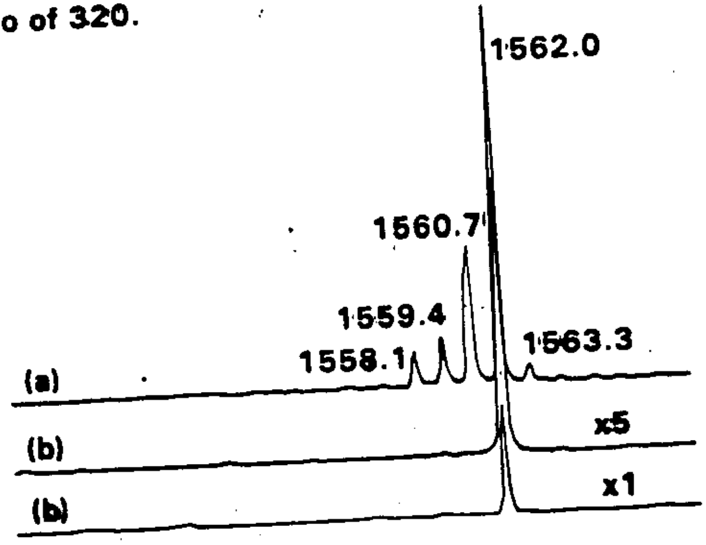

## Delayed Self Heterodyne Spectrum Around 80MHz of a Multimode Laser Coupled to an Equivalent 11cm Fibre Grating External Cavity

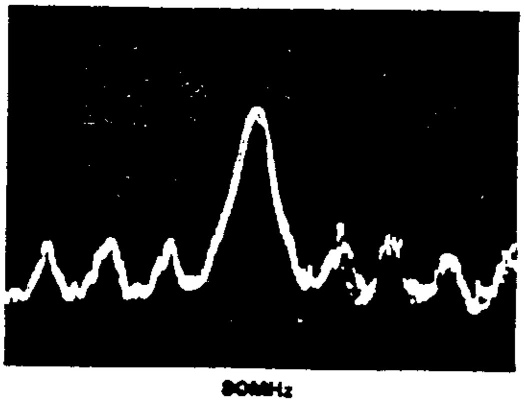

Horizontal 100KHz/cm

Vertical 10dB/cm

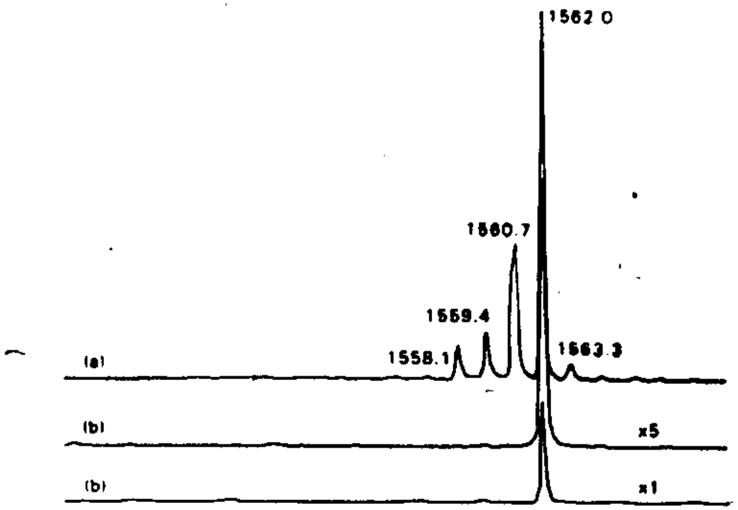

Fig. 2 SPECTRA OF 1.55 LASER. (a) WITHOUT. (b) WITH FIBRE GRATING EXTERNAL CAVITY. ONE MODE IS SELECTED AT 1562 nm WITH A SIDE MODE REJECTION RATIO OF 320.

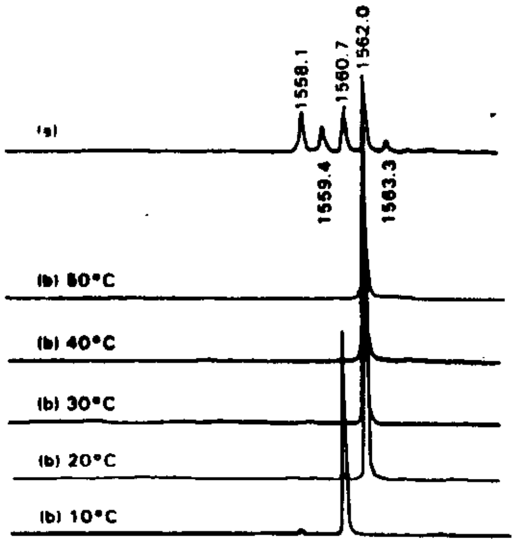

Fig. 3 SPECTRA OF MULTIMODE 1.55 LASER. (a) WITHOUT. (b) WITH EXTERNAL FIBRE GRATING, SHOWING THE EFFECT OF GRATING TEMPERATURE.

Reflection Characteristics of One of a Pair of Fibre Grating Devices Operating at 1536nm

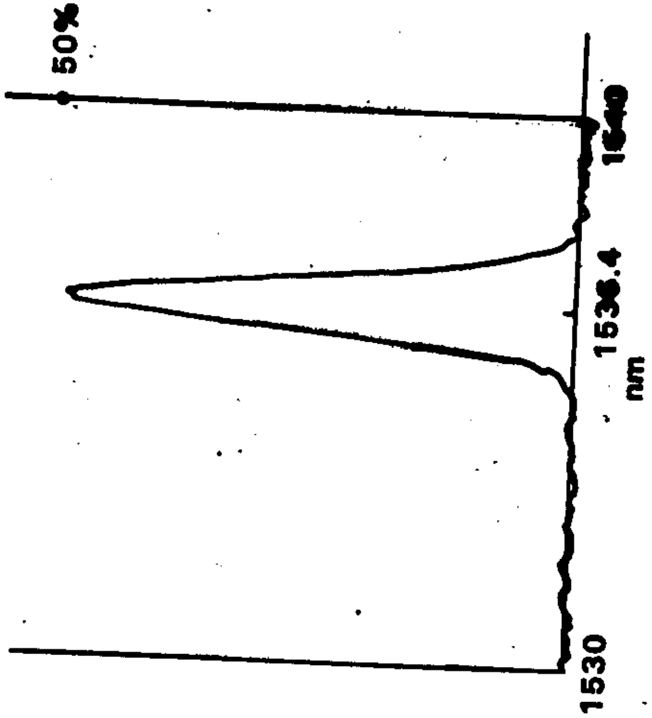

## Spectra of 1.55 Laser at Different Temperatures Coupled to a Fibre Grating

Grating reflects at 1536nm

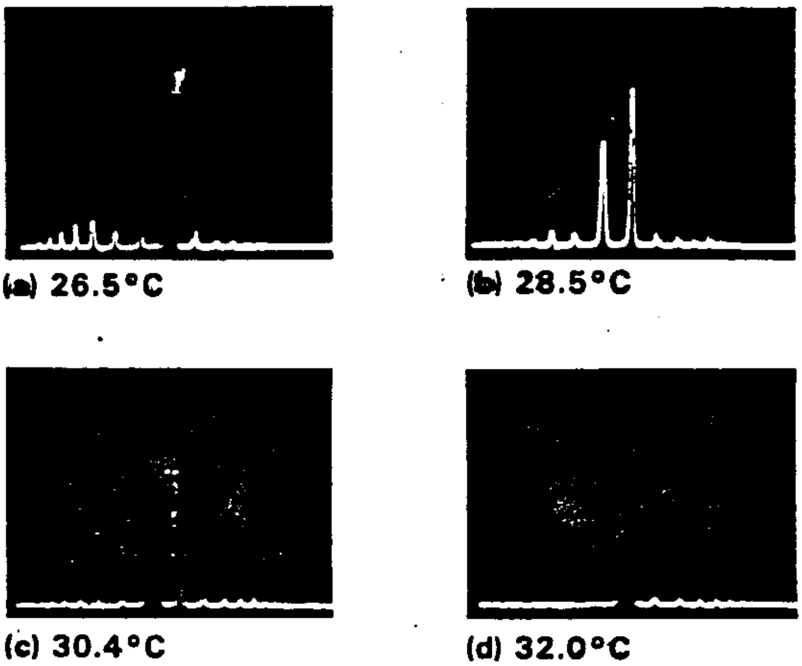

(a) 26.5°C

(b) 28.5°C

(c) 30.4°C

(d) 32.0°C

## Spectra of Two Fabry Perot Lasers each Coupled to a Fibre Grating at 1536nm

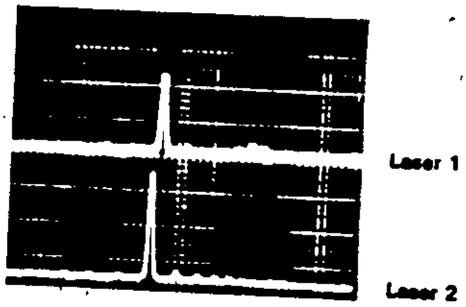

this letter a newly developed 1·5 μm wavelength-tunable DBR laser with both a phase control region and a Bragg wavelength control region is reported.[6] Tuning was performed by injecting currents into the PC and DBR regions. This changed the refractive index of the regions because of the plasma effect. Large-range continuous wavelength tuning was achieved by controlling the PC and DBR region currents simultaneously.[7,8]

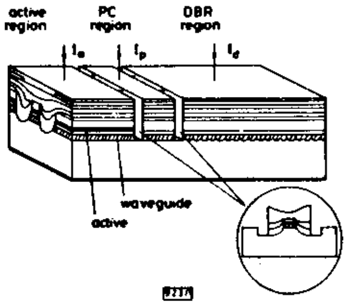

Fig. 1 *Wavelength-tunable DBR laser structure and cross-sectional view of groove position*

The device structure is shown in Fig. 1. The structure was basically the same as that of the previously reported DBR laser,[5] which had no phase control region. The DBR laser consists of three current injection regions: a 190 μm-long active region, an 80 μm-long phase control (PC) region and a 700 μm-long DBR region. The waveguide layers of the PC and DBR regions, which were coupled to the active region optically, were transparent to laser light. For transverse mode control, the DC-PBH configuration was adopted for all regions. The three regions were electrically isolated from each other by 20 μm-wide etched grooves, which were formed on both sides of the centre mesa stripe area. A cross-section at the groove position is shown in the circle in Fig. 1. Isolation resistances were about 600 Ω. The sample was mounted on a silicon heat sink with a junction-up configuration.

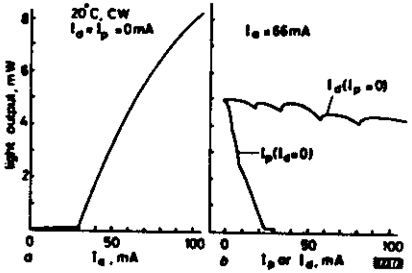

Fig. 2 *Light-output characteristics*

*a* Light output as a function of active region current $I_a$
*b* Light output as a function of DBR region current $I_d$ and of PC region current $I_p$

Light output as a function of active region current $I_a$ is shown in Fig. 2*a*, when currents are not injected into either the PC or DBR regions. The threshold current was 29 mA, and the external quantum efficiency was 19% per front facet at 20°C. Fig. 2*b* shows light output as a function of DBR region current $I_d$ and of PC region current $I_p$. The active region current $I_a$ was fixed. As the DBR region current increased, the light output changed periodically and the wavelength shifted toward a shorter wavelength with mode jumps, which was expected theoretically.[1-4] On the other hand, as the PC region current increased, the light output decreased almost monotonically and the wavelength dropped continuously towards a shorter wavelength, but occasionally shifted to longer wavelengths with mode jumps. This significant

current, which increased from 29 mA to 75 mA, as the PC region current increased from 0 mA to 30 mA. The large increase in threshold current is probably due to absorption loss increase in the PC region, caused by free carrier density increase. Small negative values in $I_d$ and $I_p$ were due to the leakage currents between individual regions.

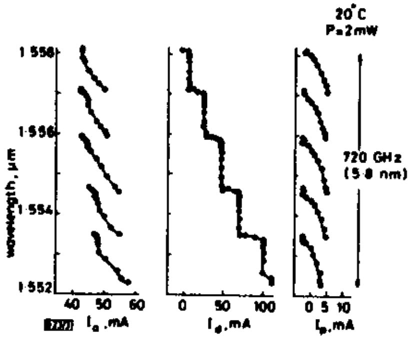

Fig. 3 *Large-range tuning by controlling three currents*

The tuning characteristics over a large wavelength range are shown in Fig. 3. Wavelengths are plotted as functions of the three currents. Large-range tuning was realised by the following procedures. First, the DBR region current $I_d$ was increased when the PC region current $I_p$ was not injected. The wavelength shifted slightly toward a shorter wavelength. More increase in $I_d$ caused a mode jump. Therefore, before the mode jump occurred, $I_p$ was increased when $I_d$ was held constant. The wavelength shifted about 1 nm toward a shorter wavelength. After $I_p$ was reset at zero the above procedures were repeated. In these processes the active-region current $I_a$ was changed to maintain light output at 2 mW. Consequently, over 720 GHz (5·8 nm) continuous tuning was achieved by controlling the three currents simultaneously. At all data points, single-longitudinal-mode oscillations, with a submode suppression ratio of more than 30 dB, was maintained.

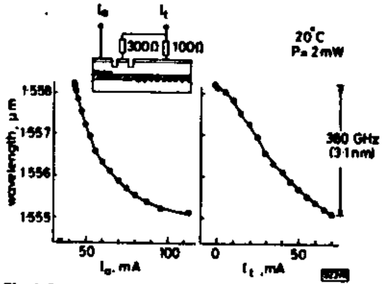

Fig. 4 *Smooth tuning by controlling two currents*

Fig. 4 shows a smooth wavelength tuning result for the same laser. In this case, tuning was performed by controlling only two currents. These were the active region current $I_a$ and the tuning current $I_t$, which was the sum of the PC and DBR region currents. The current ratio of the PC and DBR regions $I_d/I_p$ was kept nearly constant by using fixed load resistances of 100 Ω and 300 Ω for the DBR region and PC region, respectively, as shown in the Figure. The current ratio was about 3 to 1. The maximum tuning range was 380 GHz (3·1 nm) when the light output was kept constant at 2 mW. This range was restricted by an increase in threshold current, as mentioned previously. Nonetheless, it is very advantageous to be able to obtain both the desired wavelength and light output by controlling only two currents.

Spectral linewidth was also measured as a function of the wavelength by the delayed self-homodyne method. In a large-range tuning case (Fig. 3), the linewidth changed periodically

MURATA, MITO,
KOBAYASHI. NEC. 00

---

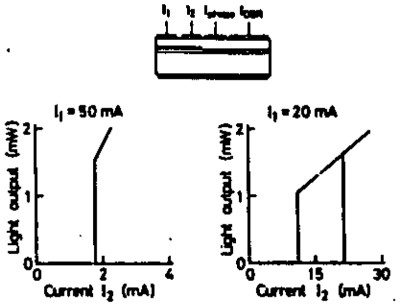

Fig.2 Current-light output characteristics.

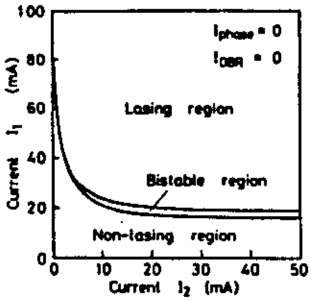

Fig.3 Lasing, bistable and non-lasing regions.

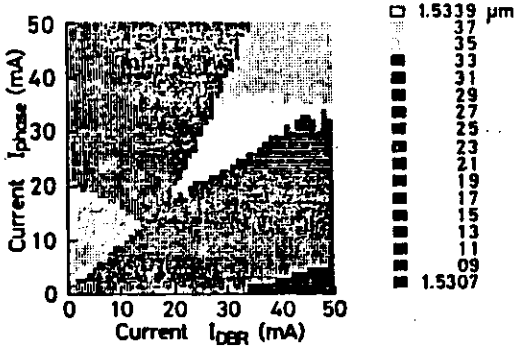

Fig.4 Lasing wavelength map as functions of $I_{phase}$ and $I_{DBR}$.

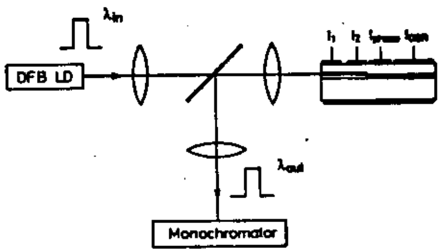

Fig.5 Experimental set-up for optical-wavelength conversion.

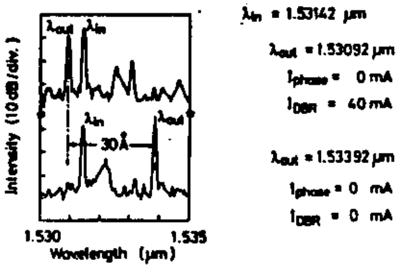

Fig.6 Results of optically triggered wavelength conversion.

100

YAMAKOSHI et al
OFC 88 (Fujitsu)

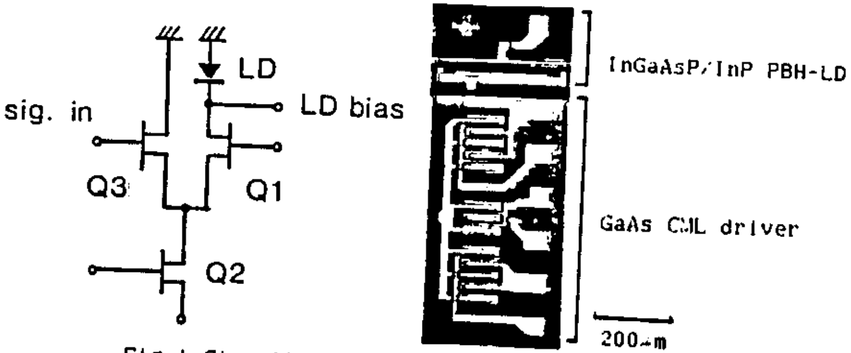

Fig.1 Circuit diagram and chip photograph for transmitter OEIC

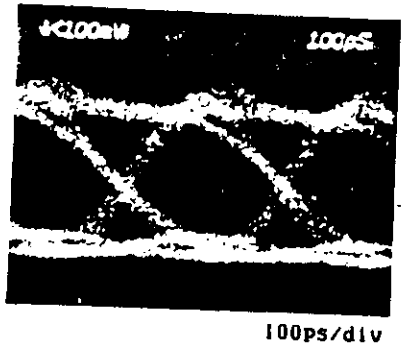

Fig.2 2.4Gb/s NRZ output waveform for transmitter OEIC

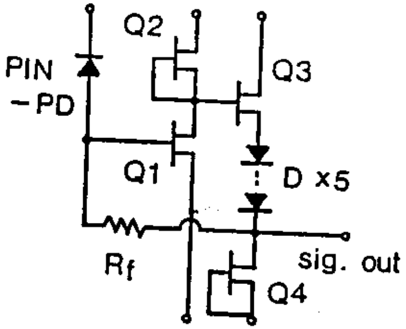

Fig.3 Circuit diagram for receiver OEIC

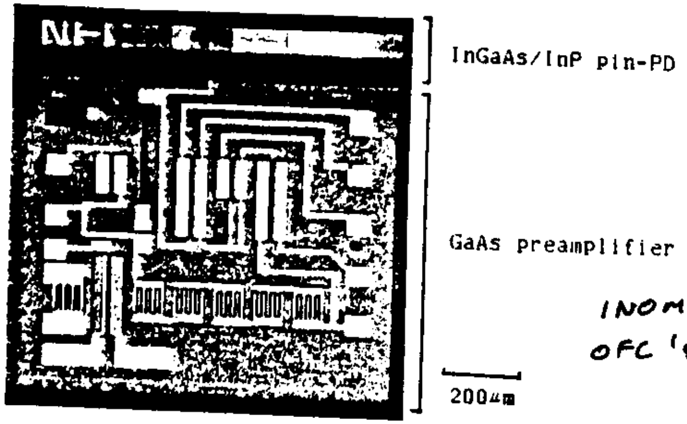

Fig.4 Chip photograph for receiver OEIC

INOMOTO ET AL
OFC '88 (NEC)

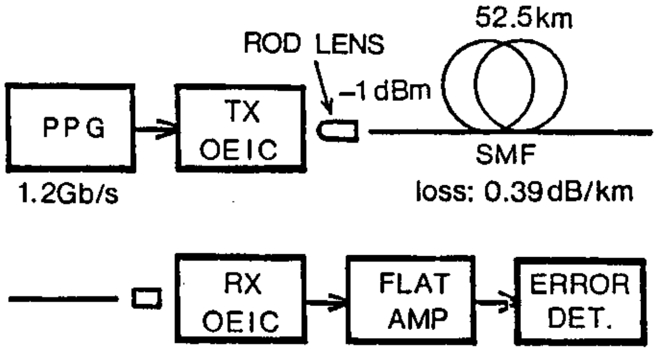

Fig.5 Blockdiagram for optical fiber transmission experiment

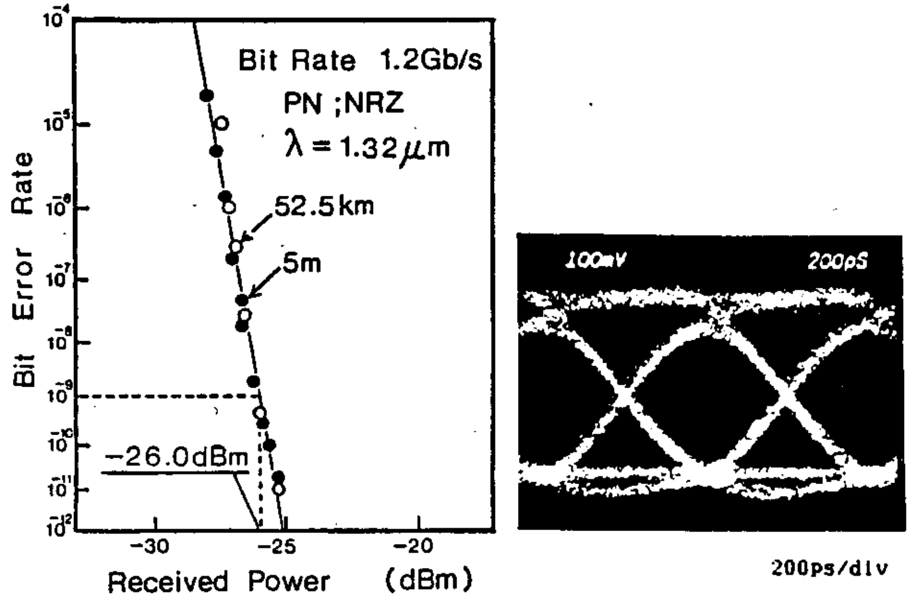

Fig.6 Receiver OEIC bit-error-rate characteristics and received signal waveform (1.2Gb/s NRZ)

INOMOTO ET AL
OFC '88 (NEC)

DETECTORS LECTURE WILL BE BASED ON THIS DOCUMENT

# DETECTORS AND THEIR CHARACTERISTICS

B T Debney

## 1. INTRODUCTION

This lecture will review the role of semiconductor detectors in fibre optic telecommunication systems. The emphasis will be on direct detection systems where the detector performance is of crucial importance in the system design. Some mention will be given to the detector requirements of systems based on coherent detection, but only briefly since this will be considered more fully in a later lecture.

Early fibre optic telecommunication systems operated at a wavelength of 0.85μm. These were based on LED and laser sources fabricated in the GaAs/GaAlAs system, and Si photodetectors of either the unity gain PIN diode type, or the avalanche photodiode (APD). The latter device provides gain through the process of avalanche multiplication. Silicon devices have provided good performance in systems at data rates up to 140 Mb/s.

The need for high data rates and repeaterless transmission over larger distances has led to the move to longer wavelength operation, and with it the requirement for new sources and detectors. Multimode laser sources can be used at a wavelength of 1.3μm, where the fibre dispersion is a minimum, and very long transmission links can be established which are attenuation limited. For 1.3μm operation, lasers based on the III-V system GaInAsP/InP have been developed. This material system is also the basis of low noise unity gain PIN diode detectors. The direct band-gap of the III-V compounds leads to narrow depletion regions, resulting in detectors with high quantum efficiency and fast response. For 1.3μm operation Ge detectors have also been successfully used, and at the present time are the basis of the only commercially available APD at this wavelength.

Lower attentuation and longer links can be achieved through operation at the longer wavelength of 1.55μm. The GaInAsP/InP material system also provides suitable sources and detectors at this wavelength. The use of Ge detectors at 1.55μm is not so attactive, particularly at higher data rates, because it is close to the absorption edge for Ge and the large depletion depths required lead to low quantum efficiency and slow response.

Present day research and development in detectors for the long wavelength requirements is aimed at producing low noise detectors which can also provide substantial levels of gain. Such detectors will lead to higher sensitivity direct detection receivers which could approach the performance realisable with transmission systems based on the coherent detection principle.

B T Debney is with the Plessey Company at the Allen Clark Research Centre, Towcester, Northants.

## 2. BASIC DETECTION PRINCIPLES

### (i) Intensity Modulation and Direct Detection (IM/DD)

This is the basic principle of all present day fibre optic transmission systems. A laser or LED source is intensity modulated, by modulating the drive current, and a photocurrent is generated at the detector which is proportional to the received power (Figure 1a). The detector is essentially a power detector and basic principles can be illustrated through considering the simplest form of semiconductor detector, the PIN diode. The detection process is illustrated in figure 2.

Photons with energy hν greater than the bandgap $E_g$ enter the semiconductor and are able to excite electrons from the valence band to the conduction band. The electrons and holes produced can, if they reach the junction or are created within the depletion region, be swept through the device and so generate a photocurrent. The depth over which optical absorption occurs is characterised through the absorption coefficient $\alpha$ (hν). If $\Phi(x)$ is the optical intensity within the material at a depth of x,

$$\Phi(x) = \Phi(0) \exp(-\alpha x)$$

$\alpha$ is important because it is a measure of the thickness of material required to absorb the radiation. e.g. if $\alpha = 2/x$, 86% absorption is achieved, and if $\alpha = 3/x$ this rises to 95%. The absorption coefficient depends on wavelength and the bandstructure of the material (see figure 4). Direct gap semiconductors have absorption which rises steeply at the absorption edge, e.g. GaAs, InP. Indirect gap materials require phonons to mediate the absorption process and hence the absorption is not so strong, e.g. Si.

An important detector parameter is the quantum efficiency ($\eta$). This is defined as the ratio of the number of photogenerated electrons which are collected (traverse the depletion region and contribute to the photocurrent) to the number of photons which are incident on the detector. If $\Phi$ is the photon intensity and $J_{ph}$ the photocurrent density.

$$\eta = J_{ph}/e\Phi$$

Denoting $P_r$ as the power incident on the detector surface, area A, we can write

$$\eta = \frac{I_{ph}\, h\nu}{eP_r}$$

This leads to the definiton of detector responsivity R as

$$R = e\eta_{/h\nu} \quad \text{Amps/Watt}$$

so that the detector photocurrent is given by

$$I_{ph} = RP_r$$

This is the basic result for direct detection.

A high value of quantum efficiency depends on the ability to:

(a) Reduce reflections from the detector surface (AR coating).

(b) Maximise absorption within the depletion region (device design, $W \sim (2+3/\alpha)$.

(c) Avoid carrier recombination (device design, minimise absorption outside the depletion region).

For a PIN diode detector reverse bias is applied so that a wide depletion zone is created and carrier generation predominantly takes place here. Carriers are swept through by the drift field with little or no recombination. Generation outside the depletion zone has the effect that electrons and holes generated diffuse towards the junction, and can contribute to the photocurrent if they reach it before recombining. Carrier generation outside the depletion region can lead to recombination losses and affect the rise and fall time of the detector, influencing the speed/bandwidth.

If the reverse bias is increased then a point is reached when the electrons and holes can acquire sufficient energy from the field to be able to impact ionize and create additional electron-hole pairs (see figure 3). This carrier multiplication process gives rise to avalanche gain and is the principle behind the avalanche photodiode (APD).

For this case

$$I_{ph} = MR\,P_r$$

where M is the current gain, or multiplication factor.

### (ii) Coherent Detection

For completeness we describe the basic principle of coherent detection. This is illustrated in figure 1b. At the detector the signal field and local oscillator field are combined. Because the detector is a power detector, and the optical power is proportional to the square modulus of the combined optical field, the photocurrent produced is proportional to,

$$\left| E_S\, e^{j(\omega_S t + \phi_S)} + E_L\, e^{(j(W_L + \phi_L)} \right|^2 \text{ TIME AVERAGED}$$

which is $$\frac{E_S^2}{2} + \frac{E_L^2}{2} + E_L E_S \cos(\omega_{IF} t + \Delta\phi)$$

where $\omega_{IF} = \omega_S - \omega_L$ is referred to as the intermediate frequency (IF). The resulting photocurrent is then

$$I_{ph} = RP_S + RP_L + 2(P_L P_S)^{\frac{1}{2}} \cos(\omega_{IF} t + \Delta\phi)$$

The detector therefore acts as a mixer to produce an output electrical signal at an intermediate frequency (heterodyning). This expression illustrates the basic principle of coherent detection. The signal modulation appears either in amplitude ($P_S$), frequency ($\omega_S$) or phase ($\Phi_S$). The intermediate frequency signal can be made large by increasing the local oscillator power $P_L$ thus improving the SNR.

## 3. MATERIALS FOR DETECTORS

Detection of light at a wavelength λ, or equivalently photons of energy $h\nu = {}^{hc}/_{\lambda}$ requires a material with band gap Eg which is less than the energy hν. Figure 5 can be used to investigate the range of materials which are available to perform the detection process in the wavelength region of 0.85 → 1.55μm. Silicon with a band gap of 1.1 eV is well suited for operation at wavelengths below 1.1μm and generally offers the best solution for the 0.8 → 0.9μm band.

The requirement for detection of light out to 1.55μ limits the choice of suitable materials to those of bandgap less than 0.8eV. Materials with band gaps much smaller than this will still respond to 1.55μm radiation but will have the disadvantage of high levels of dark current and undesirable temperature sensitivity. A direct gap semiconductor material is also an advantage as this results in more efficient light absorption. Germanium, with its band gap of 0.7eV and an indirect gap below 1.53μm (0.8eV) is an illustration of these points and although it can be used at 1.55μm is far from ideal, particularly for high data rates. Germanium has found better application at 1.3μm, particularly when an APD is required.

The group III-V semiconductors are also providing suitable detector materials for the range 1.3 → 1.55μm. As can be seen from figure 5, none of the binary semiconductors, with the exception of GaSb have bandgaps near 0.8eV. It is possible, however, to form ternary and quaternary solid solutions and to tailor the band gap to a desired value over a wide range. These solid solutions are usually prepared by epitaxial growth either from the vapour (VPE) or the liquid (LPE) phase onto a binary substrate. The preferred material system for 1.3 to 1.55μm devices, based on proven performance, is the quaternary GaInAsP range of alloys which can be grown epitaxially lattice matched to InP with bandgaps between that of the binary InP (1.3eV, or 0.95μm) to that of that of the ternary GaInAs (0.75eV, or 1.6μm). The system AlInAs provides larger bandgap materials and can also be grown lattice matched to InP, allowing a further degree of freedom in the design of more sophisticated detector structures.

## 4. DETECTOR TYPES

### (i) Detectors without Internal Gain: The p-n and p-i-n Junction Diodes

The mode of operation of these devices has already been briefly described in section 2. Whether the device structure is of the p-n or p-i-n type makes little difference to the basic principles. The choice of structure depends largely on the width of depletion region required and this will be discussed shortly. But first we consider some basic parameters which are necessary to characterise the device for use in an optical receiver.

#### Device Capacitance

The small signal equivalent circuit for the junction photodiode is shown in figure 6. For a p-i-n diode in which the 'i' region is lightly doped the electric field is approximately uniform and the junction capacitance is easily shown to be that of a parallel plane capacitor. The detector junction capacitance $C_D$ is therefore given by

$$C_D = \varepsilon\varepsilon_0{}^{A}/_{W}$$

where W is the depletion width.

This also applies to the abrupt p/n junction case with W suitably interpreted.

#### Bandwidth

The frequency response, or impulse response, is ultimately limited by the transit time for carriers to drift across the depletion region. If we define $\tau_{av}$ as the mean of the transit times for electrons and holes then the detector 3db bandwidth is given by

$$f_{3db} = {}^{0.44}/\tau_{av}$$

The bandwidth is here defined as the frequency at which the current falls by the factor of √2 for a sinusoidal modulation at frequency $f_{3db}$.

## Noise

In the dark the current-voltage characteristic for the diode is as depicted in figure 6b. When biased as a photodiode the reverse bias saturation current $I_D$ flows through the device. This leakage current can arise from a variety of mechanisms: minority carrier injection, generation - recombination within the depletion region, band to band tunnelling. Which occurs depends on the semiconductor material and the field conditions. Current fluctuations appear at the device terminals due to the random nature of the process by which the carriers traverse the depletion region. The process gives rise to what is known as shot noise, and is characterised by the mean squared current fluctuations being proportioned to the average detector current. For the dark current process the single sided (positive frequencies only) noise spectral density function is given by

$$S_I = 2qI_D$$

so that in a bandwidth Δf the total mean square current fluctuations are,

$$\overline{I_{dn}^2} = 2qI_D\Delta f$$

The photocurrent $I_{ph}$ also exhibits shot noise due to the quantum nature of the generation process and so

$$S_I^{PIN} = 2q\ (I_D + I_{ph})$$

## Design Considerations

One of the main design considerations is to ensure that most of the incident radiation is absorbed within the depletion region. For Si operating at ~0.85μ a depleted zone of typically 30μm is required. In the case where wide depletion zones are necessary the p-i-n structure is preferred, since the lightly doped 'i' material can be depleted at relatively low voltages. For Si devices the reach-through structure of figure 7 is therefore adopted, so called because the depletion zone 'reaches through' depleting the 'i' region and stopping at the heavily doped substrate. When only a microns or so of material needs to be depleted, e.g. when using GaInAs for long wavelength detection (see figure 8a) a p-n junction diode often suffices.

Another design point is the avoidance of absorption outside of the depleted zone, in order to reduce absorption loss and speed limitations. This can be achieved through making the heavily doped surface region very thin. The problem is particularly important when direct gap semiconductors are used because substantial absorption can occur in the surface and within thin layers. This is avoided in the device shown in figure 8b by using a substrate entry structure in which the large bandgap of InP makes it transparent to the radiation. Absorption takes place within the n GaInAs layer, which would be fully depleted so as to avoid a diffusion contribution to the photocurrent.

Alternative solutions to the avoidance of surface absorption are the use of heterojunction or Schottky barrier structures.

## (ii) The Avalanche Photodiode

The avalanche photodiode (APD) is in essence a p-n junction diode reverse biased close to the point where the junction begins to break down. Under very high electric fields electrons and holes can impact ionise and give rise to carrier multiplication, e.g. a highly energetic electron can collide with a valence band electron and transfer sufficient energy to it to cause excitation into the conduction band. In this way one electron gives rise to two free electrons in the conduction band and a free hole in the valence band. The basic processes are illustrated in figure 3. When the electrons initiating the ionisation are photogenerated electrons the multiplication process gives rise to photocurrent gain at the device terminals. Gains of the order 100 have been obtained in well designed Si devices.

Important material parameters determining the behaviour of a device are the electron and hole ionisation coefficients α and β. These quantities define the probability of an ionising event taking place per unit distance travelled. They are strongly field dependent and also temperature dependent. If eg. α >> β then this would indicate that the impact ionisation is predominantly due to electrons so that the current gain is associated with the primary electron photocurrent. Some typical ionisation coefficient data is given in figure 9.

Avalance photodiodes have the advantage of providing current gain which can substantially improve the performance of an optical receiver. They do, however, have the drawbacks of requiring very high voltages to establish the device fields necessary, and the gain is very sensitively dependent on bias voltage and temperature so that the operating conditions need to be very stable. A typical gain-voltage characteristic for a Si device is shown in figure 10b.

## Device Capacitance

As for p-n junction diodes. The important parameters are device area and depletion width.

## Bandwidth

We consider here the optimum situation where all carriers are generated within the depletion region. The analysis of the bandwidth of an APD is a complex problem because the presence of the gain process results in a gain-bandwidth relationship. This has been analysed by Emmons (ref. 1) for a p-i-n diode structure in which the whole of the depletion region contributes to the multiplication process. For this case the transit time which enters the calculations is that for the depleted layer, which also defines the avalanche zone. If the width of the avalanche region is $L_a$ and $\upsilon$ is an effective drift velocity for the carriers, then the transit time $\tau_a$ is given by $L_a/\upsilon$. It is found that for a particular value of multiplciation factor M, the bandwidth is given by

$$f_{3db} = \frac{\chi_a(M)}{2\pi\tau_a}$$

$\chi_a$ is a factor which depends on the gain M and the $\alpha/\beta$ ratio for the device, and can be extracted from figure 11. An effective transit time, or what is sometimes referred to as the avalanche build up time can be defined according to

$$\tau_a^{eff} = \tau_a 2.8/\chi_a(M)$$

The factor of 2.8 enters as the limit of $\chi_a$ when the gain is unity so that this has the correct limiting form for a non-avalanching diode.

It can be seen from Figure 11 that when $M < \alpha/\beta$ the bandwidth is approximately independent of the gain, whereas for $M > \alpha/\beta$ there is a constant gain-bandwidth product.

## Noise

When the APD is operating at an average gain M not all photogenerated carriers are multiplied by exactly M. There is a distribution of gains which is produced by the statistical nature of the avalanche process and this introduces noise into the multiplication process. The problem has been analysed by McIntyre (ref. 2) and shown that if a primary current $I_0$ is injected into the avalanche region the spectral density of the shot noise in the multiplied current is given by

$$S_I^{APD} = 2q\, I_0\, M^2 F(M)$$

F(M) is the excess noise factor, and is the measure of how much the noise exceeds that of an ideal current multipler. F(M) depends on the material and junction characteristics through the ionisation coefficient data, as well as the nature of the primary excitation, i.e. electron injection, hole injection, or both. If an effective ionisation coefficient ratio $K_{eff} = (\beta/\alpha)eff$ is defined for the avalanche zone and the avalanche is initiated by electrons ($\alpha$), then,

$$F(M) = M\,\{1 - (1-K_{eff})\,(\frac{M-1}{M})^2\,\}$$

In the limit where the electron ionisation coefficient is very much larger than that for holes ($K_{eff} \ll 1$), $F(M) \rightarrow 2$, independent of the gain and this is essentially the result for a photomultiplier, which is the best which can be achieved. If $K_{eff} = 1$, then $F(M) = M$, yielding the strongest dependence of the excess noise factor on the gain, reflecting the maximum feedback between the electrons and holes in the multiplication process and hence the greatest noise. However, if the ionisation is initiated by electrons, but the holes possess the largest ionisation coefficient ($K_{eff} > 1$) then in the limit of large gain $F(M) \rightarrow K_{eff}$. This emphasises the importance of ensuring that the carrier with the largest ionisation coefficient initiates the avalanche.

In the APD not only the photocurrent undergoes multiplication, but also any component of the device leakage current which flows through the junctions is also multiplied and contributes to the noise. Therefore the full noise spectral density can be represented as

$$S_I^{APD} = 2q\,\{I_D^{(1)} + (I_D^{(2)} + I_{ph})\,M^2\,F(M)\,\}$$

## Design Considerations

The comments made concerning the requirements for achieving high quantum efficiency and bandwidth in the case of unity gain junction photodiodes apply equally well to the APD.

Material quality is very important. Defects and dislocations within the material can cause local enhancement of the electric field, and thus cause premature avalanching in their vicinity, referred to as microplasmas. This can give rise to non-uniform carrier multiplication across the illuminated surface area of the device.

In structures requiring large optical absorption depths, such as Si, the simple p-i-n structure is unsatisfactory. Instead a similar reach-through structure is adopted but where the lightly doped region occurs after the $n^+p$ junction as depicted in figure 10a. This has the action of providing an appropriate thickness of depleted material for absorption, but the high field avalanching region is confined to the more heavily doped, but thin, $n^+$-p junction. This provides for a much more stable device than would be the case if the whole of the highly doped region sustained a breakdown field.

The device shown in figure 10a also indicates the use of a guard ring structure. The ring of comparatively low n-type diffusion creates a p-n junction which consists of a wider depletion region and hence lower field compared with the $n^+$-p junctions. This has the effect of confining the avalanche within the ring and inhibiting premature breakdown near the surface at the $n^+$-p junction.

The choice of materials with high $\alpha/\beta$ ratios is clearly preferred, but moveover it must also be ensured that the carrier with the largest ionisation coefficient initiates the multiplication. These conditions influence the bandwidth of the device, its noise performance, and also ensures a more stable and uniform gain.

Work in developing APDs for long wavelength operation based III-V materials has presented a new range of design problems. Because of the narrow band gap associated with long wavelength detecting materials there is a tendency for band-to-band tunnelling to take place before sufficiently high fields are reached to achieved carrier multiplication. The large tunnelling currents which occur and their associated shot noise rule out homojunction structures formed in e.g. GaInAs. To overcome this problem the structure depicted in figure 13 has been devised. This is referred to as a SAM APD (Separate Absorption and Multiplication APD). Carriers are photogenerated in the narrow gap material (GaInAs) where the field is high enough to cause depletion, but not tunnelling or multiplication, and drift into the wide gap more highly doped InP junction where the field is high enough to cause avalanching. The constraints imposed by the field requirements and depletion requirements for this structure make it a difficult device to fabricate.

## 5. WHAT MAKES A GOOD DETECTOR?

In this lecture we are considering the behaviour of detectors in the context of an optical receiver. Whether it is digital or analogué transmission there is the requirement to maximise the signal to noise ratio at the receiver. The noise contributions from the detector can be important in determining the receiver sensitivity, but more subtly other parameters can also influence the receiver performance through their influence on the electrical characteristics of the receiver. Receiver sensitivity analysis will not be given here, but we will briefly describe those detector attributes which influence the receiver sensitivity and their significance at different data rates.

For all detector types it is important to maximise the quantum efficiency in order to maximise the signal photocurrent and this need not be discussed further.

The detector parameter requirements for the PIN diode (non-avalanching) and the APD are summarised below.

### PIN Diode (Unity Gain)

1. Low leakage current (minimise shot noise).
2. Low capacitance (minimise contribution to total input capacitance, and hence receiver noise - higher data rates).

3. High bandwidth (for detector response at high data rates).

**APD**

1,2,3 as above, plus

4. High gain, or combined with 3, large gain bandwidth product (in order for achieve optimum gain condition and maximise receiver sensitivity).
5. Large $\alpha/\beta$ ratio (to minimise excess noise factor and maximise value of optimum gain).

These detector features have varying levels of significance depending on the data rate, and trends are summarised in Table 1.

## 6. PRESENT DAY TECHNOLOGY

For 0.85μm wavelength operation Si detectors presently offer the best solution. The technology is well developed and excellent performance can be obtained from both PIN diodes and APDs. Commercially available Si PIN diodes can typically achieve quantum efficiencies of ~75% and subnanoamp leakage currents at 25°C. Operating at 10V reverse bias, a bandwidth of approximately 500 MHz is achievable. The Si APD is an excellent device, as a result of the fact that the ionisation coefficient for electrons is much greater than that for holes ($\alpha \gg \beta$). Devices exhibit values of $K_{eff}$ in the range 0.1 to 0.01, with 0.03 being typical. Coupled with subnanoamp leakage currents, this results in a very low noise APD which permits the device to be operated at multiplication factors of around 100. Bias voltages of 200-300V are required to achieve such gain, though it can be obtained simultaneously with a frequency response up to ~500 MHz. The APD can offer very significant receiver sensitivity improvements over the PIN diode as is illustrated in figure 14

Germanium detectors, though capable of operation out to 1.55μm, have predominantly been used at a wavelength of 1.3μm. The Ge APD has found the greatest application because at this wavelength it is at present the only commercially available APD. The easist to fabricate and hence commonest device uses the $n^+p$ configuration produced by diffusing n-type donors into a p-type substrate. This structure sustains the avalanching field near the $n^+$ layer and hence electrons predominantly initiate the ionisation. Unfortunately, in Ge the ionisation coefficient for electrons is less than for holes ($\alpha < \beta$), though only slightly, with the result that the excess noise factor $F(M) \sim M$ giving rise to a noisy device. Leakage currents in Ge devices tend to be rather high, being typically 0.1μA unmultiplied at room temperature. This limits the useful gain in a receiver to around 10, beyond which the receiver noise increases more rapidly than the signal, and hence the SNR degrades. Operating voltages for Ge APDs are lower than for Si devices, being typically 30-40V, and bandwidths of up to ~1 GHz are available from commercial devices.

Operation can be extended out to 1.55μ, but large depletion depths of ~10μm are required. A reach-through type $p^+nn^-$ structure has been developed for this wavelength, which has the added advantage that the ionisation is initiated by holes. The result is that $K_{eff}$ of less than unity has been achieved, with the corresponding $F(M) < M$, so that avalanche noise is reduced. Leakage currents have been reduced somewhat by using smaller area diodes (30μm diameter as opposed to the more conventional 100μm). Operation at 1.55μm tends to be a feature of the move to ever higher data rates and it is in this respect that the Ge APD HAS limited application. Best reported results indicate a bandwidth of 700 MHz at a gain of 10.

At long wavelengths (1.3 → 1.55μm) the GaInAs PIN diode is the detector favoured for high data rate operation. For the lowest receiver noise this is usually coupled to a GaAs FET preamplifier. The GaInAs PIN/GaAs FET front end is the basis of commercially available receivers for data rates up to 565 Mb/s. Although the bandgap and wavelength of peak response of a III-V detector could be optimised by appropriate choice of the GaInAsP alloy compositions most longwavelength detectors in this system have in fact been developed using $Ga_{0.53}In_{0.47}As$ which is lattice matched to InP and responds to wavelengths out to 1.7μm. This results in a broadband detector with a response from 0.8 → 1.7μ, although the quantum efficiency is usually optimum near 1.3 and 1.55μm, being typically 75 and 90%. Interestingly the device has a useful response at 0.85μm, ($\eta \sim 40\%$). Both the top entry and substrate entry devices of figure 8 have been successfully developed. In both cases a depleted GaInAs layer of ~3μm is used which provides high quantum efficiency and bandwidth. Low doping permits full depletion of the GaInAs at low reverse bias. Because of the narrow depletion layers and the associated short transit times the device is intrinsically very fast with a theoretical bandwidth of approximately 15 GHz. However, the bandwidth of commercially available packaged detectors is usually limited to 1-2 GHz, due to the properties of the package. The devices operate under a reverse bias of approximately 5V and exhibit low leakage currents of typically 10nA or less. Low capacitance is a very important feature of the PIN diode detector and a device capacitance of less than 0.5pF is normal. With one particular design of substrate entry device in which the detector is flip-chip bonded a GaAs FET IC preamp, a detector capacitance of ~0.05 pF has been achieved (ref. 3).

In recent years there has been considerable R & D effort worldwide aimed at producing a III-V APD for longwavelength operation, which will surpass the performance offered by Ge. The SAM APD structure illustrated in figure 13 has been the subject of most investigation. Promising device and system results have been reported in the literature but up to the present time no device has been commercially available. However, preliminary specification sheets are now being issued by some companies indicating that a GaInAs/InP SAM APD will be available in the near future. Typical performance specifications are: quantum efficiency better than 80%, leakage current (unmultipled) of 10nA or less, capacitance of less than 0.5 pF, and an operating voltage of ~100V. For the InP junction used in the device the effective $\alpha/\beta$ ratio is approximately 0.5 which, coupled with the lower leakage current, suggests a lower noise performance compared to Ge APDs. As indicated in section 4 the gain-bandwidth relationship for an APD is complex, therefore though incomplete information it is useful to note that at a gain of 10 a bandwidth of ~ 2GHz is achievable with this device.

## 7. DETECTORS FOR THE FUTURE

For trunk applications the drive is towards higher data rates (over 1 Gbit/s), higher receiver sensitivity, and probably 1.55μm wavelength operation. Detector developments are continuing with the aim of achieving wider bandwidth, lower noise, and internal gain. We have already mentioned in the introduction systems based on the principle of coherent detection. In a coherent receiver the local oscillator power provides the gain mechanism and, assuming adequate local oscillator power to achieve shot noise limited operation, the ideal detector is a low noise unity gain PIN diode. The motivation for future detector development is therefore to enhance the performance of direct detection systems and a common theme which features in these developments is to seek structures with internal gain.

In the last few years new concepts have been emerging for APDs with the aim of achieving higher effective $\alpha/\beta$ ratios, and hence lower noise. Two such ideas have arisen out of work on semiconductor superlattices. The first is depicted in figure 15 and represents a structure comprising alternate layers of wide and narrow bandgap materials. By choosing materials such that the conduction and valence band discontinuities are significantly different it is possible to achieve an effective $\alpha/\beta$ ratio for the structure which is very different from unity, even though the ratio may be close to unity for the constituent bulk semiconductors. The concept has been realised in the GaAs/GaAlAs system but not yet in materials suitable for longwavelength operation. A second multilayer concept is shown in figure 16. This is referred to as the staircase APD. Device operation is based on the idea that if the conduction band discontinuity is sufficiently large the electrons drifting across the discontinuity will find themselves with sufficient energy to immediately impact ionise in the narrow gap region. This device could operate on a very low bias voltage and in the limit of no hole impact ionisation it becomes a solid state photomultiplier with an excess noise factor of unity! The present challenge is to find suitable materials in which to realise the structure. The band structure requires the ability to grade continuously in alloy composition. The only suitable candidate material system to date is GaAlAsSb.

A third idea for improving the ionisation coefficient ratio arises out of the observation that in certain material systems the hole ionisation coefficient exhibits a resonant characteristic as a function of the alloy composition. The phenomenon is a band structure effect and occurs when the band gap energy becomes equal to the spin-orbit splitting energy. The two material systems which have been found to exhibit this behaviour and which are suitable for long wavelength operation are $Ga_{1-x}Al_xSb$ and $Hg_{1-x}Cd_xTe$. At resonance an enhancement in the $\alpha/\beta$ by up to a factor of ~20 has been observed. However, considerable improvement in the quality of these materials is necessary before high performance devices will be forthcoming.

Also in the category of future developments are included the phototransistor and photoconductor. These are not so new in concept but are included here because at present no suitable devices are commercially available for longwavelength operation. The heterojunction phototransistor (HPT) has been investigated for a number of years as an alternative to the APD. The HPT combines the detection process, at the base-collector junctions, and current gain, but is more analogous in operation and performance to that of an integrated PIN diode and bipolar transistor, rather than an APD. The InGaAs/InP HPT has been the subject of most development work, but results to date suggest that it will not be a serious contender for high data rate, high sensitivity receivers.

The photoconductor is an inherently simple device both in concept and structure, and can operate from a bias of only a few volts. Photoconductors have been produced in GaInAs, and demonstrated a photoconductive gain of 10. It has so far proved difficult to fabricate devices which simultaneously achieve low noise, high bandwidth, and high quantum efficiency. Compared with the PIN diode the photoconductor is inherently slower and hence is less suitable at high data rates. Additionally, because the device is gain-bandwidth product limited the gain available at high data rates is small.

It is interesting to speculate on the performance that could be achieved with optimised receivers based on the spectrum of detectors which could be available in the forseeable future and for gigabit per second data rates. An attempt at such a comparison is presented in figure 17.

## LITERATURE

### References

1. R B Emmons, 1967, J.A.P., Vol. 38, No.9, p.3705.

2. R J McIntyre, 1966, IEEE Trans. Elec. Dev., ED-13, No.1, p.164.

3. R S Sussmann et al, 1985, Elec. Lett., Vol.21, No.14, p.593.

### Detectors/General

J Gower, 'Optical Communication Systems', Prentice-Hall, International Series in Optoelectronics, Ed-P.J. Dean.

S M Sze, 'Physics of Semiconductor Devices', 2nd Edition, Wiley.

### Detectors/Receivers

M Brain and T P Lee, 1985, J.L.T., LT-3, No.6, p.1281.

### Detector Developments

G E Stillman et al, 1982, IEEE Trans. Elec. Dev., ED-29, No.9, p.1355.
F Capasso et al, 1983, IEEE Trans. Elec. Dev., ED-30, No.4, p.381.
F Capasso, 1985, Physica 129B, pp.92-106.

| DETECTOR ATTRIBUTE | PIN DIODE |  | APD |  |
|---|---|---|---|---|
|  | DATA RATE |  | DATA RATE |  |
|  | LOW | HIGH | LOW | HIGH |
| LOW LEAKAGE CURRENT | 3 | 1 - 2 | 4 | 2 - 3 |
| LOW CAPACITANCE | 1 - 2 | 3 | 1 | 2 |
| HIGH QUANTUM EFFICIENCY | 4 | 4 | 4 | 4 |
| HIGH BANDWIDTH | 1 | 4 | 1 | 4 |
| HIGH GAIN | 1 | 1 | 3 | 2 |
| LARGE RATIO OF IONISATION COEFFICIENTS | 1 | 1 | 3 | 3 |

1. Not significant/not applicable
2. Significant
3. Important
4. The highest importance

Table 1

Assessment of the relative importance of detector characteristics to the optical receiver performance.

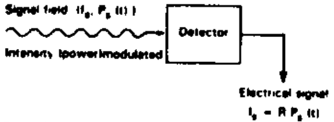

Figure 1(a)

The Principle of Intensity Modulation and Direct Detection

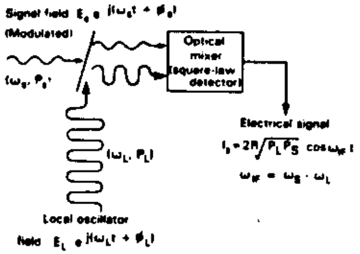

Figure 1(b)

The Principle of Coherent Detection

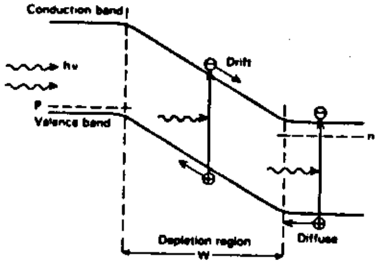

Figure 2

Enery Band Diagram for a Reverse Biased PIN Junction Photodiode Illustrating Electron-hole Pair Generation via Photon Absorption

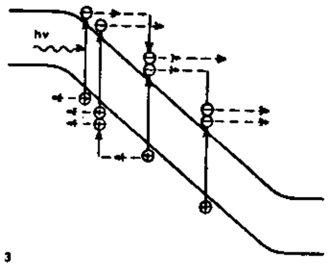

Figure 3

The Principle of Avalanche Multiplication in an avalanche Photodiode (APD)

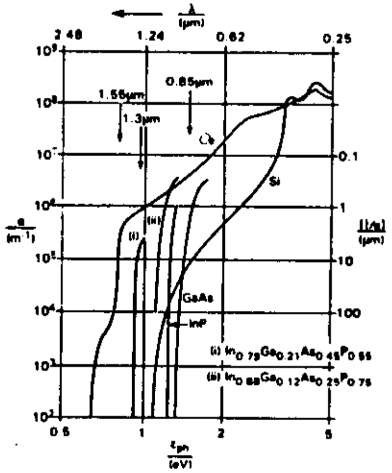

Figure 4

Variation of Absorption Coefficient with Photon Energy

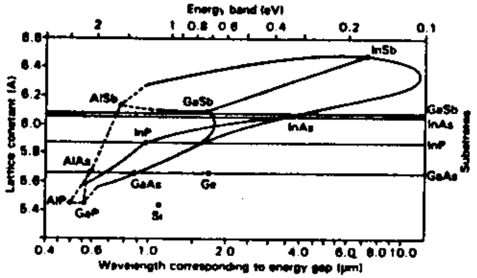

Figure 5

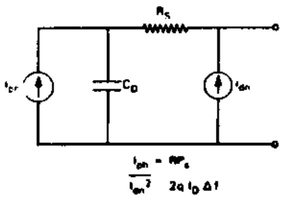

Figure 6a
Equivalent Circuit Model for a Reverse Biased Photodiode

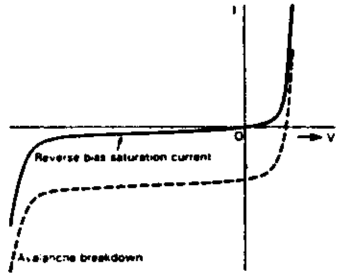

Figure 6b
Current Voltage Characteristic for a PIN Photodiode, in the Dark (Solid) and when Irradiated (Dashed)

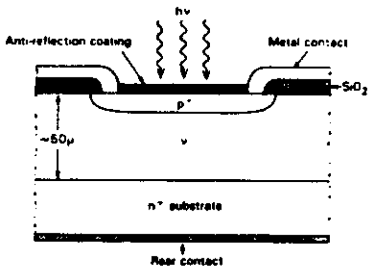

Figure 7
Structure of a Si PIN Photodiode.
The device is of the reach-through type in which the low doped v layer depletes through to the $n^+$ substrate at low voltages

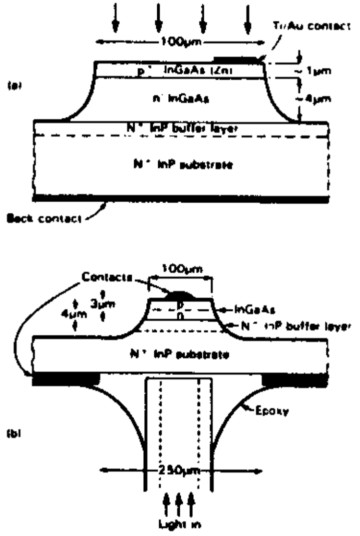

Figure 8
GaInAs PIN Photodiodes, (a) Front Entry, and (b) Substrate Entry

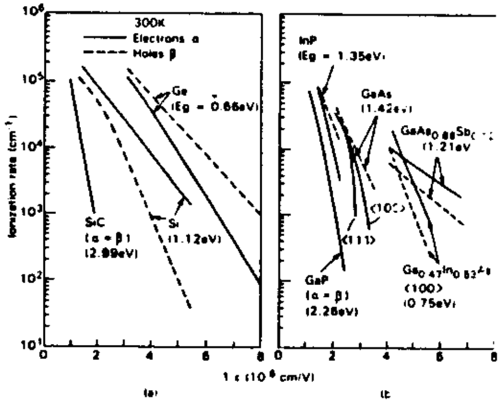

Figure 9
Ionization Rates at 300K versus Reciprocal Electric Field for Ge, Si, GaAs and some IV-IV and III-V Compound Semiconductors

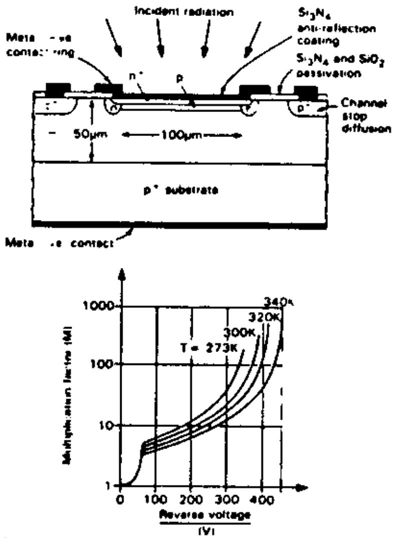

Figure 10
A Planar Epitaxial Silicon reach-through APD (a) Schematic cross-section (b) Variation of the Avalanche Multiplication factor, M, with applied Voltage and Temperature (taken from H. Melchior et al, Planar Epitaxial Silicon Avalanche Photodiode, Bell Syst. Tech. J., 57, 1781-7 (1978))

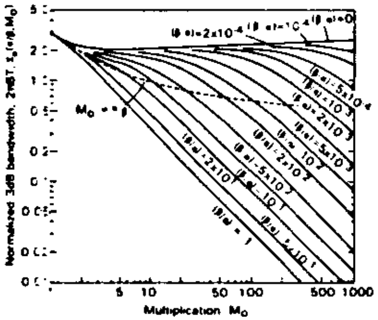

Figure 11
Bandwidth as a Function of Multiplication and β for Pin Photodiode

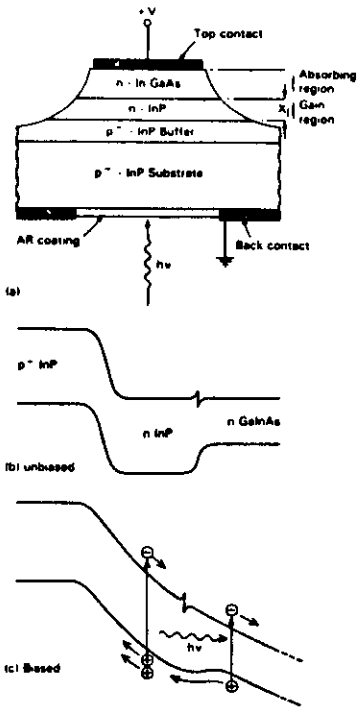

Figure 13
The Structure and Band diagram of the GaInAs/InP SAM APD

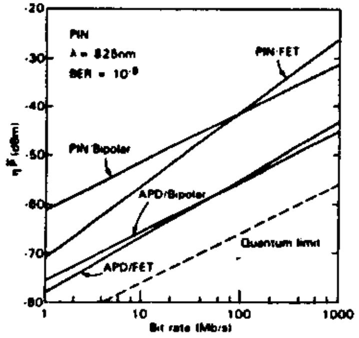

Figure 14
Calculated Receiver Sensitivity of Si PIN Diodes and APDs (K = 0.03)

117

118

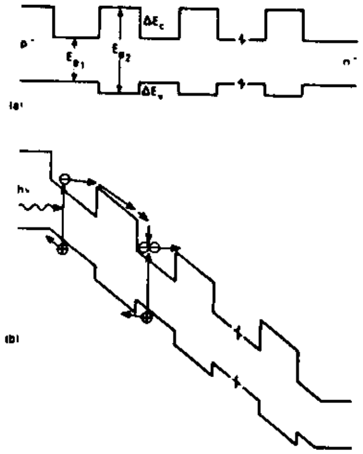

Figure 15

Energy Band diagram of the Superlattice APD, (a) Unbiased (b) Biased. The structure would comprise ~100 layers of alternate wide and narrow gap semiconductors

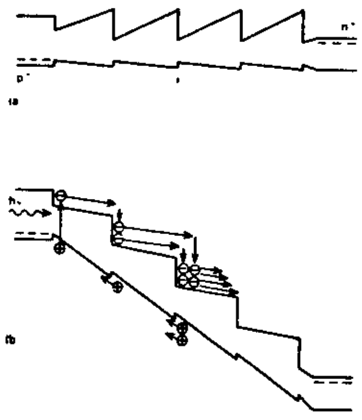

Figure 16

The Staircase Avalanche Photodiode. Depicted here in the Photomultiplier mode with an electron multiplication of two at each stage, and no hole ionisation. (a) is the situation for the unbiased device. (b) illustrates the device biased for normal operation

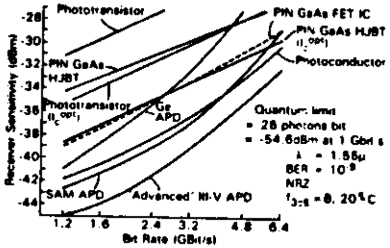

Fig. 17. Receiver sensitivities as a function of data rate.

RECEIVERS FOR HIGH-SPEED SYSTEMS AND PARAMETERS TAKEN FOR EACH AND USED TO DERIVE RECEIVER SENSITIVITY IN FIG 17

| | |
|---|---|
| ● Phototransistor | (Base contacted $f_T$ = 17GHz<br>$C_{bc} = C_{be}$ = 0.03pF |
| ● Germanium Avalanche Diode | (5μm depletion, α/β = 1,<br>1nA leakage 20°C) |
| ● Separate Absorption-Multiplication Avalanche Diode | (3.5μ depletion, α/β = ½,<br>1nA @ 20°C) |
| ● Photoconductor | (2×2μm², R=2kΩ,<br>peak gain=10, gB=16GHz |
| ● PIN-HJBT | ($C_{PIN}$ = 0.05pF) |
| ● PIN-FET I C | (Dynamic range >20dB,<br>Cgs=0.17pF, $g_m$=19mS |
| ● Advanced Avalanche Diode | (α/β = 10, 2μm depletion,<br>1nA @ 20°C |